

HUNGARIAN

AGRICULTURAL

ENGINEERING



40/2021





HUNGARIAN
ACADEMY
OF SCIENCES

Hungarian Agricultural Engineering

N^o 40/2021

Editors-in-Chief:
Dr László TÓTH
Dr. István SZABÓ

Managing Editor:
Dr. Csaba FOGARASSY

Secretary of Editorial board:
Dr. László MAGÓ

Editorial Board:

Dr. David C. FINGER
Dr. György SITKEI
Dr. Gábor KESZTHELYI-SZABÓ
Dr. László TÓTH
Dr. János BEKE
Dr. István SZABÓ
Dr. István J. JÓRI
Dr. Béla HORVÁTH
Dr. Péter SEMBERY
Dr. László FENYVESI
Dr. Csaba FOGARASSY
Dr. Zoltán BÁRTFAI
Dr. László MAGÓ
Dr. Bahattin AKDEMIR
Dr. R. Cengiz AKDENIZ
Dr. József NYERS
Dr. Mičo V. OLJAČA
Dr. Zdenek PASTOREK
Dr. Vijaya G.S. RAGHAVAN
Dr. Lazar SAVIN
Dr. Bart SONCK
Dr. Goran TOPISIROVIĆ
Dr. Valentin VLADUT
Dr. László KÁTAI

**PERIODICAL OF THE COMMITTEE OF
AGRICULTURAL AND BIOSYSTEM
ENGINEERING OF THE
HUNGARIAN ACADEMY OF SCIENCES**

Published by

**Hungarian University of
Agriculture and Life Sciences
Institute of Technology
H-2103 Gödöllő, Páter K. u. 1.**



HUNGARIAN UNIVERSITY OF
AGRICULTURE AND LIFE SCIENCES

Institute of Technology

**Gödöllő
2021**

Technical Editor: Dr. László MAGÓ

Published online: <http://hae-journals.org>
HU ISSN 0864-7410 (Print)
HU ISSN 2415-9751(Online)

PREFACE

In the name of the Committee of Agricultural and Biosystem Engineering of the Hungarian Academy of Sciences we would like to welcome everyone who is interested in reading our journal. The Hungarian Agricultural Engineering (HAE) journal was published 33 years ago for the very first time with an aim to introduce the most valuable and internationally recognized Hungarian studies about mechanisation in the field of agriculture and environmental protection.

In the year of 2014 the drafting committee decide to spread it also in electronic (on-line and DOI) edition and make it entirely international. From this year exclusively the Hungarian University of Agriculture and Life Science's Institute of Technology (former Szent István University's Faculty of Mechanical Engineering) took the responsibility to publish the paper twice a year in cooperation with the Hungarian Academy of Sciences.

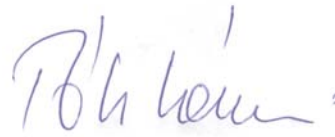
Our goal is to occasionally report the most recent researches regarding mechanisation in agricultural sciences (agricultural and environmental technology and chemistry, livestock, crop production, feed and food processing, agricultural and environmental economics, energy production, engineering and management) with the help of several authors. The drafting committee has been established with the involvement of outstanding Hungarian and international researches who are recognised on international level as well. All papers are selected by our editorial board and a triple blind review process by prominent experts which process could give the highest guarantee for the best scientific quality.

We hope that our journal provides accurate information for the international scientific community and serves the aim of the Hungarian agricultural and environmental engineering research.

Gödöllő, 20.12.2021.



Dr. István SZABÓ
editor in chief



Dr. László TÓTH
editor in chief

CONSTRUCTION OF A PACKED-BED PYROLYSIS REACTOR FOR CHARCOAL PRODUCTION

Author(s):

A. Dhaundiyal¹, G. Bercesi¹, L. Toth¹

Affiliation:

¹ Institute of Process Engineering, Hungarian University of Agriculture and Life Sciences (MATE), 2100 Gödöllő, Páter Károly u. 1., Hungary

Email address:

Alok.dext@hotmail.com; Bercesi.Gabor@uni-mate.hu; laszlotothdr@t-online.hu

Abstract: The paper pivoted on processing forest waste, Austrian Pine, for producing carbon enriched char. A small-packed bed reactor was developed to pyrolysis the processed char. The preparation of feedstock was carried out in an improvised muffle furnace. The following parameters were obtained to determine the potential of pine waste: thermal effectiveness, oil yield, char yield, gas yield, specific biomass consumption, and carbon conversion efficiency of the unit. The absolute increase in the cold gas efficiency of pine needles after torrefaction was 44%. As compared to Acacia wood chips (G30 and G50), a 4.8% rise in the carbon conversion efficiency was seen after thermal pre-treatment of pine needles. However, it was relatively dropped by 2% to the wood pellets. The obtained char yield from torrefied pine needles as to the wood pellets was augmented by 160%. On the contrary, the oil yield derived from torrefied pine pellet was dropped by 65% while comparing it with the wood pellets. The carbon dioxide emission was mitigated by 3.4% after torrefaction of raw pine needles, whereas it was reduced by 11.71% when it was compared with commercial wood pellets. A pronounced rise of 123% in the clean gas production was noticed after the torrefaction of pine needles, while it was 14.96% when it was compared with the wood pellets.

Keywords: packed bed, char, pine waste, thermal performance, wood pellets, clean gas

1. Introduction

Diversification of fuel sources has become a common practice for energy generation, but some waste materials are abundant in nature and could be exploited for the same. The majority of energy companies focuses on the standard fuel for domestic and international consumption, but it could be economically more viable and environmentally friendly if the waste loose biomass is also used. However, some designing complications are appended with them, but with the suitable processing technique, it could be utilised in different thermochemical processes.

According to the general policy framework of the EU, the share of renewable energy must be increased by 32%, an improvement of 32.5% in the energy efficiency of the system, and carbon emission must be abridged by 40% as compared to the base year 1990 [1]. For promoting bioenergy, another initiative was taken in Paris Climate Agreement by the EU that functioning of the coal-based power plant would be shunned by 2030 [2]. What are alternatives do we have to get clean energy? Either tap the solar energy or go for waste biomass management. In 2014, the parallel experiments were conducted on the 120 kW and 10 kW of the throat-less gasifiers to know the suitability of the loose biomass, pine needles, and it was found that the overall thermal efficiency of the system was 76.66% for 120 kW, whereas it was 76.5% for a small-scale unit. It was noticed that the loose biomass could be used in the different sizes of gasifiers with marginal change in its thermal performance [3, 4]. Similarly, a small unit for pyrolysis purpose was developed in the Institute of Agriculture Mechanisation. were thermally decomposed, and the thermal efficiency of 47–48% was obtained while carrying out the thermal decomposition of the Austrian standard wood chips, ONORM G30 and G50 (if the unit height is 320 mm) [5, 6]. Similarly, various technologies were used for the thermal decompose of woody biomass and it was noticed that thermal efficiency varied from 36.1% to 58.6% [7]. So, even state-of-art thermochemical transformation was not much promising for biomass conversion.

After reviewing the different types of technologies, it was noticed that the thermal effectiveness of the unit was not much influence despite using miscellaneous solid biomasses.

In this paper, a miniature of the pyrolysis reactor was constructed for thermally processed black pine needles pellets. The assessment of a unit was based on the cold gas efficiency (CGE), carbon conversion efficiency (CCE), apparent thermal efficiency, specific biomass consumption, and yield of char, gas and pyrolysis oil.

2. Materials and Methods

The pine waste was collected from Pest County of Hungary. The net 10 kg of pine needles were prepared and processed at the National Centre for Agriculture Research and Innovation, whereas the fabrication of a small-scale reactor was done at Edison Energetic Lab, Institute of Process Engineering, Szent Istvan University, Hungary.

2.1. Preparation and processing of loose biomass

For the milling purpose, a 1.5 kW rotor grinding machine (Retsch SM 2000) was used. The feed rate of the material was kept between 0.2 to 0.3 kg·h⁻¹. A sieve of 1.5 mm was considered for filtering the milled material. The milled form of pine needles is shown in Fig. 1. After finishing the milling process, the moisture content of the end product was measured before the densification process.



Figure 1. The milled pine needles for the densification process

A 1–2% of water was added to the milled pine needles which were thereby heated to 70°C approximately. The heat is usually supplied to ensure that the lignin is released, and it would impart the binding ability to the particles.

For densification purposes, a ring-type pellet machine (CL3, Pellet mill) was used (Fig. 2). A screw extrusion of milled feedstock was carried out by feeding the material into a barrel via a hooper. The screw aims to push the material into the chamber where the roller presses the material against the ring die. The length and diameter were calculated to be 25.95 mm and 6.39 mm, respectively. It is worth mentioning that the gap between the die and roller impacts the quality of the pellets, wearing of the machine components and the energy consumption during the densification process.



Figure 2. The ring-type pellet machine

Around 20% of extra energy is required if the gap is increased by 1 mm. However, it also reduced the dust content by 30% in the final product. Another factor is the pressure required to form a pellet. The compacting process elevates the temperature of the input feedstock. A material that requires a higher pressure would

ultimately block the holes in the die and thus hamper the densification process. The densified form of pine needles is shown in Fig. 3.



Figure 3. The pellet form of pine needles

2.2. Modification of muffle furnace

The thermal pre-treatment was performed in an improvised furnace that is based on the principle of the Joule heating system. A digital furnace (Nabertherm GmbH) was programmed to suit the quasi-static condition. The furnace used during the experimental task is illustrated in Fig. 4.



Figure 4. The improvised furnace for the torrefaction process

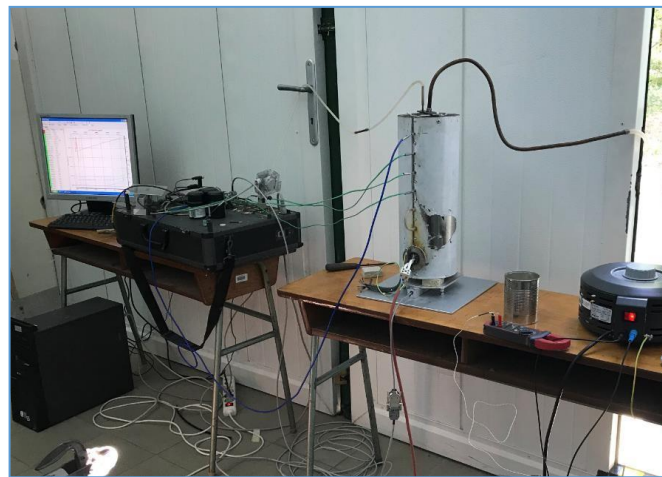
The nitrogen gas flowing at the volumetric rate of $42 \text{ L} \cdot \text{min}^{-1}$ was used to inert the furnace chamber. The mass measurement was performed by connecting the mass holder to the weighing machine via a mechanical link. The lid ($313.15 \text{ mm} \times 250 \text{ mm}$) for the furnace was modified to hold the pine pellets until the furnace attains a predetermined torrefaction temperature. For the flow of nitrogen, ducts of 21.5mm diameters were provided on the hollow cylinder and the rectangular frame of the lid. To cool down the system, a fan was bolted along the structure to inhibit the heating of protruded cylindrical section. The volumetric flow rate of the nitrogen was measured by the gas flow meter (Ganz 2000). Once the furnace attained the desired temperature, the sample was immediately fed into the chamber. The thermal profile for the torrefaction process was controlled by a digital console. The thermally processed material is shown in Fig. 3.7.



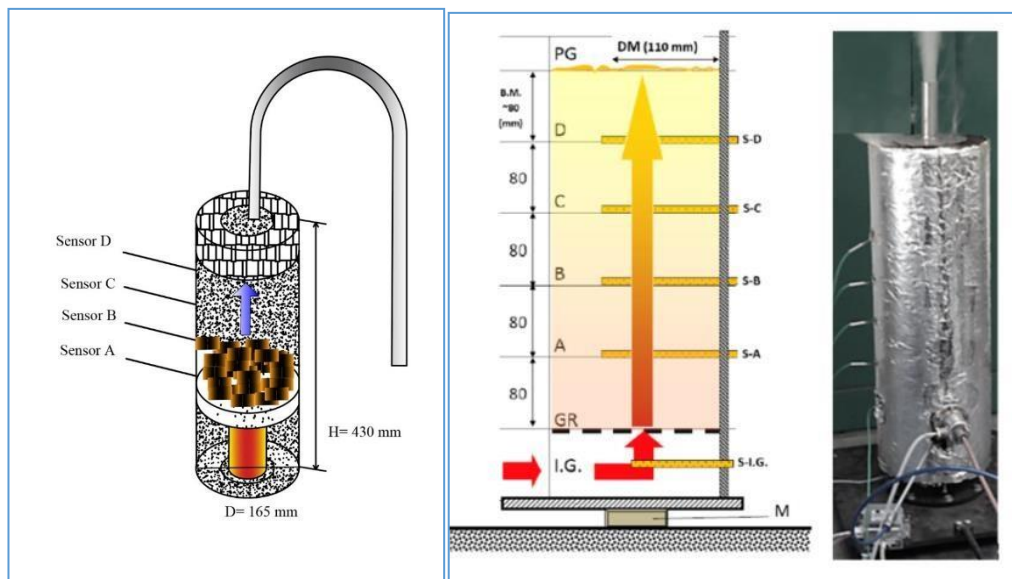
Figure 5. Thermally pre-treated pine pellets

2.3. Fabrication of the experimental rig

The preliminary drafting of the pyrolysis unit was carried out in AutoCAD (Autodesk, 2019). The inner shell of the reactor was fabricated from 1.45 mm thick welded carbon steel. The height of the reactor from the base is 430 mm, whereas the inner length was measured to be 400 mm. A clearance of 30 mm was provided between the inner and the outer shells. A 41.5 mm thick rock wool coating was provided to prevent heat across the outer shell of the reactor. The outer covering of the rock wool was done by a galvanised steel sheet. The diameter of the outer and inner shells of the reactor was 165 mm and 85.2 mm, respectively. For temperature measurement, the ports were produced along the length of the reactor. The distance between ports was kept at 43.8 mm. A small duct of 5mm diameter was provided for pressure measurement. A lid was also fabricated for providing additional heat insulation to the main body. The length and diameter of the lid were 71.6 mm and 118.4 mm, respectively. A grate of 79.55 mm in diameter was formed to carry the ash and char of feedstock. A concentric ceramic casing was provided for securely holding the heating element in the helical grooves engraved on the inner ceramic casing. The height of the heating unit was 153 mm from the bottom of the inner shell. The inner and outer diameter of the concentric casing was measured to be 47 mm and 73mm, respectively. To prevent the ingress of air, an airtight gasket was placed between the lid and flange provided at the bottom of the shell.



(a)



(b)

(c)

Figure 6. a: A small-scale pyrolysis unit; b: technical drawing of the proposed unit [8]; c: MGI pyrolysis unit (inert gas-based) [5, 6]

2.4. Metrology of the thermal system

The temperature measurement was performed by a 16-channel data acquisition unit (HBM). The thermogravimetric evaluation was carried by a strain gauge. The thermocouples type K (Ni-Cr) was used to measure the temperature at the designated ports. The producer gas measurement and its sampling were conducted by the Wood gas analyser (VISIT-03H, Messtechnik EHEIM GmbH). The sampling rate was preset at a volumetric rate of $0.7 \text{ L} \cdot \text{min}^{-1}$. The wood gas analyser involved in the measurement process is shown in Fig. 7. The gas wash bottles filled with refined oil and distilled water were used to trap the gaseous byproducts during pyrolysis reactions. Once the gas got cleaned, it went for further processing in the wool filter, activated carbon, and activated alumina soaked in potassium permanganate so that the dry producer gas could be obtained. The remaining condensate formed during the cleaning process was expelled through the water port provided on the console of the gas analyser. It is to be noted that before letting the gas be washed, a condensate trap was provided to remove the pyrolytic oil formed during the thermal decomposition of processed pine needles pellets. The dust and tar collection were performed at a sampling rate of $0.6 \text{ L} \cdot \text{min}^{-1}$. A 50 mL of isopropanol was used to dissolve the collected oil in the bottle placed in an ice bucket. Before beginning the sampling process, the volumetric suction rate of the pump was calibrated by a gas meter.



Figure 7. The wood gas analyser for the gas measurement



Figure 8. The single-stage rotary evaporator for distillation [8]

The filtration of pyrolysis oil was done at Regional Knowledge Centre, Szent Istvan University. A 50 mL of isopropanol was used as a solvent to collect the oil, which was later distilled by a rotary evaporator (RVO 400, Boeco). The single-stage evaporator is shown in Fig. 8. The operating conditions used during distillation are provided in the literature [4]. To distil the isopropanol, the vacuum pressure and temperature of the water bath were kept at 0.137 bar and 60°C , respectively. The decanter was allowed to undergo 70 revolutions per minute until no further condensation of isopropanol was noticed. The mass of the mixture along with the decanter was measured before starting distillation.

2.5. Performance assessment of a reactor

To measure thermal as well as the energetic aspect of pre-treated pine pellets, the following parameters were calculated

Carbon conversion efficiency (CCE)

The percentage of the total carbon converted to those components of producer gas that contain carbon is defined by CCE. The CCE can be given by Eq. 1. [9]

$$CCE \% = 12 \times V_g \times \frac{[CO\% + CH_4\% + CO_2\%]}{22.4 \times C\% \times W(1 - X_{ash})} \times 100 \quad (1)$$

In case the additional gas components C_2H_4 , C_2H_2 and C_2H_6 are also measured along with the producer gas, Eq. (1) can be written as

$$CCE \% = 12 \times V_g \times \frac{(CO\% + CH_4\% + CO_2\%) + 2(C_2H_4\% + C_2H_6\% + C_2H_2\%)}{22.4 \times C\% \times W(1 - X_{ash})} \times 100 \quad (2)$$

where CO, CH₄, CO₂, C₂H₄ and C₂H₆ are measured on a vol% basis, whereas C% is the carbon fraction in the feedstock. W is the biomass feeding rate (g·h⁻¹), V_g (Nm³·h⁻¹) and X are the volumetric flow rate of producer gas and the ash content in biomass, respectively.

Steam decomposition (SD)

Decomposition of steam during thermochemical transformation can be given by Eq. (3) [9]

$$SD\% = V_g \times \frac{((H_2 + 2 \times CH_4) + 2 \times C_2H_4) \times \frac{18}{22.4}}{W_1 + W_2} \times 100 \quad (3)$$

Here, W_1 and W_2 are the steam flow rate and the moisture content in feedstock, respectively.

Apparent thermal efficiency (ATE)

Correspond to the oxidation of the feedstock, the energy conversion was presented in the context of apparent thermal efficiency. However, this factor is based on the effect of reactor temperature on energy yield. The producer gas to solid fuel energy ratio is defined as, [10]

$$ATE = \frac{Y \times HHV_g}{W \times HHV_b} \quad (4)$$

where Y and W denoted the gas yield and mass of solid biomass

Gas yield (Y)

The nitrogen content of the feedstock is relatively low therefore it was excluded while computing the gas yield. The dry gas yield, Y , based on ash-free biomass can be given by Eq. 5. [11].

$$Y = \frac{V_g \times 0.79}{W \times (1 - X_{ash}) \times N_2} \text{ Nm}^3 \cdot \text{kg}^{-1} \quad (5)$$

Here, N_2 volumetric percentage of nitrogen in the producer gas.

Higher heating value (HHV_g)

The heating value of the producer gas was measured with the help of a volumetric percentage of H₂, CO and CH₄. The higher heating value of gas can be derived from Eq. 6. [11]

$$HHV_g = 0.0418 \times (3.018 \times CO\% + 3.052 \times H_2\% + 9.5 \times CH_4\%) \text{ MJ} \cdot \text{Nm}^{-3} \quad (6)$$

Cold gas efficiency (CGE)

The cold gas efficiency of the reactor can be defined as the ratio of chemical energy of the producer gas to that of feedstock. Mathematically, it can be written as [11]

$$\eta_c = \frac{Y \times HHV_g}{HHV_b} \quad (7)$$

2.6. Physicochemical properties of raw and torrefied pine needles

The physical and chemical analyses of pine needles were conducted into two phases: Ultimate and proximate and Calorimetry. The ash measurement of the torrefied material was determined according to the NREL method [12]. The following equation was used to estimate the fixed carbon in the raw and thermally pre-treated samples. The material tested in the proposed pyrolysis unit was pre-treated at 250°C for 5 minutes.

$$F.C\% = 100 - \text{Ash}\% - M\% - V.M\% \quad (8)$$

The ultimate analysis of the samples was performed using a CHNS analyser (Vario MACRO elemental). The detailed analysis information is provided in the literature [8]. Information about physical and proximate analysis and the chemical composition of raw/ processed pine needles, hog fuel, wood chip and Mengxi coal are tabulated in Table 1 and Table 2, respectively.

Table 1. Variation in physical properties and proximate analysis of material upon thermal pre-treatment

Material	ρ_b (kg·m ⁻³)	HHV (MJ·kg ⁻¹)	Ash%	*F.C %	**V.M%
Raw	179.20	22.32	2.92	7.16%	89.92
Densified [13]	788	22.32	2.92	7.16%	89.92
Torrefied (250°C, 5 min.)	720.64	23.45	2.07	73%	21.48

*Fixed carbon ** Volatile matter

Table 2. Chemical composition of different biomasses and coal

Material	C%	H%	N%	S%	O%
Raw	50.91	7.02	1.01	0.11	41.43
Torrefied	53.40	6.54	0.68	0.09	40.53
Wood pellet (Hog fuel) [15]	49.35	5.23	0.10	0.06	41.95
Wood chip (Acacia) [5]	50.03	5.84	0.07	0.06	42.94
Mengxi Coal [14]	87.50	6.50	1.00	1.50	3.50

3. Results and discussion

3.1. Thermal performance of the reactor

A comparative assessment has been conducted based on the thermal potential of different biomasses that were tested in different kinds of reactors (Table 3). A non-inert powered reactor was compared with a microwave-based pyrolysis unit [14] and the MGI reactor [5]. It was found that the cold gas efficiency of pre-treated pine needles pellets was 31% lower than that of the wood pellets (hog fuel), whereas the carbon conversion efficiency of torrefied pine needles was found to be 4.8% higher than the wood chips, but 70.23% lower than that of raw pine needles. The absolute increase in the gas yield of raw pine needles after torrefaction was 83%, whereas it was 17.47% lower than that of the wood pellets. The char production ability of densified- pre-treated pine needles was increased by 689.47%. The derived char yield was found to be 122.71% higher than the wood pellets, but it was 25.90% lower than the char yield derived from microwave pyrolysis of coal [14]. The steam decomposition (SD) percentage during pyrolysis was calculated to 47.14% for torrefied pine needles pellets, which was 13.48% and 1745.51% higher than wood chips and wood pellets, respectively. The relative energy conversion was assessed with the help of apparent thermal efficiency (ATE). The apparent thermal efficiency of torrefied pine needles was computed to be 30% lower than that of the wood pellets, whereas the absolute percentage rise in ATE was 182% after the thermal pre-treatment of pine needles. The oil yield derived after torrefaction was noticed to be reduced by 65% while comparing it with the wood pellets. Similarly, the conventional pyrolysis of coal provided 94% less oil yield than the thermally processed pine needles. The heating value of the producer gas derived after thermal decomposition of the torrefied pine pellets was 1.57%, 142%, 99%, and 72.95% higher than that of wood pellets, wood chips, coal and the raw pine needles, respectively.

Table 3. Performance parameters for different types of biomasses and coal

Parameters	Processed pine needles	Wood chips	Wood pellets	Coal [14]	Raw pine needles
ATE	1.93	0.0038	2.76	0.0045	0.11
CGE %	44.53	0.18	64.38	0.20	0.63
Y (Nm ³ ·kg ⁻¹)	0.85	0.0065	1.03	0.0066	0.02
CCE %	13.66	13.03	13.94	0.96	45.89
Char yield %	60	26.94	23	80.98	7.6%
Oil yield %	10.48	-	30	0.62	-
HHV _g (MJ·Nm ⁻³)	12.28	5.06	12.09	6.17	7.1
W (kg·h ⁻¹)	0.23	0.47	0.24	0.44 [9]	0.055
SD%	47.14	41.54	17.11	2.02	10.75
V _g (Nm ³ ·h ⁻¹)	0.036	0.2	0.036	0.006	0.036
Medium	-	Nitrogen	-	-	-

It was noticed that the thermal pre-treatment alongside densification of pine needles improved thermal efficiency, carbon conversion ability, char yield and quantitative aspect of the proposed design; however, it is still relatively lag behind the commercial hog fuel in the context of carbon conversion and cold gas efficiency. But the overall objective of charcoal production was drastically higher than the commercially available biomasses (G30, G50 and the wood pellets). Moreover, the fuel consumption rate (W) was noticed to 4.34% higher than that of thermally processed pine needles, where it was increased to 104.34% when it was compared with the Acacia wood chips (G30 and G50). Similarly, coal pyrolysis consumes 91% more fuels than that of the proposed design. However, the raw pine needles require 76% less fuel to generate gas, but the overall charcoal production from the unit was exceptionally low, therefore the proposed packed-bed reactor was found to be not suitable for loose biomass. The solid material can generate up to 60% or more charcoal without any significant interrupt during the functioning of the small-scale reactor. The minimum ingestion period of the reactor was 3.60 min for processed pine needles, whereas it is around 12 minutes, so the overall delay of 8.4 minutes was seen during thermal decomposition of commercial biomass. The reason for higher carbon conversion efficiency is the relatively low thermal immunity of commercial pellets as compared to the torrefied pine pellets. The cold gas efficiency of processed pine pellet was attributed to the reduction in the dry gas yield obtained from the processed pine pellets. It could be controlled by adding a suitable catalyst to increase the hydrogenation of carbon monoxide and carbon dioxide and thus the overall clean gas production would also be influenced. Albeit the overall clean gas production after torrefaction was amplified by 14.96%. Another means of improvement is the water-gas shift reaction or expelling out nitrogen from the system via the Haber-Bosch process.

3.2. Thermogravimetry / Evolved gas analysis

The change in the extensive and intensive properties of the reactor with time are shown in Fig. 8 and Fig. 9, respectively. The initial mass of 0.3 kg had undergone thermal decomposition. The mass plateau was decreased by 56% during dehydration of the torrefied pine needles pellets when it was compared with the wood chips [5]. The ripples were noticed at the beginning of the pyrolysis. The reason for this effect was either owing to a sudden change in the heating rate of the system or evolving intermediate compounds. Since the applied voltage and power supply was kept constant, a thermal lag was seen during the pyrolysis of processed pine pellets. It indicated that thermal immunity of pre-treated biomass at a reduced temperature range was improved due to the cross-linking reactions. The surfacer adsorption was observed while carrying out the thermal decomposition of processed pine pellets and consequently, the system temperature was dropped by 15°C at the onset of the char formation stage. The dynamic pressure of the system was decreased from 0.6 Pa to 0 Pa during surface adsorption. It could be concluded from the thermogravimetric (TG) curve that surface defects formed during thermal pre-treatment have changed the TG behaviour of the processed pine pellets.

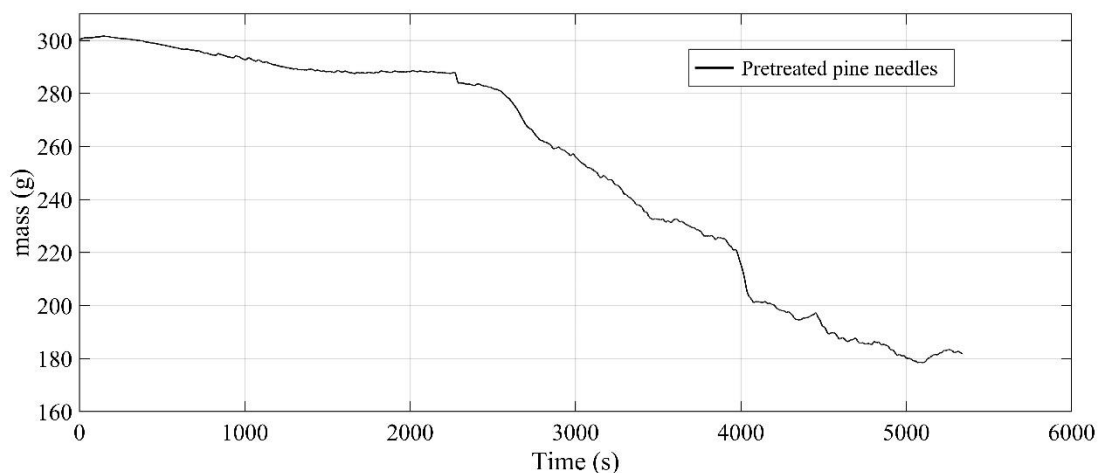


Figure 8. Thermogravimetric variation in pre-treatment pine needles with time

Besides thermogravimetric variation in the processed pellet mass, the intensive properties (Fig. 9) were also monitored. At the constant power supply, a steep rise in the lower bed temperature (A) was observed at the onset of the pyrolysis process. The corresponding heating rate calculated during the thermal event was 3.89

$^{\circ}\text{C}\cdot\text{min}^{-1}$. The sigmoidal nature in the thermal profile shows the simultaneous dissipation of heat and pressure taking place within the system. Once the lower bed (A) approached the cut-off point, the upper bed temperature tried to maintain the thermal equilibrium with the lower bed. A 24.26% rise in heating rate was seen during the desorption of moisture. The drying of processed pine pellets brought a significant rise of 76% in pressure that showed that eventually drifted away from the system from its thermal equilibrium. This was happened due to a rise in the partial vapour pressure of water content in the cellulose structure. The structural rapture of pine needles during the torrefaction increased the pressure-driven flow of fluid across the reactor and thus reduced the residence time of volatile in the reactor. The evolution of volatile during thermal decomposition of the processed pine pellets was seen in a temperature interval of 406–577 $^{\circ}\text{C}$. The formation of the process was observed at 577–690 $^{\circ}\text{C}$. The pressure drops while the formation of char was 212 Pa.

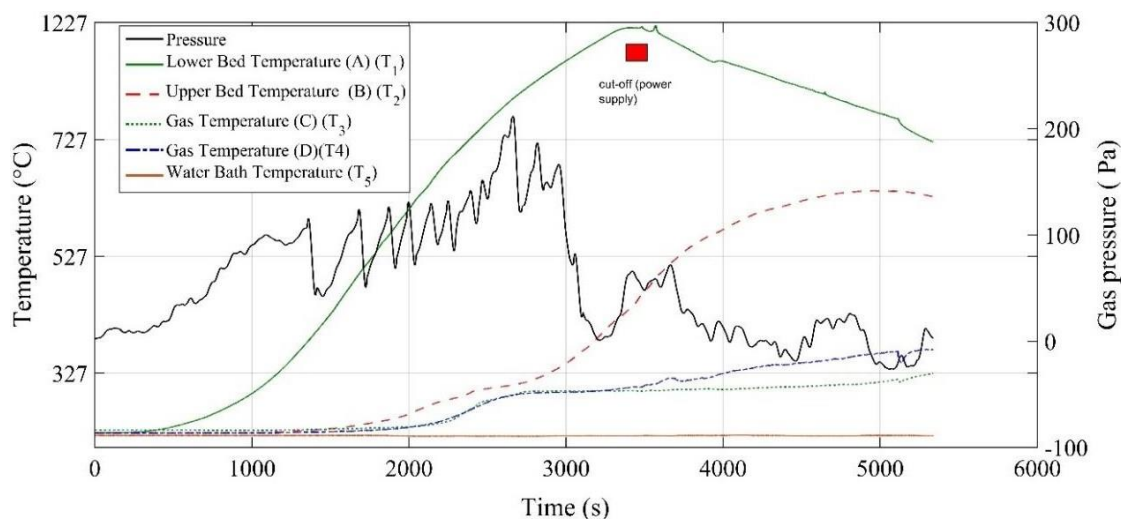


Figure 9. The change in the intensive properties of the system with time

The deviation in producer gas composition derived from processed pine pellets is illustrated in Fig. 10. The average gas composition derived during pyrolysis of the processed pine needle pellets, coal, raw pine needles, wood chips and wood pellets is shown in Table 4. It was seen that the emission of CO_2 and CO fraction was decreased by 8.2% and 12%, respectively. Similarly, the rise in hydrogen and methane gases composition was 91.2% and 11%, respectively, when it was compared with wood chips [5]. It was observed that the release of volatiles was very abrupt as time proceeds. It happened due to water-gas shift reaction that eventually bolstered the percentage of hydrogen gas percentage in the producer gas. Once the hydrogen began to increase, the carbon dioxide and methane were got saturated with time.

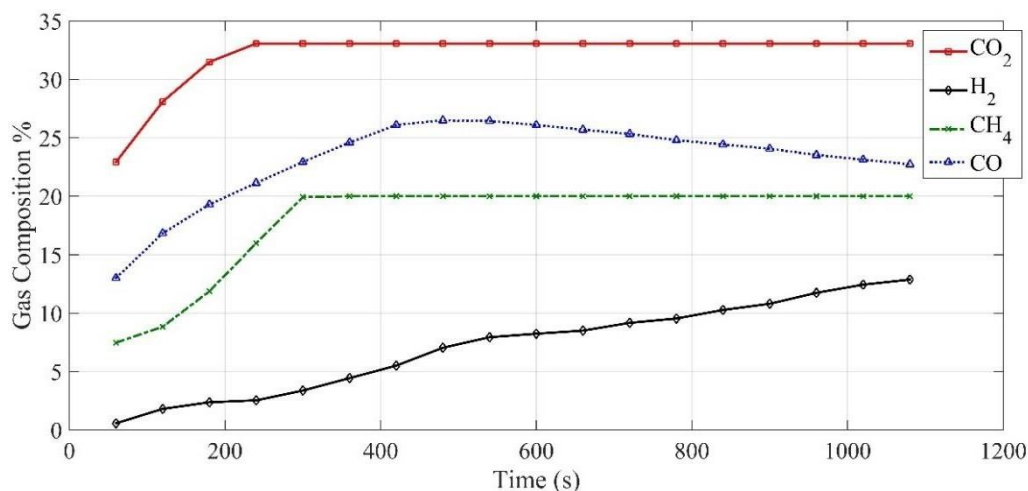


Fig.

Figure 10. The fluctuation in the producer gas composition with time

As compared to raw pine needles, coal, the wood pellets, the carbon dioxide emission was, respectively, seen to be reduced by 3.43%; 50.59% and 11.71%. The clean gas generation increased by 123.40% after the

torrefaction of raw pine needles, which was correspondingly 45.16 %, 14.96% and 200% higher than wood chips [5], wood pellets and Coal [14]. The operating medium also influences the gas composition as it was seen that the gas composition derived from wood chips had 250% higher nitrogen content in the producer gas than that of the processed pine needles pellets, whereas it was noticed to be the least during coal pyrolysis [14]. The influence of the medium affects the thermal performance of the reactor; therefore, it should be minimised during thermal decomposition.

Table 4. Gas composition derived from thermal decomposition of different biomass (vol%)

Material	CO%	CO ₂ %	H ₂ %	CH ₄ %	N ₂ %
Processed Pine Needles	22.80	30.90	11.50	20	14.80
Raw pine needles	24.50	32	5.90	8.20	29.40
Wood Chips [5] (Nitrogen reactor)	14.3	12.2	19.9	1.8	51.8
Wood pellets	25.40	35	7.40	20	12.20
Coal [14] (conventional pyrolysis)	23.07	62.54	3.35	7.14	2.02

4. Conclusion

The following noteworthy points were derived during analysis:

- The proposed reactor was able to assimilate properly the solid biomass, but it had shown anomaly with loose biomass.
- The carbon conversion efficiency of the raw pine needles was decreased by 70.23% after torrefaction. The reason is thermal immunity is imparted due to cross-linking reactions.
- The fuel consumption of the processed pine pellets was reduced by 4.166% when it was compared with the commercial wood pellets.
- The gas derived from processed pine needles pellets was 5.96% and 14.96% cleaner than the wood chips and the wood pellets, respectively.
- The carbon dioxide emission was curtailed by 3.43% after the torrefaction of the raw pine needles, whereas it was further decreased as compared to coal and woody biomasses.
- The dry gas yield of processed pine pellets to the wood pellets was dropped by 17.45%. The reason is the excessive formation of nitrogen gas during the thermal decomposition of processed pine needles. It could be curtailed if the methanation and water-gas shift reactions are promoted via catalytic pyrolysis.
- The adsorption of gas accompanied a drastic drop in the pressure of the system.
- A sudden rise in hydrogen gas formation was owing to the exothermic reaction between water vapour and carbon monoxide.
- The steam decomposition was found to be maximum in the torrefied pine needles pellets among other biomasses and coal.
- The following reactor can be further modified if nitrogen is transformed into ammonia and thus the overall producer gas yield can be improved.

Acknowledgment

Thanks to GINOP-2.1.2-8-1-4-16 for “Research and Development for Decentralized Energy Production” for assisting in the performance of laboratory experiments.

References

- [1] <https://www.europarl.europa.eu/factsheets/en/sheet/68/energy-policy-general-principles> (Accessed: 19-07-2021)
- [2] <https://www.carbonbrief.org/daily-brief/eu-must-shut-coal-plants-2030-meet-paris-climate-pledges-work-restarts-dakota-access-oil-pipeline> (Accessed: 19-07-2021)
- [3] **Dhaundiyal, A. & Gupta, V.K.:** (2014) The Analysis of Pine Needles as a Substrate for Gasification. *Hydro Nepal: Journal of Water, Energy and Environment*. 15:73–81.

- [4] **Dhaundiyal, A. & Tewari, P.C.:** (2016) Performance evaluation of throatless gasifier using pine needles as a feedstock for power generation. *Acta Technologica Agriculturae*. 19(1):10–18.
- [5] **Dhaundiyal, A., Toth, L., Bacskai, I. & Atsu, D.:** (2020) Analysis of pyrolysis reactor for hardwood (Acacia) chips. *Renewable Energy*. 147:1979–1989.
- [6] **Dhaundiyal, A. & Atsu, D.:** (2021) Exergy analysis of a pilot-scale reactor using wood chips. *Journal of Cleaner Production*. 279:123511.
- [7] **Patuzzi, F., Basso, D., Vakalis, S., Antolini, D., Piazzzi, S., Benedetti, V., Cordioli, E. & Baratieri, M.:** (2021) State-of-the-art of small-scale biomass gasification systems: An extensive and unique monitoring review. *Energy*. 223
- [8] **Dhaundiyal, A., Singh, S.B. & Toth, L.:** (2021) Experimental investigation of a small-scale reactor with processed bio-fuel pellets. *Biofuels, Bioprod. Bioref.*. <https://doi.org/10.1002/bbb.2256>
- [9] **Lv, P. et al.:** (2004) An experimental study on biomass air–steam gasification in a fluidized bed. *Bioresource Technology*, 95(1), pp.95–101.
- [10] **Nipattummakul, N., Ahmed, I. I., Kerdsuwan, S., & Gupta, A. K.:** (2010). Hydrogen and syngas production from sewage sludge via steam gasification. *International Journal of Hydrogen Energy*, 35(21), 11738–11745.
- [11] **Xiao, R., Zhang, M., Jin, B., Huang, Y., & Zhou, H.:** (2006). High-Temperature Air/Steam-Blown Gasification of Coal in a Pressurized Spout-Fluid Bed. *Energy & Fuels*, 20(2), 715–720.
- [12] **Dhaundiyal, A., Bercesi, G., Atsu, D., & Toth, L.:** (2021). Development of a small-scale reactor for upgraded biofuel pellets. *Renewable Energy*, 170, 1197–1214.
- [13] **Sluiter, A et al.** (2005). Determination of Ash in Biomass (NREL/TP-510-42622). <https://www.nrel.gov/docs/gen/fy08/42622.pdf>
- [14] **Shi, K. Q., Wu, T., Zhao, H. T., Lester, E., & Wang, Y. D.:** (2013). Microwave Induced Co-Processing of Biomass/Coal Blends. *Applied Mechanics and Materials*, 319, 227–232.

SOIL STRENGTH AND LOAD BEARING CAPACITY MEASUREMENT TECHNIQUES

Author(s):

A. E. Eltayeb Ahmed¹, A. El Hariri¹, P. Kiss²

Affiliation:

¹ Mechanical Engineering Doctoral School – Hungarian University of Agriculture and Life Sciences, 2100 Gödöllő, Páter Károly u. 1., Hungary;

² Institute of Technology - Hungarian University of Agriculture and Life Sciences, 2100 Gödöllő, Páter Károly u. 1., Hungary;

Email address:

Ahmed.Ahmed.Elawad.Eltayeb@phd.uni-mate.hu; El.hariri.alaa.2@phd.uni-mate.hu; Kiss.peter@uni-mate.hu

Abstract: In this research, the interest will be given to studying the load bearing capacity and strength of soil terrain, resulting from machine-soil interaction. A small introduction will define terramechanics studies and its importance when dealing with machine-terrain interaction. The axial load acting on a terrain will lead to the sinkage of the machine, thus considering this load will help in studying the load bearing capacity of the soil and ending up with results that are beneficial to terramechanics studies, so improvement in the machine design or choosing the suitable machine for specific terrain. This review shows the studies and models that researchers obtained and dealt with regarding the load bearing capacity. The techniques and the measurements used in finding the load bearing capacity of soil will be explained (Bevamer, Cone penetrometer).

Keywords: Load bearing capacity; Vehicle-terrain interaction; Bevamer; Cone penetrometer; Terrain; Soil pressure-sinkage; Terrain properties; Soil strength

1. Introduction

Off-road vehicles are used in many worldwide fields such as agricultural, construction, cross-country transportation, and also in military missions. Scientists have made heavy endeavours through the history in the fields of agriculture, logging, construction, mining, exploration, recreation, and military operations aiming to study locomotion over unprepared terrain.

Designing off-road vehicles and studying their interaction with the terrain have attracted many researcher's interests.

Studying the performance of an off-road vehicle on a terrain has become known as "Terramechanics". Terramechanics plays an important role in the development and evaluation of off-road equipments to be used on a specific terrain.

Over the years variety of methods of approach for studying off-road vehicles mobility have been developed including empirical methods, computational methods and methods for parametric analysis (Wong, 2010).

The forces and moments between the machine and the ground reflect the performance of the vehicle (Taheri, et al., 2015). So, the mobility of the vehicle and its dynamical performance are determined by the terrain-soil interaction during operation (Shibly & Iagnemma, 2005).

Terrain-vehicle machines provide guiding principles to understand better the soil-vehicle interaction. Most frequent problems faced during soil-machine interaction are encountered in the categories of excessive soil compaction, excessive wheel or track sinkage due to ground pressure, physical characteristics of both soil and vehicle, excessive wheel or tracks slippage and insufficient traction resulting from internal soil shear or surface friction failure (Yong et al., 1984).

Terrains mechanical properties are divided into two directions: the normal (load bearing capacity; pressure-sinkage relationship equations) and the tangential (shear load; shear-slippage relationship equations) (Bekker, 1969).

Normal load applied by the wheel on the terrain will compact the soil (reduction of soil pores volume), thus the wheel sinks until soil produces resistance load opposing the sinkage (is the load bearing capacity). The soil resistance to the wheel normal load is directly affected by the two soil parameters: cohesiveness (bonding of soil particles) and angle of internal friction (resistance of movement between soil particles), thus the soil resistance is influenced by the soil density, shear strength, and the load coming from the vehicle (Meirion-Griffith & Spenko, 2014).

Classifying the soil from its colour detected using a colour technique will help in determining the attributes of the (soil), so documenting differences between different soil types and their structures. Specifying the color of the soil would greatly help in avoiding overloading the soil beyond its capacity, so preventing soil compaction and other degradation factors.

The forces and moments acting at the interaction level are proportional to operating factors as slip ratio, slip angle, normal load, and tyre inflation pressure.

The pressure (stresses) at the contact part cause geometrical and mechanical changes in the tyre and the terrain as changing in the tyre belt deformation, soil sinkage, soil deformation, erosion, and particle's movement.

Mechanical changes in the tyre and the terrain occur upon interaction (bulk density, compaction, water content).

The deformable terrains in off-road scenarios increase the complexity of modelling the cases at the contact zone (Gallrein & Bäcker, 2007). For simplifying this interaction majority of terramechanics models make certain prior assumptions. These simplifications depend on the model's applicability and necessitates computational and experimental resources (Gipser, 2007).

2. The Structure and the Strength of the Soil

The soil is divided into two main types: cohesive and a frictional type; In general soils are combination of both friction and cohesive (Inns & Kilgour, 1978).

Cohesive forces depend on soil moisture suction rather than soil moisture content (Earl, 1996). Friction is the resistance between the soil particles when sliding over each other (Increase with the increase in the number of particles contacts per unit volume) (Dumbleton & West, 1970). The increase in soil bulk-density will increase the soil friction (Godwin et al., 1991).

Figure 1. shows the Mohr-Coulomb diagrams of the three soil classes are:

- a- Pure cohesive soil and possess only a cohesive (non-frictional) strength component; the water-saturated clay is an example of it.
- b- Pure frictional soil and has only frictional (zero cohesion) strength component; the dry sand is an example of this kind.
- c- Cohesive-frictional soil class and contains both cohesive and frictional strength components; the saturated clays, loams, and sands are examples of this soil class.

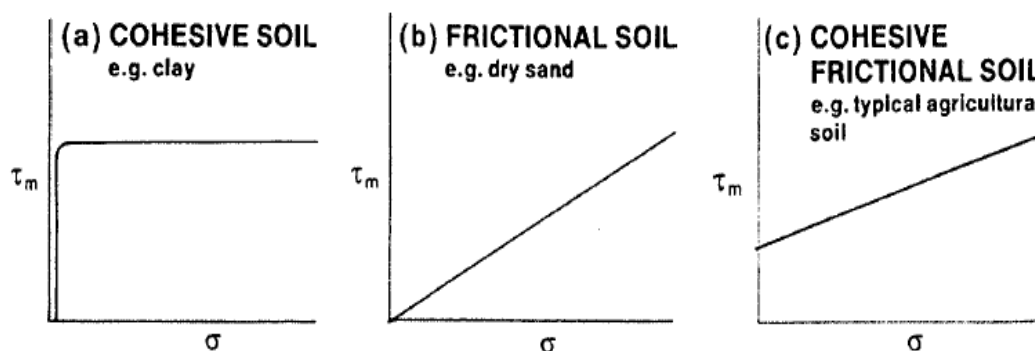


Figure 1. Graphs showing the strength of different soil types (Inns & Kilgour, 1978).

Freitag reported that it is important to consider the tractive performance on the three different soil classes (cohesive, frictional, cohesive-frictional) (Freitag, 1965).

2.1. Distribution of the Applied Load Stresses in the Terrain

The terrain under the vehicle is modelled as either elastic medium or as a rigid, perfectly plastic material (Wong, 2010). The elastic behaviour of a material is its tendency to return back to its original geometry, but when the material enters the plastic region then it is permanently deformed and will not return back to its initial geometry when removing the exerted load. The two regions are shown in the stress strain diagram shown in Figure 2.

The elasticity theory leads to the development of most theoretical investigations dealing with dense soil (for the limitation of need exceeding load bearing capacity the plastic theory reflect the soil failure) (Taghavifar & Mardani, 2017).

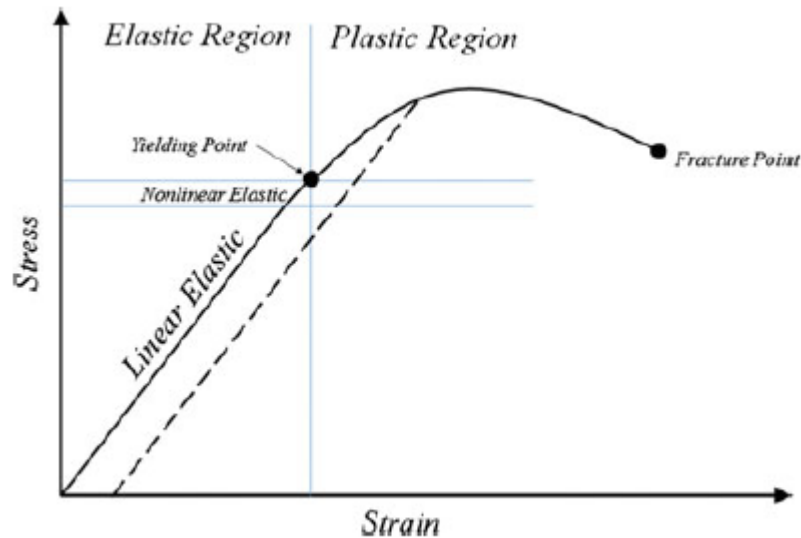


Figure 2. Soil Stress-Strain curve showing the elastic and plastic regions (Taghavifar & Mardani, 2017).

2.2. Moisture Content

The moisture is a component present in the soil structure, and that is based on the soil's three phase-system (minerals, moisture, and air). The moisture affects the characteristics of the soil such as consistency, compatibility, cracking, swelling, shrinkage, and the density.

Determining the water content in the soil is important in agriculture, mechanical, geotechnical, hydrological, and environmental engineering since moisture has impact on the soil's characteristics (Susha et al., 2014).

3. Load Bearing Capacity Measurement Techniques

Bevameter and cone penetrometer are two techniques that are used for measuring the terrain properties. Specifying which technique will be used depends on the type of vehicle used on the terrain, as an example for that the technique used in military vehicles is much different than the technique required by normal non-military vehicles. Selecting the suitable technique among both depends on the method of approaching the purpose. In case a technique is required by an off-road vehicle engineer in the development of new products, then the targeted technique is much different than the technique used for military vehicle trafficking on a go/no go basis (Wong, 2010).

3.1. Cone penetrometer Technique

This technique was initially used by the US army Engineer for evaluating the strength of soil (Freitag, 1966). In agricultural field the cone penetrometer is standardized as ASAE S313.2; by following the standard, the findings are compared to the standardized data (Figure 3.).

The index application range, penetration speed, and the depth increment for various penetrometer types are defined by the ASAE standard.

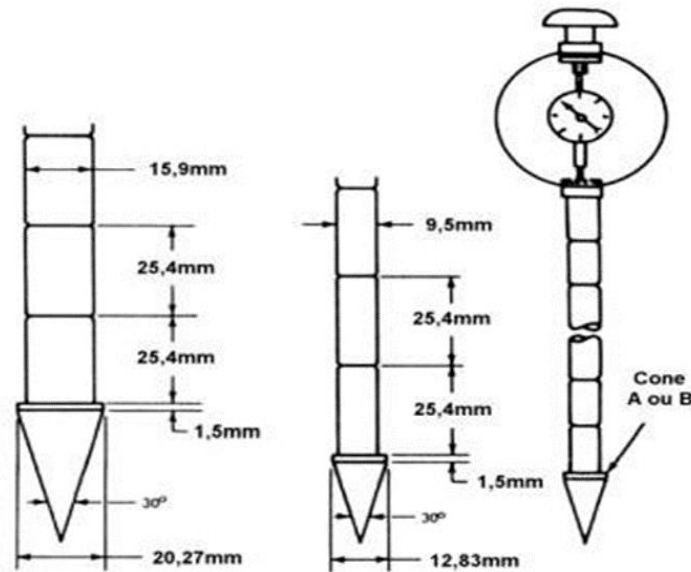


Figure 3. ASAE S313.2 Standardized cone penetrometer (Wong, 2010).

The value obtained from the cone penetrometer test is the cone index. This value indicates the average penetration force and is the force exerted by the soil against the conical head per unit projected cone base. The soil is penetrated by the cone to a given depth at a rate 3 cm/sec (suggested by ASAE). The value (cone index) is a composite value embedding the impact of shear, compression, and even soil metal friction (ASAE, 1988).

The CI (cone index) varies depending on the depth, so averaging of the CI values taken at different depths corresponding to the track or tyre sinkage will help in predicting the traction (Wismer & Luth, 1973).

The remoulding index (RI) is a value that measures the change in the terrain strength resulting from the passage of vehicles over terrains (recurrent activity). RI is the ratio of the soil's cone index after remoulding to that before remoulding (CI before). Regarding the remoulding test in case of fine-grained soils 100 blows of 1.135 kg (2.5 lb) hammer dropped from height 30.5 cm (12 in) on the soil sample in the remoulding cylinder, and in case of having coarse grained with fines soil type the hammer is dropped on the soil cylinder 25 times from 15.2 cm (6 in) height (SAE, 1967).

The RCI value-rating cone index-is the product of the remoulding index (RI) and the cone index (CI) before remoulding. The RCI shows the strength of terrain under repeated vehicle passage on it. In addition to this value there is the vehicle cone index, a value indicating trafficability and is the minimum soil CI at the critical layer level that allows the vehicle to move without getting immobilized. Considering the depth of the critical layer is dependent of the vehicle and its weight (Wong, 2010).

The cone index was calculated in term of terrain's angle of internal shearing resistance, cohesion, density, apparent shear modulus, and the cone shape and penetration depth (Rohani & Baladi, 1981).

An equation was developed by Hettiaratchi and Liang for the load acting on the cone or on a wedge-shape indenter. The equation was as function of the cone or wedge geometry, penetration depth, angle of internal shearing resistance, and terrain cohesion (Hettiaratchi & Liang, 1987).

The Cone index (CI), Remoulding index (RI), Rating cone index (RCI), Vehicle cone index (VCI), and slope index are values obtained by the penetrometer test (Taghavifar & Mardani, 2017).

The depth in the terrain influences the resulting CI value upon implementing the cone penetrometer test, so the CI value utilized for traction prediction is the average value of set of CI values recorded across different depths that correspond to maximum tyre or track sinkage (Wismar & Luth, 1973).

3.2. Bevameter Technique

This technique was developed by Bekker aiming to measure the strength of soil and its sinkage parameters upon being subjected to running wheel. The wheel or the running gear connected to the vehicle applies both the normal load (vertical) and the shear load (tangential stresses) on the terrain. The wheel contacts the terrain, thus transferring the power taken from the transmission to the wheels as tractive forces, so ending with the vehicle's movement.

For simulating the real wheel-terrain contact case through studying the normal and shear loads applied on the terrain, the Bevameter technique is the best among the others (Wong, 2010), (Wong, 2001).

The Bevameter technique (Figure 4.) embeds:

- The plate sinkage test; and it simulates the normal load applied from the running gear on the terrain, thus the pressure sinkage relationship of the soil.
- A shear test ending up with the In-situ shear strength parameters of the soil.

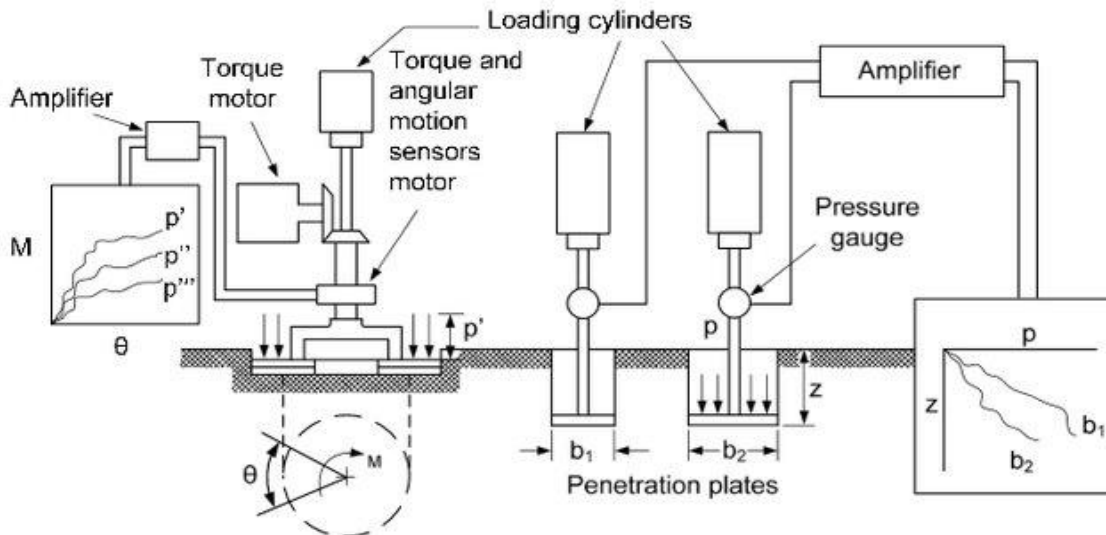


Figure 4. Bevameter schematic diagram (Bekker, 1969).

The shear device of the Bevameter holds an annular groused ring that is applied by a constant vertical load on the terrain, and when contacting the terrain, it is rotated at constant velocity. The torque and angular displacement are recorded for calculating the shear strength.

The normal load (in normal load test) is applied on the sand sample (terrain in reality) using different plates. Different sizes of flat plates are forced into the soil, and the penetration results are then recorded; reaching the load bearing capacity.

The Bevameter is associated with the following parameters: Cohesion (C), Angle of internal friction (ϕ), Sinkage moduli (k, k_c , k_ϕ), Sinkage exponent (n) (Taghavifar & Mardani, 2017).

A custom built Bevameter at NASA Glenn research centre and is able to perform the two tests: the normal and the shear. For the normal test the instrument use a piston to press plate down (load cell measures the force, and a laser is measuring the vertical displacement) (Edwards et al., 2017).

When it comes to shearing the terrain (contact part), the same apparatus used in the normal test is also used for shearing having torque applied and the angular motion is measured by sensors (the resistance to rotation); simultaneously with the normal load applied.

4. Studying the Normal Load Acting on the Terrain

Based on Boussinesq theory in elastic half-space, Saakyan (1965) suggested a pressure sinkage equation (Boussinesq, 1885; Nihal et al 2021).

$$p = k \left(\frac{Z}{D} \right)^n \quad (1)$$

where p is the average pressure under indenter, D is the diameter of the indenter, Z is the vertical soil deformation (sinkage), k is the sinkage modulus.

Bernstein in his field of expertise (agricultural engineering field) has demonstrated that if a plate penetrates soil (normal load) the pressure-sinkage curve arising is represented by the equation.

$$p \cong kz^{0.5} \quad (2)$$

where k is the modulus of inelastic deformation; 0.5 is the sinkage exponent (power); z is the depth (Bekker, 1969; Bernstein, 1913).

Later a Russian researcher adjusted the equation (2) by reducing it to the form.

$$p = kz^n \quad (3)$$

Considering the pressure-sinkage is of a power function form, then the above equation is an applicable equation, where k and n are curve fitting constants obtained experimentally for specific soil type with n ranging from 0 to 1 (represented in Figure 5)

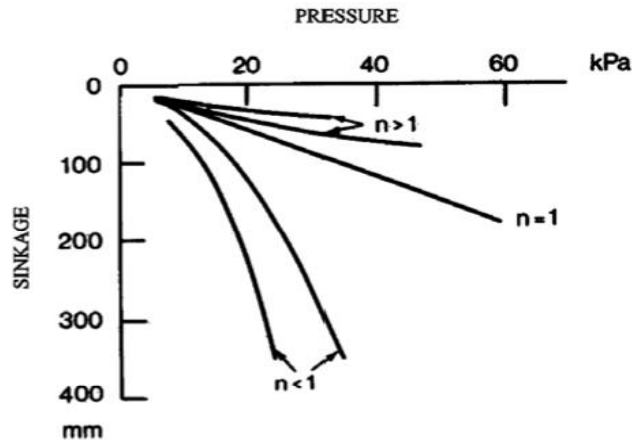


Figure 5. Typical pressure-sinkage curves (Bekker, 1969).

The limitations of this equation is that (k) and (n) are values of a particular soil type despite changing with surface load and the load range (Ageykin, 1973).

The plates used for performing the plate-sinkage experiment are either circular or rectangular considering that the width or the radius of plate influences the measured data (Bekker, 1956).

For homogeneous soil Bekker deduced that the above equation (3) can be reduced to the form:

$$p = \left(\frac{k_c}{b} + k_\phi \right) z^n \quad (4)$$

where b is the width used, k_c the pressure-sinkage parameter due to the cohesive effects, k_ϕ the pressure-sinkage parameter due to the frictional effects, z is the sinkage of the plate, and $n \in IR^*$ is the deformation exponent. (The k_ϕ and k_c values are Independent of n value)

The equation above has shown its ability to measure the soil resistance to penetration over a wide soil range in addition to its ability in predicting trends when there isn't direct experimental data available (Wong, 2001).

In the above equation p and z are measured values, while k_c , k_ϕ and n are derived from the above equation (4).

Later Bekker modified equation 4 by introducing the weight of the vehicle:

$$z = \frac{3W}{\left((3-n)(K_c + bK_\phi) d^2 \right)^{\frac{2}{2n+1}}} \quad (5)$$

where W is the wheel normal load, d is the tyre diameter, and b is the tyre width (Bekker, 1960).

Afterwards Onafeko and Reece mentioned that the pressure-sinkage relation depends on n.

Thus,

$$p = (c\hat{k}_c + \gamma b\hat{k}_\phi) \left(\frac{z}{b} \right)^n \quad (6)$$

where \hat{k}_c , \hat{k}_ϕ , and n are new dimensionless pressure-sinkage parameters, and γ is the specific weight of the terrain (Onafeko & Reece, 1967).

Wong proposed a weighted least squares method to obtain the parameters n, k_c , k_ϕ , \hat{k}_c and \hat{k}_ϕ (Wong, 2010). Thus, minimizing the function using a weighting Factor p^2

$$F = \sum p^2 [\ln p - \ln k_{eq} - n \ln z]^2 \quad (7)$$

Where: $k_{eq} = \frac{k_c}{b} + k_\phi$

Taking two partial derivatives of F (with respect to n and the other with respect to k_{eq}) so, decreasing the values of F.

These two equations appear

$$\ln k_{eq} \sum p^2 \ln z + n \sum p^2 (\ln z)^2 = \sum p^2 \ln p \ln z \quad (8)$$

$$\ln k_{eq} \sum p^2 + n \sum p^2 \ln z = \sum p^2 \ln p \quad (9)$$

Since n depends on the size of the plate it is required to use an average n-value resulting from two different plates when calculating $\ln k_{eq}$. The usage of two different plates will result in two k_{eq} values (for b_1 and b_2 plates sizes).

The following equations can be used for determining k_c and k_ϕ .

$$k_c = \frac{(k_{eq})_{b_1} - (k_{eq})_{b_2}}{b_2 - b_1} b_1 b_2 \quad (10)$$

$$k_\phi = (k_{eq})_{b_1} - \frac{(k_{eq})_{b_1} - (k_{eq})_{b_2}}{b_2 - b_1} b_2 \quad (11)$$

Wong defined the error between the experimental and theoretical data by developing a method known as “Goodness-of-fit” equation. This equation is the ratio of the mean square error to the mean value of pressure.

$$\varepsilon = 1 - \frac{\sqrt{\frac{\sum (p_m - p_{lc})^2}{N - 2}}}{\frac{\sum p_m}{N}} \quad (12)$$

where p_m is the measured pressure, p_{lc} is the calculated pressure (using above procedures), N is the number of data points used for the curve fitting $\varepsilon = 1$ (perfect fit).

The increase in soil resistance is at greater depth since the pressure was not increasing the sinkage, and that results in a hyperbolic pressure-sinkage relation, and that is recognized in Figure 6, showing hyperbolic curves with the increase in the sinkage. Relying on semi-empirical methods for studying the soil behaviour under normal load would be better than extending the theory of elasticity and plasticity (Kougre et al., 1983).

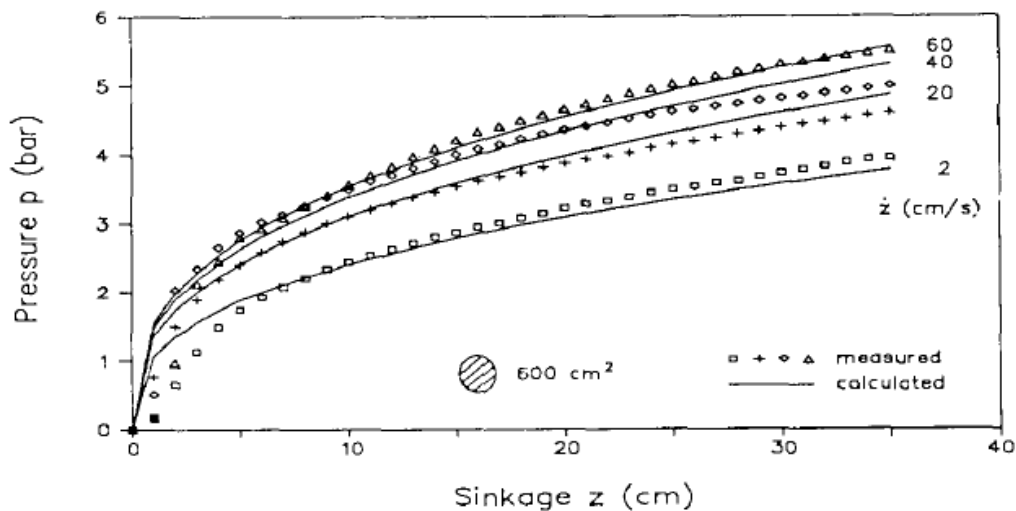


Figure 6. Measured and calculated pressure-sinkage curves (correlation) at different penetration velocities under 500 cm² loading surface (Grahn, 1991).

Emori and Schuring have shown that the force pushing the plate is function of the depth penetration (Z^*), plate velocity (\dot{Z}), and acceleration (\ddot{Z}).

$$F_s = f_1(Z^*) + f_2(Z^*, \dot{Z}) + f_3(Z^*, \ddot{Z}) \quad (13)$$

f_1 is the static force, f_2 is the force resulting from lateral acceleration of soil particle and viscosity, f_3 is the inertial force vertically accelerated soil particles (Emori & Schuring, 1966).

The soil sinkage was smaller at higher penetration velocities and the modulus of soil deformation in Bekker's equation was equal to $(K_0 \dot{Z}^m)$ where (\dot{Z}) is the vertical velocity, (K_0) is static modulus of soil deformation and (m) is the exponent of soil penetration.

$$p = K_0 \dot{Z}^m Z^n \quad (14)$$

4.1. Influence of the Plate Size and Shape

The plate penetration rate should always emulate the realistic case as in the track or wheel contact area. From a proof it is impossible to apply the load at high rate, because relating the load coming from a vehicle is not applied at high rate (major cases). Altering Bekker and Reece model resulting in equation (15).

$$p = (K_1 + 0.5bK_2)\beta^n Z^n \quad (15)$$

where β is a geometric constant (depends on plate shape). (Youssef & Ali, 1982).

Using plates that are of same sizes as the contact patch requires an increase in the plate's geometry with sinkage, also a new diameter would be required to be used in the equation. As a result of that Meirion-Griffith and Spenko worked on the effect of wheel diameter change on pressure sinkage.

Bekker model was modified to

$$p = \hat{K} z^{\hat{n}} D^{\hat{m}} \quad (16)$$

where D is the diameter, \hat{K} is the proposed sinkage modulus ($\text{kN}/\text{m}^{\hat{n}+\hat{m}+2}$), \hat{n} is the proposed sinkage exponent, D is the wheel diameter, and \hat{m} is the diameter exponent. (Meirion-Griffith & Spenko, 2011).

The effect of the wheel width on sinkage was later used plus considering the effect of diameter.

$$z_0 = \frac{3W}{b(3 - \hat{n})\hat{k} \left(b\sqrt{Dz_0 - z_0^2} \right)^{m+0.5}} \quad (17)$$

W is the normal load from the wheel and z_0 is now a function of itself and cannot be separated. Such equation has no closed form solution. However, if every possible value of z_0 inside the length function is plotted against the solution for z_0 it can be seen that the two converge only once for sinkages less than the wheel radius, and yielding the correct solution (Meirion-Griffith & Spenko, 2013).

It is important to have proper and accurate prediction of the contact patch stresses, in addition to specifying the wheel load, tyre inflation pressure, recommended tyre inflation pressure, tyre width and diameter as input data to the soil compaction models increasing the accuracy of soil stress and compaction. (Keller, 2005).

Giving consideration to the pressure sinkage rate, Pope assumed that this relation fit as power law forming (Pope, 1969):

$$p = p_0 \left(\frac{u}{u_0} \right)^m \quad (18)$$

Using Reece model, the new equation is;

$$p = (ck_c + \gamma bk_\phi) \left(\frac{z}{b} \right)^n \left(\frac{u}{u_0} \right)^m \quad (19)$$

u is the sinkage velocity, u_0 is the plate sinkage; m , n sinkage exponent.

It is important to note that an inclined load applied on a horizontal plate leads to more sinkage when compared to having the same load applied normally on the same plate. The sinkage of an inclined plate under an inclined load is less than the sinkage upon having vertical load applied on an inclined plate. (Xuewu et al, 1996).

5. Bevameter test at the University Laboratory

A bevameter test was carried out at the Hungarian University of Agriculture and Life Sciences laboratory. The bevameter used is shown in the Figure 7 and of a pressing plate diameter 20 cm. The load (normal load of increasing value) was applied using hydraulic force to press down the loam sand soil; loads were measured using a load cell and provided to the computer. Upon having the plate sinking the longitudinal deformation was also recorded using a displacement sensor and provided to the computer through the data logger. The results (load and displacement) recorded by the computer using the Catman 4.5 software, the results are shown in graphs plotted using excel as in Figure 8; of the soil at different moisture contents (0%, 10%, 20%).



Figure 7. Bevameter test at the university laboratory testing the loam sand soil at different moisture contents

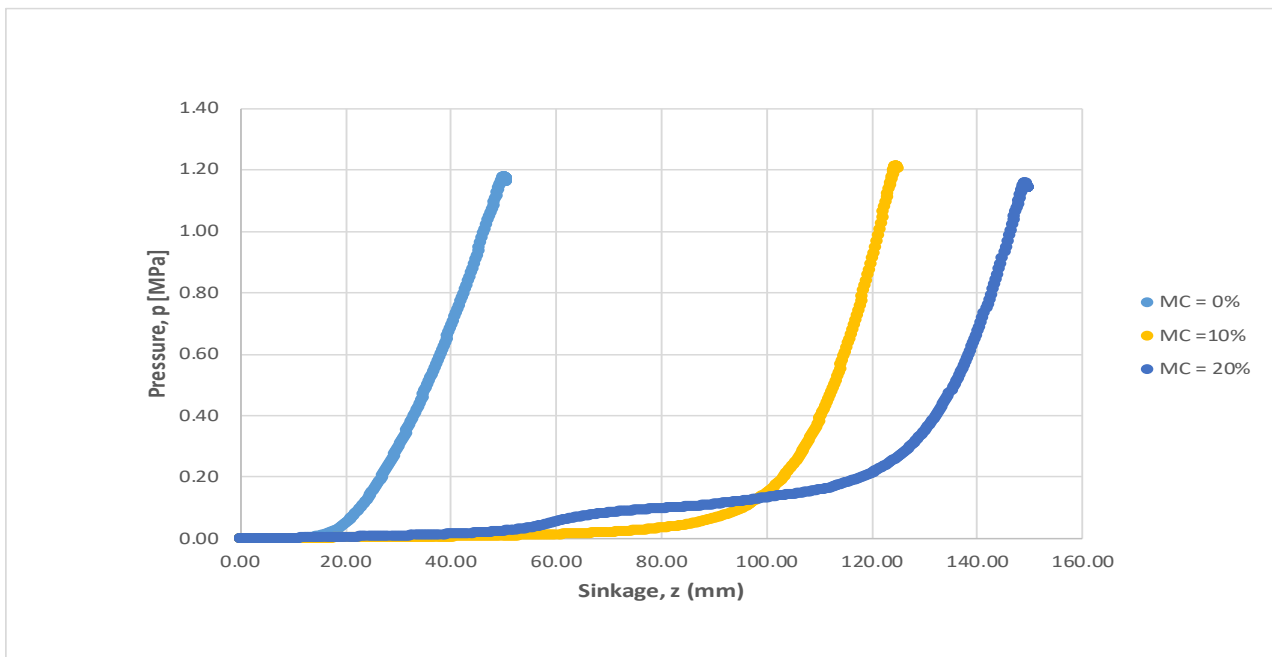


Figure 8. Pressure-sinkage curves at different moisture contents (0%, 10%, 20%) under plate size (D = 20 cm)

6. Numerical methods

The finite and discrete element methods are practical tools used for analysing complicated systems. These methods have been used in terramechanics modelling since 1970s and the popularity of using these methods continued to increase due to providing improved computational results (Wong, 2001).

Finite element method was used to study the potential self-excitation of wheeled-vehicles operating on soft soil. The discrete element method terramechanics is able to deal with complex effects arising during traversal through rough terrains by modelling the individual grain particles (Smith & Peng, 2013).

7. Conclusion

Many fields (agricultural, military...) require enhancements in the vehicles used and if not enhancing, choosing the suitable vehicle for the specified mission might be helpful in accomplishing it. The load bearing capacity will help in this enhancement by measuring the normal interaction between the vehicle and the terrain. The Bevameter and the cone penetrometer have facilitated measuring the resulting load bearing capacity between the vehicle and the terrain.

The cone penetrometer results with index value that is used for deducing many properties regarding the interaction, and the other technique (Bevameter) helps in measuring the normal displacement upon having normal load pressing on the terrain having at the same time the displacement being measured with the sinkage, so the resulting curve will help in studying the bearing capacity of the terrain.

Studying this normal load based on the equations and models proved by researchers, and by linking these models accurate study of the load bearing capacity as mentioned in the section (4) will be reached, in addition to considering the change in the wheel diameter, width, and tyre inflation on the load result and the geometry of the track in case of tracked vehicles.

Based on our experimental test made on loam sand soil, it has appeared that with the increase in the amount of moisture content present in the soil, the sinkage of the Bevameter plate increased upon applying the same load. So, we can deduce that the bearing capacity of the soil decreases with the increase in the moisture content. In reality this deduction is recognized when having a vehicle moving on wet soil (of the used type), that the increase in the amount of water in soil (wet soil) leads to the sinkage of the vehicle. We should also consider that on dry soil types (dry sand soil) the behaviour will be the opposite, where the increase in moisture content will increase the traction and the load bearing capacity of the soil.

Finally, even though using the Bevameter and the cone penetrometer techniques end up with beneficial results, in case of dealing with complicated cases (complicated interaction flow) numerical methods might be helpful in solving these cases by having these methods emulating the real interaction, such as using the finite element method or the discrete element method (studying the motion at the particle level).

Acknowledgement

This work was accomplished by the help of the Mechanical Engineering Doctoral School at the Hungarian University of Agriculture and Life Sciences, Gödöllő, Hungary. Also, we would like to thank The Stipendium Hungaricum foundation for funding our Ph.D. program.

References

- [1] **Ageykin, Y. S.** (1973). Evaluation of ground deformability with respect to vehicle mobility. *Journal of Terramechanics*, 10 (1), 105–111.
- [2] **Bekker, M.**, (1956). *Theory of Land Locomotion: The Mechanics of Vehicle Mobility*. University of Michigan Press, Ann Arbor, MI.
- [3] **Bekker, G.**, (1960). *Off-road Locomotion*. University of Michigan Press, Ann Arbor, MI.
- [4] **Bekker, M. G.** (1969). *Introduction to terrain-vehicle systems*. University of Michigan Press; First Edition edition (March 1, 1969).
- [5] **Bernstein, R.** (1913). Probleme zur experimentellen Motorpflugmechanik. *Der Motorwagen*, 16(9), 199–206.
- [6] **Boussinesq, J.**: Application des potentials a l'etude de l'equilibre et due mouvement des solides elastique, Gauthier-Villars, Paris, 1885. [Google Scholar](#).
- [7] **Dumbleton, M. J., & West, G.** (1970). the suction and strength of reivoloulded soils. Berkshire.

- [8] Earl, R. (1996). Prediction of Trafficability and Workability using Tensiometers. *Journal of Agricultural Engineering Research*, 63(1), 27–33. <https://doi.org/10.1006/jaer.1996.0004>.
- [9] Edwards, M. B., Dewoolkar, M. M., Huston, D. R., & Creager, C. (2017). Bevameter testing on simulant Fillite for planetary rover mobility applications. *Journal of Terramechanics*, 70, 13–26. <https://doi.org/10.1016/j.jterra.2016.10.004>.
- [10] Emori, R., & Schuring, D. (1966). static and dynamic penetration test of soil. *Journal of Terramechanics*, 3(1), 23–30.
- [11] Freitag D.R., (1965), Wheels on soft soils, an analysis of existing data. Technical Report No. 3-670 USAE Waterways Experiment Station.
- [12] Freitag, D. R. (1966). A dimensional analysis of the performance of pneumatics tires on clay. *Journal of Terramechanics*, 3(3), 51–68. [https://doi.org/10.1016/0022-4898\(66\)90106-6](https://doi.org/10.1016/0022-4898(66)90106-6).
- [13] Gallrein, A., & Bäcker, M. (2007). CD Tire: a tire model for comfort and durability applications. *Vehicle System Dynamics*, 45 (sup1), 69–77. <https://doi.org/10.1080/00423110801931771>.
- [14] Gipser, M. (2007). FTire – the tire simulation model for all applications related to vehicle dynamics. *Vehicle System Dynamics*, 45 (sup1), 139–151. <https://doi.org/10.1080/00423110801899960>.
- [15] Godwin, R. J., Warner, N. L., & Smith, D. L. O. (1991). The development of a dynamic drop-cone device for the assessment of soil strength and the effects of machinery traffic. *Journal of Agricultural Engineering Research*, 48(C), 123–131. [https://doi.org/10.1016/0021-8634\(91\)80009-4](https://doi.org/10.1016/0021-8634(91)80009-4).
- [16] Grahn, M. (1991). Prediction of sinkage and rolling resistance for off-the-road vehicles considering penetration velocity. *Journal of Terramechanics*, 28 (4), 339–347. [https://doi.org/10.1016/0022-4898\(91\)90015-X](https://doi.org/10.1016/0022-4898(91)90015-X).
- [17] Griffith, G. M., & Spenko, M. (2014). Simulation and experimental validation of a modified terramechanics model for small-wheeled vehicles. *International Journal of Vehicle Design*, 64(2/3/4), 153. doi:10.1504/ijvd.2014.058499.
- [18] Hettiaratchi, D. R. P., & Liang, Y. (1987). Nomograms for the estimation of soil strength from indentation tests. *Journal of Terramechanics*, 24 (3), 187–198. [https://doi.org/10.1016/0022-4898\(87\)90040-1](https://doi.org/10.1016/0022-4898(87)90040-1).
- [19] Inns, F. M., & Kilgour, J. (1978). *Agricultural tyres*. London: Dunlop. Retrieved from http://books.google.co.uk/books/about/Agricultural_tyres.html?id=JB8NAQAAMAAJ&pgis=1.
- [20] Keller, T. (2005). A Model for the prediction of the contact area and the distribution of vertical stress below agricultural tyres from readily available tyre parameters. *Biosystems Engineering*, 92 (1), 85–96. <https://doi.org/10.1016/j.biosystemseng.2005.05.012>.
- [21] Kogure, K., Ohira, Y., & Yamaguchi, H. (1983). Prediction of sinkage and motion resistance of a tracked vehicle using plate penetration test. *Journal of Terramechanics*, 20 (3–4), 121–128. [https://doi.org/10.1016/0022-4898\(83\)90043-5](https://doi.org/10.1016/0022-4898(83)90043-5).
- [22] Meirion-Griffith, G., & Spenko, M. (2011). A modified pressure-sinkage model for small, rigid wheels on deformable terrains. *Journal of Terramechanics*, 48 (2), 149–155. <https://doi.org/10.1016/j.jterra.2011.01.001>.
- [23] Meirion-Griffith, G., & Spenko, M. (2013). A pressure-sinkage model for small-diameter wheels on compactive, deformable terrain. *Journal of Terramechanics*, 50 (1), 37–44. <https://doi.org/10.1016/j.jterra.2012.05.003>.
- [24] Onafeko, O., & Reece, A. R. (1967). Soil stress and deformation beneath rigid wheels. *Journal of Terramechanics*, 59 (1), 59–80.
- [25] Pope, R. G. (1969). The effect of sinkage rate on pressure sinkage relationships and rolling resistance in real and artificial clays. *Journal of Terramechanics*, 6 (4), 31–38. [https://doi.org/10.1016/0022-4898\(69\)90015-9](https://doi.org/10.1016/0022-4898(69)90015-9).
- [26] Rohani, B., & Baladi, G. Y. (1981). Correlation of mobility cone index with fundamental engineering properties of soil. U. S. Army Grgnee Watewy xprmn Station. Vicksburg.
- [27] SAE. (1967). *Off-road Vehicle Mobility Evaluation*. S.A.E.
- [28] Salman, N.D.; Pillinger, G.; Hanon, M.M.; Kiss, P. (2021) A Modified Pressure–Sinkage Model for Studying the Effect of a Hard Layer in Sandy Loam Soil. *Appl. Sci.* 2021,11, 5499. <https://doi.org/10.3390/app11125499>.

- [29] Shibly, H., & Iagnemma, K. (2005). An equivalent soil mechanics formulation for rigid wheels in deformable terrain , with application to planetary exploration rovers, 42, 1–13. <https://doi.org/10.1016/j.jterra.2004.05.002>.
- [30] Smith, W., & Peng, H. (2013). Modeling of wheel-soil interaction over rough terrain using the discrete element method. Journal of Terramechanics, 50 (5–6), 277–287. <https://doi.org/10.1016/j.jterra.2013.09.002>.
- [31] Susha Lekshmi S.U., D.N. Singh, Maryam Shojaei Baghini, (2014) A critical review of soil moisture measurement, Measurement, Volume 54, 2014, Pages 92-105, <https://doi.org/10.1016/j.measurement.2014.04.007>.
- [32] Saakyan, S. (1965) ‘Soil resistance under load’, Szbornyik trudov po zeml, Vol. 3, pp.24–31.
- [33] Taghavifar, H., & Mardani, A. (2017). Off-road Vehicle Dynamics (Vol. 70). Switzerland: Springer International Publishing. <https://doi.org/10.1007/978-3-319-42520-7>.
- [34] Taheri, S., Sandu, C., & Taheri, S. (2014). Finite Element Modeling of Tire Transient Characteristics in Dynamic Maneuvers. SAE International Journal of Passenger Cars - Mechanical Systems, 7 (1), 2014-01–0858. <https://doi.org/10.4271/2014-01-0858>.
- [35] Wismer, R. D., & Luth, H. J. (1973). Off-road traction prediction for wheeled vehicles. Journal of Terramechanics, 10 (2), 49–61. [https://doi.org/10.1016/0022-4898\(73\)90014-1](https://doi.org/10.1016/0022-4898(73)90014-1).
- [36] Wong, J. Y. (2001). Theory of Ground Vehicles (Third). Canada: JOHN WILY and SONS.
- [37] Wong, J. Y. (2010). Terramechanics and Off-Road Vehicle Engineering (Second). Oxford, UK: Elsevier Ltd. <https://doi.org/10.1016/C2009-0-00403-6>.
- [38] Xuewu, J., Jide, Z., & Xiding, Q. (1996). Effects of loading patterns on the pressure-sinkage relation of dry loose sand. Journal of Terramechanics, 33 (1), 13–20. [https://doi.org/10.1016/0022-4898\(96\)00005-5](https://doi.org/10.1016/0022-4898(96)00005-5).
- [39] Yong, R. N., Fattah, E. A., & Skiadas, N. (1984). Vehicle Traction Mechanics. Amsterdam: Elsevier Science.
- [40] Youssef, A.-F. A., & Ali, G. A. (1982). Determination of Soil Parameters using Plate Test. Journal of Terramechanics, 19 (2), 129–147. [https://doi.org/10.1016/0022-4898\(82\)90016-7](https://doi.org/10.1016/0022-4898(82)90016-7).



THE MAIN INFLUENCING FACTORS OF MOBILE BANKING ADOPTION IN THE OPEN INNOVATION BUSINESS ENVIRONMENT (CASE STUDY)

Author(s):

T. Atobishi¹, M. Bahna¹, Cs. Fogarassy²

Affiliation:

¹ Doctoral School of Management and Business Administration – Hungarian University of Agriculture and Life Sciences, 2100 Gödöllő, Páter Károly u. 1., Hungary;

² Institute of Agriculture and Food Economics - Hungarian University of Agriculture and Life Sciences, 2100 Gödöllő, Páter Károly u. 1., Hungary;

Email address:

thabet.tubashi@moj.gov.jo; miriam.bahna@phd.uni-mate.hu; fogarassy.csaba@uni-mate.hu

Abstract: Mobile banking is a mobile commerce application that is revolutionizing financial services. Accepting and using a virtual system is not easy for users, either technologically or emotionally. The purpose of this research is to find out the effects of "Effect of Risk Perception", "Perceived Ease of Use" and "Perceived Usefulness of Mobile Banking" on mobile banking attitude and adoption. For this study, data was collected in 2019 from N=220 participants using 19 items of five Likert-type questionnaires. The data was analyzed using Statistical Package for Social Sciences and Regression Analysis through the enter method was used. It was found out that there is a positive significant effect of perceived ease of use and perceived usefulness of mobile banking on mobile banking attitude. The results also showed, that attitude towards switching to mobile banking has a positive significant effect on the intentions of mobile banking adoption. It can be concluded that the perceived ease of use of mobile banking will have a significant impact on attitudes towards switching to mobile banking services. The results of the research show that the perceived risk has a significant effect on the mobile. Also, for the practitioners it is very important to take into consideration these results to promote the usage of mobile banking among the customers in Jordan. Our research results also show similarities and differences from previous research results, confirming the unique characteristics of the rapidly developing Arab region. User behavior related to mobile banking is shaped by the combined effect of custom and culture. Mobile banking services may be a very efficient and cost-effective tool in the future, accelerating industry development processes.

Keywords: mobile banking; technology adoption; consumer behavior; technology acceptance; banking service; perceived usefulness; behavior intention; mobile platforms

1. Introduction

Electronic banking is a huge step in the field of finance [1]. It can be a useful tool for the banks to improve their relations with the customers through enhancing the customer loyalty, affective commitment and the satisfaction [2]. Although still mobile banking started adoption from only 1999 and now everyone uses mobile banking to make transactions and to send and receive payments or to purchase products. Mobile banking is "instance of a mobile commerce (commerce) application by which financial institutions enable their customers to carry out banking activities via mobile devices" [3]. In every decade various scientific changes occur similarly now mobile banking is giving ease and enhancing its services everyone is involved either as a user or a service provider [4] mortgage and credit cards play a vital role in influencing the use of electronic banking [5]. However, in research internet banking is further divided into three phases the first is to analysis and to know what is internet banking also known as descriptive type, second is to adopt internet banking after understanding it and by using it also known as relational. The third type is comparing two or more types of internet banking to conclude better results and improve this technology in the better way known as comparative [6]. In the very beginning this area was not focused to attain the betterment, but now it is expanding exponentially. The internet banking even introducing few new or improved methods to be used in

the financial and banking sector, such models and theories like TAM (Technology Acceptance Model), Structural Equation Modeling (SEM), Unified Theory of Acceptance and Usage of Technology (UTAUT), Task-Technology Fit (TTF), Initial Trust Model (ITM), diffusion of innovation theory, unified technology acceptance theory and various such theories were presented to improve mobile banking adoption [7]. In Jordan mobile banking services are growing rapidly and the growth rate jumped to 140% in 2012 [8], also the study by Gharaibeh, Arshad, & Gharaibeh [9] showed that only 8% of the banks customers in Jordan have used the mobile banking services and according to the 2019 digital financial country report 79% used the mobile devices to conduct their banking transactions. In the Jordanian economy 44% of the small enterprises would not use the digital financial services in their businesses, also the report assured that Jordan has a fine digital financial services foundation due to its modern ICT infrastructure and adequate regulations (Digital Finance Country Report Jordan, 2019). However, the use of smart phones shows a different picture in the country. According to the report [10] in Jordan mobile banking took over the e-banking and became more popular, but unfortunately the usage of mobile banking (with safety smart phones) is still at low-level and only 2% of adults used mobile banking. The report showed that culture, cost and low technological knowledge level of the customers are the main obstacles for usage of mobile banking services. In this study we empirically tested the major factors affecting the customers' adoption of the mobile service banking in Jordanian market. Our research question was what main factors (risk perception, the perceived easy of using, usefulness and the technology acceptance attitude) influence the use of mobile banking services in the context of mobile phone use in rapidly evolving economic systems.

2. The Technology Acceptance Model (TAM) and other adoptions theoretical concepts

Mobile banking can be defined as "Mobile banking, also referred to as cell phone banking, is the use of mobile terminals such as cell phones and Personal Digital Assistants (PDAs) to access banking networks via the Wireless Application Protocol (WAP)" [11]. Mobile banking is adding a facility for the users it is being used to deploy betterment in business and even in the daily routine. The main advantage of providing mobile banking is to enable the customers to make transactions at any place and time [12].

The adoption of mobile banking is expanding exponentially, it is witnessed that the demand and the user both are increasing in the same ratio. Various applications and products use the internet or mobile banking to increase their sell ratio. In a survey, it was reported that eighty percent of people are now using their mobile banking, and it is increased sixty percent as compared with previous years [13]. The significant increase in the use of mobile banking needs a comparatively strong architect to design the models for mobile banking and to be adopted as well. In terms of financial usage, automated teller machines known as ATM were used widely from last decade and give growth to internet banking [14]. However, the current era is dealing with mobile adoption as the use of mobile is increased exponentially similarly mobile banking is increased as it saves the time in transactions and it is also a secure method to transfer or to withdraw amount or to purchase products [15]. In other fast developing countries, for example the statistics from Malaysia show enormosity of smart mobiles usage which reported that 65% of population of Malaysia owns mobile phones [16]. A study by Alalwan, Dwivedi, Rana, & Williams [8] about consumer adoption of mobile banking in Jordan showed that perceived usefulness, perceived ease of use and perceived risk are significantly influence the behavioral intention to use mobile banking. Furthermore, this leads the innovation models, to tackle mobile adoption in the banking sector and integrate the innovative tools to emerging technology in one place [17]. While discussing the innovation models the previous methods have limited prediction power to tackle innovative technical change in the field of internet banking, to relate cross co-relation [18].

TAM (Technology Acceptance Model) was an effective model used to predict the new information and the adoption in the new information of the technologies. The proposed TAM (Technology Acceptance Model) process is shown in the Figure 1.

It is one of the most used models at individualistic level and has been proved in term of validity by many studies [20], [21], [22]

Basically, it was based on the model Theory of Reasoned Action (TRA) and later on it was improved and the new model was known as TAM [23]. The similarity of TAM with other models is still a part but considered as a better solution than other models. As TAM is based on TRA the basic aim of the developing this model was to make further predictions, to use with new technical systems [4]. TAM operates to provide benefits given by the information systems and parsimonious, and innovation [24]. The adoption rate basically depends on the five basic things complexity, compatibility, trainability, relative advantage, and observability as this theory is the oldest and known as diffusion of innovation theory. Similarly, the theory of planned

behavior model improves the predictive power [25]. This theory of planned behavior base on attitude, subjective norm, perceived behavioral control, and these three basic modules then processed with intentions and by this behavior is judged. Likewise, like the theory of planned behavior the diffusion of innovation theory explains, what, how, when and why the new mobile adoption and the technology are spreading. This theory explains the process of diffusion is like the innovation communication depends on the time and the users in the social circle [26]. The most complete model Decomposed Theory of Planned Behavior DTPB, known as an improved model and based on the innovation diffusion theory, it is a multidimensional solution and considered as having multi-impact factors in the adoption of the technology. Decomposed Theory of Planned Behavior has two peer constructs peer influence and superior influence [27]. These all theories explain how, when and why the mobile adoption is increasing its use, increasing its popularity, and demand. As the technology is advancing, and changing diversely and adopting new technical changes in mobile banking is already been adopted widely. The excessive number of users now making it hard to remain constant, there is a need to adopt new technical changes and enhance the abilities of mobile banking, the previous models are already performing for what they were developed, but there is a need to improve the models to handle such increased users [28], [29]. The mobile adoption is increased and needs the models to improve and give same and better results for the users. The sudden need to improve models is because of the exponential increase in the users and their requirements according to the current era. So TAM model has been extended or modified by many scholars and these new versions of the TAM model is called TAM++ [30], trust and perceived risk were among the most used factors in extended the TAM model [2].

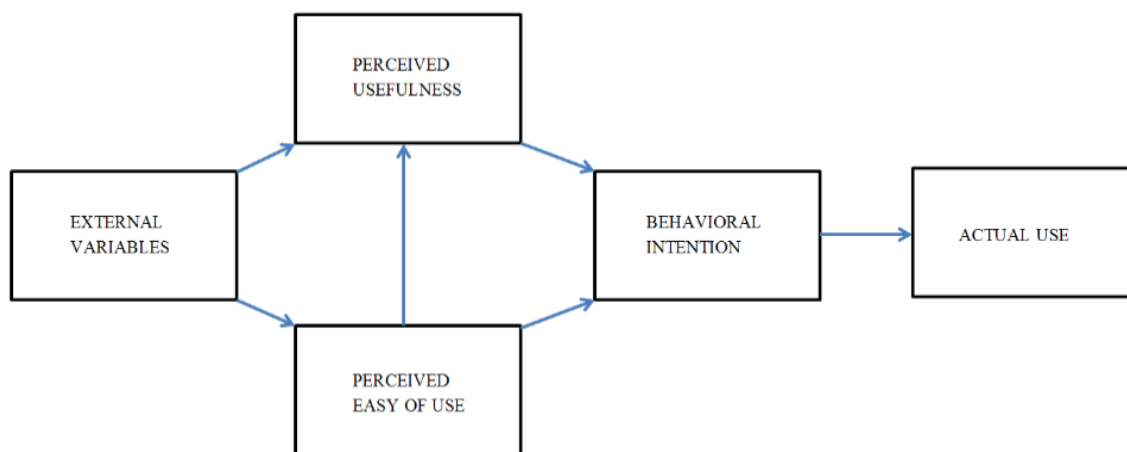


Figure 1. Proposed Technology Acceptance Model (TAM)[[19].

In mobile banking adoption to analyses the current technical aspects as a unified view, the theory of unified acceptance and the use of the technology will be used [31]. To analyze the facilitating condition, performance expectancy, social influence, and effort expectancy, of the mobile banking unified theory of acceptance will perform better than other theories, like TPB (theory of planned behavior), DTPB (decomposed theory of planned behavior), TRA (theory of reasoned action) [32]. Unified theory acceptance is basically a technology acceptance model, this analyzes the unified view, and this theory explains the user intentions to use in the subsequent behavior of the user. To analyze the direct determinants in mobile banking adoption and the user behavior the best theory and the model is a unified theory of acceptance [25]. The improvement in the models and the study can be brought in the field of mobile banking adoption by the unified theory of acceptance [17].

The Unified Theory of Acceptance and Use of Technology (UTAUT) covered various gaps in terms of integration, and in the need of mobile banking adoption to overcome gaps of understanding between the banks and the clients. The UTAUT improved mobile bank services by providing services accordingly, by this perceived risk is reduced [33], [34], [35], [36]. The detailed UTAUT process is shown in the Figure 2. Though the unified theory of acceptance new model was built to improve the mobile banking adoption, previously it was discussed as theory and the practical work was not found. However, after the implementation of the unified theory various perspectives were now overcome but after an exponential increase in the users, various certain and uncertain gaps were still there. The unified theory of acceptance improved the interacting behavior with the clients, by including the emergence of technology, and by

implementing [4],[37]. Previous it was observed that UTAUT was capable of working two different cultural environments like, in the developing country and in a developed country. Similarly, it is concluded that now it is the time to test the UTAUT model that it could be able to tackle such exponential load of users and data. It can be now tested or checked that the UTAUT model still has the power to tackle and to produce the same high results [4].

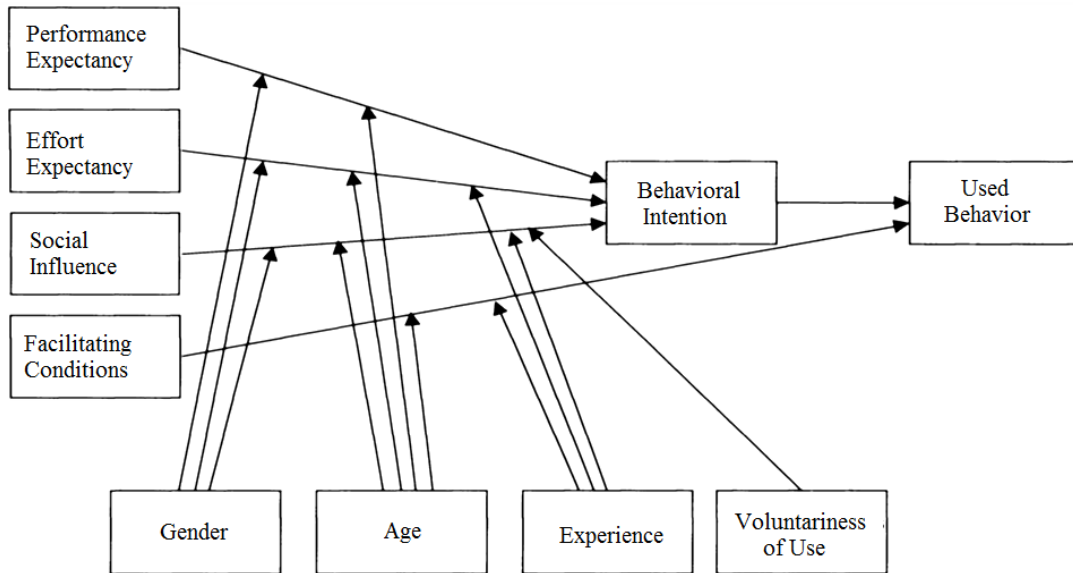


Figure 2. Proposed UTAUT [4].

New research may be conducted to test if UTAUT needs improvements in its model, either there should be a need to improve its predictive power of the UTAUT [38], [39]. The security concerns always appear in the adoption of new technologies especially if it's related to the applications of e-commerce. The perceived risk theory has been used to investigate the consumer's behaviour especially in online purchasing, the perceived risk of online banking can be seen in five dimensions: Security/privacy risk, financial risk, Social risk, Time/convenience risk and Performance risk [40]. According to Featherman and Pavlou [35], perceived risk is can be defined as "the potential for loss in the pursuit of a desired out-come of using an e-service" (Figure 3.).

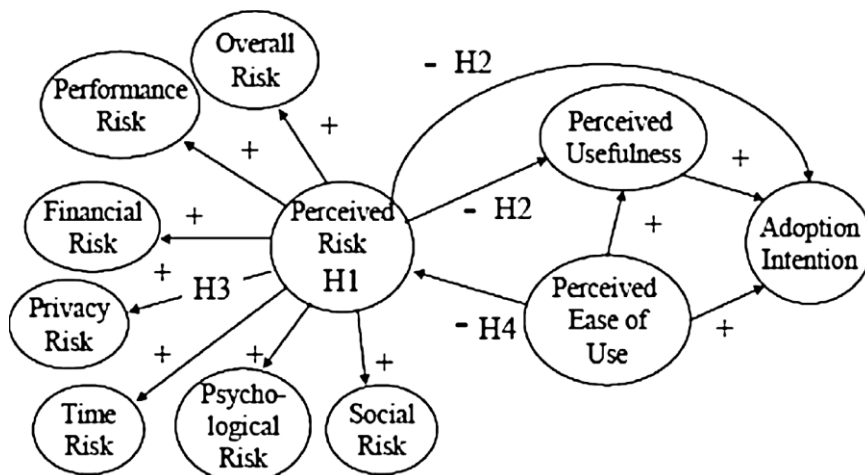


Figure 3. Proposed model based on Featherman & Pavlou [41]

After reviewing the previous studies we propose the following research framework by integrating the TAM model with perceived risk factor. Security (risk perception), perceived ease of use and perceived usefulness were the starting points in the design of the test framework (Figure 4.).

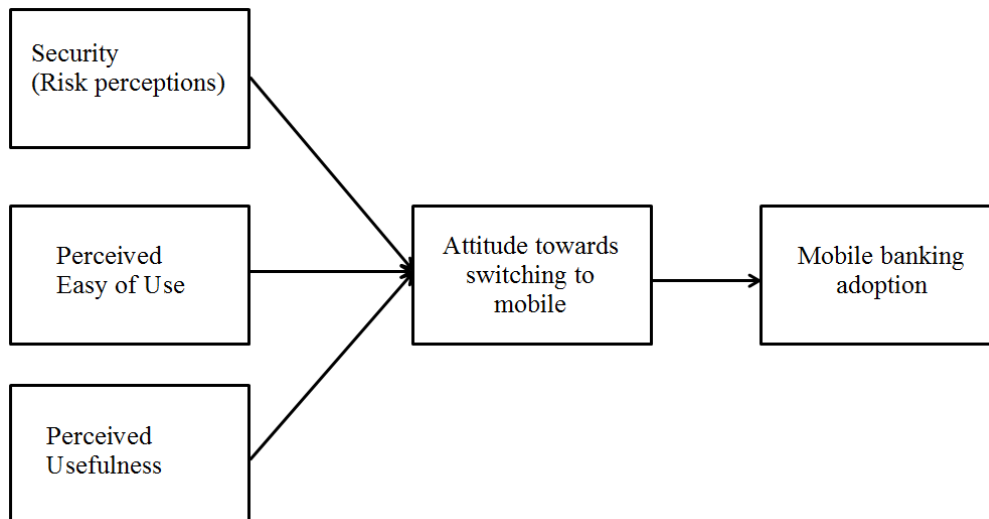


Figure 4. Proposed model to analyze the process (based on own concept)

The risk of using mobile banking services, the perceived ease of use of applications, the usefulness of available services, and changes in usage attitudes may be determinants of changes in the use of mobile banking services. Taking these aspects into account, we developed the following hypotheses:

- H1: In the use of mobile banking services, there is likely to be significant effect of ‘Risk Perception’ of Mobile Banking on Attitude towards switching to mobile banking.
- H2: There is likely to be significant effect of ‘Perceived Ease of Use’ of Mobile Banking on Attitude towards switching to mobile banking in the future.
- H3: There is likely to be significant effect of ‘Perceived Usefulness’ of Mobile Banking on Attitude towards switching to mobile banking, which can make the financial processes of certain economic sectors more efficient.
- H4: The emergence and proliferation of smart devices and phones is likely to be a significant effect of ‘Attitude towards switching to mobile banking’ on Mobile Banking service Adoption.

3. Materials and Methods

The analysis is a quantitative research based on correlational research design. The questionnaire was written in Arabic, and during the compilation of the questionnaire, the previous question sets were synthesized and updated for the study area. In our research, we focused on those banking customers who use banking services on average or above average. In the case of banking services, efficient and fast operation is important to them. The analysis sample number was set to 250 because we planned to ask additional specific questionnaires based on the results. According to the professional team (analytical economist, marketing specialist, computer engineer) participating in the research, the indicated sample number is a suitable basis for analytical purposes.

3.1 Research design

As has been mentioned this is a quantitative research based on correlational research design. Cause and effect relationship of variables were investigated. A questionnaire of 19 itemed Likert-type scale comprised of 5 subscales was designed to get the data. The subscales were; Perceived usefulness, Perceived ease of use, Attitude towards switching to Mobile Banking, Risk Perceptions and Intention to switch to Mobile Banking (Adoption). Each item was responded on range of responses from 1-5 (highly agreed to highly disagreed). Before collection of data, consent form was given that stated the purpose of the research and ensured confidentiality of each participant’s data. Before collection of data, consent form was given that stated the purpose of the research and ensured confidentiality of each participant’s data. The survey was submitted both electronically (by google doc. to their emails) and manually to the target population in the three main cities in Jordan, Amman, Zarqa and Irbid in 2019. We have submitted 250 questionnaire and get back 220 valid ones. The study involved sample of N=220 participants from which n=108 were male and n=112 were female participants who were selected using non-probability, convenient sampling technique. The participants’ age

ranged from 21-70 years. We did not increase the number of participants to over 250 because we planned to establish further research programs.

3.2 Data analysis

Data was collected using a demographic form and a 19 itemed Likert-type scale comprised of 5 subscales. The subscales were: Perceived usefulness, Perceived ease of use, Attitude towards switching to Mobile Banking, Risk Perceptions and Intention to switch to Mobile Banking (Adoption). Each item was responded on range of responses from 1-5 (highly agreed to highly disagreed). Statistical Package for Social Sciences was used to analyse data and to test the hypotheses, regression analysis through enter method was used.

4. Results

In accordance with the aim of our study, we chose quantitative research methods to meet the objectives of the study. A questionnaire based on the presented model was used for the studies. The applied descriptive statistic is a short descriptive coefficient that summarizes a particular set of data, which can be a representation of the entire mobile bank users. Descriptive statistics are broken down into measures of central trend and variability (distribution). Measurements of the central trend include mean, median, and mode, while measurements of variability include standard deviation, variance, minimum, and maximum variables. Following are the results of analyses: Demographics.

The above table shows that the majority of the sample was from age range 31-40 with 40 percentages and there were more female participants than males with 50.9 percentages. (Feedback from other comments indicated that women are more interested in easier use.)

In order to ensure the reliability (Cronbach' Alpha) has been applied on the pilot sample consisting of (50) persons, Table (1) shows that.

Table 1. Descriptive statistics of the analysis

Demographic Variables			
		Frequency	Percent
Gender	Male	108	49.1
	Female	112	50.9
Age	21-30	13	5.9
	31-40	88	40
	41-50	79	35.9
	51-60	35	15.9
	61-70	2	0.90

Table (2) shows that the highest Cronbach' alpha value reached (0.91) for domain (5) "Mobile Banking service Adoption ", then was reach (0.90) for domain (3) "Perceived Usefulness ", and the lowest alpha value was (0.87) for domain (1) "Risk Perception ". But the total alpha values of "study tool " reached (0.99) this indicates to accept reliability. According to the general rules, a very high Cronbach Alpha (above 0.9) contains redundant elements. In our case, the mean value of 0.89 was considered a borderline case.

Table 2. The result of reliability (Cronbach Alpha)

No	Domain	Cronbach Alpha
1	Risk Perception	0.87
2	Perceived Ease of Use	0.88
3	Perceived Usefulness	0.90
4	Attitude towards switching to mobile banking	0.89
5	Mobile Banking service Adoption	0.91
Total study tool		0.89

Table (3) show that correlation Coefficient between (Risk Perception) and (Attitude towards switching to mobile banking) was reach (0.616) by sig (0.000). Correlation Coefficient between (Perceived Ease of Use) and (Attitude towards switching to mobile banking) was reach (0.655) by sig (0.000). Correlation Coefficient between (Perceived Usefulness) and (Attitude towards switching to mobile banking) was reach (0.712) by sig (0.000). Correlation Coefficient between (Mobile Banking services Adoption) and (Attitude towards switching to mobile banking) was reach (0.691) by sig (0.000).

Table 3. Pearson Correlation Coefficient between study variables

Independent variable	Attitude towards switching to mobile banking	
	Correlation Coefficient	Sig
Risk Perception	0.616**	0.000
Perceived Ease of Use	0.655**	0.000
Perceived Usefulness	0.712**	0.000
Mobile Banking service Adoption	0.691**	0.000

**Pearson Correlation Coefficient: To measure the relationship between study variables, correlation Coefficient were applied, Table (3)

4.1. Statistical treatment

The following statistical treatments through statistical software packages (SPSS v27) were used: Correlation Coefficient between study variables, the reliability (Cronbach' Alpha), Multiple Regressions analysis and Simple liner Regressions were applied

Table 4. Result of the (Multiple Regressions) analysis to detect the effect of 'Risk Perception' and 'Perceived Ease of Use' and 'Perceived Usefulness' of Mobile Banking on Attitude towards switching to mobile banking (n= 220)

Independent variable	"t" value	"t" sig	Beta	R	R2	"F" value	"F" sig
Risk Perception	3.858	0.031	0.163	0.824	0.679	138.077	0.000
Perceived Ease of Use	8.087	0.000	0.603				
Perceived Usefulness	4.718	0.000	0.322				

Note: Dependent variable: Attitude towards switching to mobile banking

Table (4) shows that there is a statistically significant effect at level ($\alpha \leq 0.05$) for independent variables on Attitude towards switching to mobile banking, where "F" value reached (138.077) by statistically significant (0.000). (R) Value reached (0.824) and (R2) value reached (0.679). The results of study hypotheses depend on (t) value indicate to accept:

H1: In the use of mobile banking services, there is likely to be significant effect of 'Risk Perception' of Mobile Banking on Attitude towards switching to mobile banking. Where (t) value was (3.858) by significant (0.031).

H2: There is likely to be significant effect of 'Perceived Ease of Use' of Mobile Banking on Attitude towards switching to mobile banking in the future. Where (t) value was (8.087) by significant (0.00).

H3: There is likely to be significant effect of 'Perceived Usefulness' of Mobile Banking on Attitude towards switching to mobile banking, which can make the financial processes of certain economic sectors more efficient. Where (t) value was (4.718) by significant (0.00).

Therefore there are a statistically significant effect of 'Risk Perception', 'Perceived Ease of Use' and 'Perceived Usefulness' of Mobile Banking on Attitude towards switching to mobile banking.

H 4: The emergence and proliferation of smart devices and phones is likely to be a significant effect of ‘Attitude towards switching to mobile banking’ on Mobile Banking service Adoption.

To test the Hypothesis 4, and to detect the effect of ‘Attitude towards switching to mobile banking’ on Mobile Banking service Adoption, the (linear Regression) analysis was used; Tables (5) shows that.

Table 5. Result of the (Linear Regressions) to detect the effect of ‘Attitude towards switching to mobile banking’ on Mobile Banking service Adoption (n= 220)

Independent variable	"t" value	"t" sig	Beta	R	R2	"F" value	"F" sig
Attitude towards switching to mobile banking	24.699	0.000	0.869	0.869	0.755	110.025	0.000

Note: Dependent variable: Mobile Banking service Adoption

Table (5) shows that there are a statistically a significant effect at significant level ($\alpha \leq 0.05$) for Attitude towards switching to mobile banking on Mobile Banking service Adoption, where "F" value reached (110.025) by statistically significant (0.000), (R) value reached (0.869), (R2) value reached (0.755). Therefore, accepted H4, which indicates to there is a statistically significant effect of ‘Attitude towards switching to mobile banking’ on Mobile Banking service Adoption.

5. Discussion

The results of this research concluded that there is a positive significant effect of Perceived Ease of Use and Perceived Usefulness of Mobile Banking on Mobile Banking Attitude. Similar results have been reported by the literature review [42]. Having the positive effects indicates that as the level of Perceived Ease of Use and Perceived Usefulness increases, the level of attitude towards Mobile Banking also increases. The results also show that there is a significant effect of Perceived Risk on attitude towards Mobile Banking which is not contrary to what is stated in the literature and hypothesis. It has been proved by recent studies that perceived risk negatively affects the customer’s intention to use mobile banking [43], [44], [45]. Even though this research was conducted in a different country than the researches that are considered in the literature review. This also gives a new direction for further research work. This research also concluded that Attitude towards switching to mobile banking has a positive significant effect on Intentions of Mobile Baking Adoption which means that as the consumers get a more positive attitude towards mobile banking, they are more likely to have intentions towards adopting mobile banking. The limitation of the study is relying on self-reported quantitative data only which can be overcome by using qualitative data, mobile internet statistics, and individual records on mobile banking to avoid subjectivity in further researches. Sales platforms and services connected to mobile applications are evolving at an unexpected rate. Similar phenomena can be observed in the case of mobile health applications, the consumer attitude follows the characteristics of our use in banking applications confirmed by our research. This direction of development also makes it possible to reduce the environmental impact of consumption and service systems. Efficient and economical solutions easily find their place in the economy [46], [47]. Focusing on untapped and redundant resources is the basis of the green discourse around the sharing economy. Studies show that the sharing economy can facilitate restructuring towards more sustainable business and consumption patterns [48], [49], [50]. The growth of mobile banking services will allow banks to grow in emerging markets as well, reaching all channels where they can connect with players in the value chain. Due to the proliferation of mobile applications, customers are in constant communication with different service systems, so banks need to seriously review and redesign previous applications. It can also be stated that banks have a primary responsibility to change the way of thinking of individuals and to develop a sense of security [51]. The viral situation is good proof that we can use the resources we used to operate in different areas of the economy much more efficiently. The transformation of bank customer services is proceeding at a tremendous pace, which also means a general decrease in the quantitative use of resources [52]. Due to the virus situation, the transformed use of mobile banking services not only in the short term but also in the long term gives a prominent role in the changed services environment. The changing technological and service environment is also an effective means of reducing service fees.

6. Conclusions

Our results show convergences and differences with previous research results, confirming the unique characteristics of the rapidly developing Arab region. User behavior related to mobile banking is shaped by the combined effect of habit and culture. Mobile banking services could be very efficient and cost-effective tools in the future, which will have a fundamental impact on the infrastructures that provide banking services. Adoption models and frameworks are increasingly used in a variety of individual and organizational contexts to explore factors that influence the intent to use a particular technology, or the use itself. Examination of risk factors and perceived risk associated with use received limited attention in the research because we thought this was evident and well-justified. In the present research, we have highlighted that perceptual risk is highly dependent on the user environment. This needs to be further investigated from the point of view of the introduction of mobile banking services because it differs significantly from the characteristics of internet banking services, especially in the Arabian countries. The transformation process is rapid - however, the efficiency and speed of transformation may vary from country to country. The ability of the fast-growing economies of the Arab region to adapt is expected to be stronger than that of consumers in classical welfare states. Limitations of the research: the number of research samples and the indicators used are of course not suitable for drawing deep conclusions in the case of either sectoral differences or the characterization of individual countries in the Arab region. In line with the details mentioned in the methodological description, further analyzes were planned for different economic sectors and in several Arab countries as well.

References

- [1] **Zhang, Y., Weng, Q., Zhu, N.,** (2018) The relationships between electronic banking adoption and its antecedents: A meta-analytic study of the role of national culture. *International Journal of Information Management*, 40, 76–87. doi: 10.1016/j.ijinfomgt.2018.01.015
- [2] **Hamidi, H.; Safareeyeh, M.,** (2019) A model to analyze the effect of mobile banking adoption on customer interaction and satisfaction: A case study of m-banking in Iran. *Telematics and Informatics* 38, 166-181. doi:10.1016/j.tele.2018.09.008.
- [3] **Oliveira, T., Faria, M., Thomas, M. A., Popovič, A.,** (2014) Extending the understanding of mobile banking adoption: When UTAUT meets TTF and ITM. *International Journal of Information Management*, 34(5), 689-703.
- [4] **Munoz-Leiva, F., Climent-Climent, S., Liébana-Cabanillas, F.,** (2017) Determinants of intention to use the mobile banking apps: An extension of the classic TAM model. *Spanish Journal of Marketing-ESIC*, 21(1), 25-38.
- [5] **Szopiński, T. S.,** (2016) Factors affecting the adoption of online banking in Poland. *Journal of Business Research*, 69(11), 4763–4768. doi: 10.1016/j.jbusres.2016.04.027
- [6] **Ebie, S., Njoku, E.,** (2016) Extension of the Technology Acceptance Model (TAM) to the adoption of the electronic knowledge and skills framework (e-ksf) in the National Health Service (NHS). *Journal of Applied Sciences and Development (JASD)*, 6(1 & 2).
- [7] **Shaikh, A. A., Karjaluoto, H.,** (2015) Mobile banking adoption: A literature review. *Telematics and Informatics*, 32(1), 129-142.
- [8] **Alalwan, A. A., Dwivedi, Y. K., Rana, N. P. P., Williams, M. D.,** (2016) Consumer adoption of mobile banking in Jordan. *Journal of Enterprise Information Management*, 29(1), 118–139. doi: 10.1108/jeim-04-2015-0035
- [9] **Gharaibeh, M. K., Arshad, M. R., Gharaibeh, N. K.,** (2019) Using the UTAUT2 Model to Determine Factors Affecting Adoption of Mobile Banking Services: A Qualitative Approach. *International Journal of Interactive Mobile Technologies (IJIM)*, 12(4), 123. doi: 10.3991/ijim.v12i4.8525
- [10] **Nzebile, P., Denadi, D.,** (2019) Digital Finance Country Report Jordan, (pp. 1–62). MEDA.
- [11] **Zhou, T., Lu, Y., Wang, B.,** (2010) Integrating TTF and UTAUT to explain mobile banking user adoption. *Computers in Human Behavior*, 26(4), 760-767. doi:10.1016/j.chb.2010.01.013
- [12] **Chaouali, W.; El Hedhli, K.,** (2019) Toward a Contagion-Based Model of Mobile Banking Adoption. *International Journal of Bank Marketing* 37, no. 1: 69–96. doi.org/10.1108/ijbm-05-2017-0096.

- [13] **Aboelmaged, M., Gebba, T. R.**, (2013) Mobile banking adoption: an examination of technology acceptance model and theory of planned behavior. *International Journal of Business Research and Development*, 2(1).
- [14] **Sampat, B.**, (2016) Antecedents to Mobile Banking Adoption in India: An Extended TAM model. *Wealth: International Journal of Money, Banking & Finance*, 5(2).
- [15] **Lian, J.-W., Yen, D. C.**, (2013) To buy or not to buy experience goods online: Perspective of innovation adoption barriers. *Computers in Human Behavior*, 29(3), 665–672. doi: 10.1016/j.chb.2012.10.009
- [16] **Poushter, J., Stewart, R.**, (2016) Smartphone ownership and internet usage continues to climb in emerging economies. Pew Research Center
- [17] **Akturan, U., Tezcan, N.**, (2012) Mobile banking adoption of the youth market: Perceptions and intentions. *Marketing Intelligence & Planning*, 30(4), 444-459.
- [18] **Püschel, J., Afonso Mazzon, J., Mauro C. Hernandez, J.**, (2010) Mobile banking: proposition of an integrated adoption intention framework. *International Journal of bank marketing*, 28(5), 389-409.
- [19] **Davis, F. D.**, (1989) Perceived usefulness, perceived ease of use, and user acceptance of information technology. *MIS quarterly*, 319-340.
- [20] **Park, E.; Lim, J.; Cho, Y.**, (2018) Understanding the Emergence and Social Acceptance of Electric Vehicles as Next-Generation Models for the Automobile Industry. *Sustainability*, 10, 662. doi: 10.3390/su10030662
- [21] **Weng, F; Rong-Jou, Y; H, Hann-Jang; Su, Hui-Mei.**, (2018) A TAM-Based Study of the Attitude towards Use Intention of Multimedia among School Teachers. *Applied System Innovation* 1, no. 3: 36. doi.org/10.3390/asi1030036.
- [22] **Giovanis, A; Athanasopoulou, P; Assimakopoulos, S & Christos Sarmaniotis**, (2019) Adoption of Mobile Banking Services.” *International Journal of Bank Market-ing* 37, no. 5: 1165–89. doi.org/10.1108/ijbm-08-2018-0200.
- [23] **Baptista, G., Oliveira, T.**, (2015) Understanding mobile banking: The unified theory of acceptance and use of technology combined with cultural moderators. *Computers in Human Behavior*, 50, 418-430.
- [24] **Lee, Y.-K., Park, J.-H., Chung, N., Blakeney, A.**, (2012) A unified perspective on the factors influencing usage intention toward mobile financial services. *Journal of Business Research*, 65(11), 1590–1599. doi: 10.1016/j.jbusres.2011.02.044
- [25] **Gupta, K. P., Manrai, R.**, (2019) Prioritizing Factors Affecting the Adoption of Mobile Financial Services in Emerging Markets–A Fuzzy AHP Approach. In *Performance Prediction and Analytics of Fuzzy, Reliability and Queuing Models* , pp. 55-81
- [26] **Tao, C. C., & Fan, C. C.**, (2017) A Modified Decomposed Theory of Planned Behaviour Model to Analyze User Intention towards Distance-Based Electronic Toll Collection Services. *Promet-Traffic&Transportation*, 29(1), 85-97.
- [27] **Yu, C. S.**, (2012) Factors affecting individuals to adopt mobile banking: Empirical evidence from the UTAUT model. *Journal of Electronic Commerce Research*, 13(2), 104.
- [28] **Luo, X., Li, H., Zhang, J., Shim, J. P.**, (2010) Examining multi-dimensional trust and multi-faceted risk in initial acceptance of emerging technologies: An empirical study of mobile banking services. *Decision support systems*, 49(2), 222-234.
- [29] **Laukkanen, T.**, (2014) Consumer Adoption / Rejection Decisions In Seemingly Similar Service Innovations: The Case Of The Internet And Mobile Banking, doi: 10.15444/gmc2014.04.02.02
- [30] **Granić, A. Marangunić, N.**, (2019) Technology acceptance model in educational con-text: A systematic literature review. *British Journal of Educational Technology* 50, 2572–2593. doi:10.1111/bjet.12864
- [31] **Rana, N. P., Barnard, D. J., Baabdullah, A. M., Rees, D., & Roderick, S.**,(2019) Exploring barriers of m-commerce adoption in SMEs in the UK: Developing a framework using ISM. *International Journal of Information Management*, 44, 141-153
- [32] **Martins, C., Oliveira, T., Popovič, A.**, (2014) Understanding the Internet banking adoption: A unified theory of acceptance and use of technology and perceived risk application. *International Journal of Information Management*, 34(1), 1-13.

- [33] Venkatesh, V., Thong, J. Y., Xu, X., (2012) Consumer acceptance and use of information technology: extending the unified theory of acceptance and use of technology. *MIS quarterly*, 157-178.
- [34] Venkatesh, Morris, Davis, Davis., (2003) User Acceptance of Information Technology: Toward a Unified View. *MIS Quarterly*, 27(3), 425. doi:10.2307/30036540
- [35] Poupancas Featherman, M. S., Pavlou, P. A., (2003) Predicting e-services adoption: A perceived risk facets perspective. *International Journal of Human-Computer Studies*, 59(4), 451-474.
- [36] Laukkanen, T., (2014) Consumer Adoption / Rejection Decisions In Seemingly Similar Service Innovations: The Case Of The Internet And Mobile Banking, doi: 10.15444/gmc2014.04.02.02
- [37] Persada, S. F., Miraja, B.A Nadlifatin, R., (2019) Understanding the Generation Z Behavior on D-Learning: A Unified Theory of Acceptance and Use of Technology (UTAUT) Approach. *International Journal of Emerging Technologies in Learning*, Vol 14, No 05, <https://online-journals.org/index.php/i-jet/article/view/9993>
- [38] Bagozzi, R. P., (2007) The legacy of the technology acceptance model and a proposal for a paradigm shift. *Journal of the association for information systems*, 8(4), 3.
- [39] Dwivedi, Y. K., Rana, N. P., Jeyaraj, A., Clement, M., Williams, M. D., (2017) Re-examining the unified theory of acceptance and use of technology (UTAUT): Towards a revised theoretical model. *Information Systems Frontiers*, 1-16.
- [40] Lee, M., (2009) Factors influencing the adoption of internet banking: An integration of TAM and TPB with perceived risk and perceived benefit. *Electronic Commerce Research and Applications*, 8(3), 130-141. doi:10.1016/j.eleap.2008.11.006
- [41] Featherman ; M. S; amp; Pavlou, P. A., (2003) Predicting e-services adoption: A perceived risk facets perspective. *International Journal of Human-Computer Studies* 59(4), 451-474. doi:10.1016/s1071-5819(03)00111-3
- [42] Rehman, Z.; Omar, S.; Zabri, S.; Lohana, S., (2019) Mobile Banking Adoption and its Determinants in Malaysia. *International Journal of Innovative Technology and Exploring Engineering Regular Issue* 9(1), 4231-4239. doi:10.35940/ijitee.I3015.119119
- [43] Milchram, C.; Kaa, G. V.; Doorn, N.; Künneke, R., (2018) Moral Values as Factors for Social Acceptance of Smart Grid Technologies. *Sustainability* 10(8), 2703. doi:10.3390/su10082703
- [44] Zhao, J.; Fang, S.; Jin, P., (2018) Modeling and Quantifying User Acceptance of Personalized Business Modes Based on TAM, Trust and Attitude. *Sustainability* 10(2), 356. doi:10.3390/su10020356
- [45] Pires, I.M.; Marques, G.; Garcia, N.M.; Flórez-Revuelta, F.; Ponciano, V.; Oniani, S., (2020) A Research on the Classification and Applicability of the Mobile Health Applications. *J. Personal. Med.* 10, 11
- [46] Geissdoerfer, M.; Savaget, P.; Bocken, N.M.; Hultink, E.J., (2017) The Circular Economy—A new sustainability paradigm? *J. Clean. Prod.* 143, 757-768
- [47] Faria, R.; Lopes, I.; Pires, I.M.; Marques, G.; Fernandes, S.; Garcia, N.M.; Lucas, J.; Jevremović, A.; Zdravevski, E.; Trajković, V., (2020) Circular Economy for Clothes Using Web and Mobile Technologies—A Systematic Review and a Taxonomy Proposal. *Information* 11, 161.
- [48] Grinevich, V.; Huber, F.; Karata, s-Özkan, M.; Yavuz, Ç., (2019) Green entrepreneurship in the sharing economy: utilising multiplicity of institutional logics. *Small Bus. Econ.* 52, 859-876.
- [49] Marques, M.S.G.; Pitarma, R., (2016) Smartphone Application for Enhanced Indoor Health Environments. *J. Inf. Syst. Eng. Manag.* 1, 4.
- [50] Shuib, L.; Shamshirband, S.; Ismail, M.H. (2015) A review of mobile pervasive learning: Applications and issues. *Comput. Hum. Behav.* 46, 239-244.
- [51] Saji TG, Paul D., (2018) Behavioural Intention to the Use of Mobile Banking in Kerala: An Application of Extended Classical Technology Acceptance Model. *Metamorphosis.* 17(2):111-119.
- [52] Cordova-Pizarro, D.; Aguilar-Barajas, I.; Rodriguez, C.A.; Romero, D., (2020) Circular Economy in Mexico's Electronic and Cell Phone Industry: Recent Evidence of Consumer Behavior. *Appl. Sci.* 10, 7744.
- [53] Seo, M.-S.; Choi, J.-W.; Kim, K.-H.; Choi, H.-D., The Relationship between Risk Perception of Cell Phones and Objective Knowledge of EMF in Korea. *Int. J. Environ. Res. Public Health* 2020, 17, 7207.

THE EFFECT OF PARTICLE SHAPE ON THE ANGLE OF REPOSE TEST BASED CALIBRATION OF DISCRETE ELEMENT MODELS

Author(s):

A. Bablena, N. Schrempf, I. Keppler

Affiliation:

Institute of Technology - Hungarian University of Agriculture and Life Sciences, 2100 Gödöllő, Páter Károly u. 1., Hungary;

Email address:

bablena.adrienn@uni-mate.hu; schrempf.norbert.attila@uni-mate.hu; keppler.istvan@uni-mate.hu

Abstract: Discrete element method (DEM) is a Lagrangian description based numerical technique used for modelling the mechanical behavior of granular materials. For using the DEM model, the micromechanical parameter values used in the governing equations must be determined beforehand. This is the so-called calibration problem. In most of the cases these micromechanical parameters cannot be directly measured, their values must be systematically changed until the modeled macro behavior of the granular assembly will be the same, as the real-life behavior. In this article we propose the simplest possible calibration method, the so-called angle of repose test for application in case of agricultural crop product related problems. We examine the effect of particle shape on the value of angle of repose, and give statistically acceptable empirical function to describe this dependence mathematically.

Keywords: granular materials, discrete element method, calibration, angle of repose test, asphericity

1. Introduction

The discrete element method was developed for rock mechanics studies in the late 1970s [1]. The method, which was later developed, has now become suitable for modelling almost any problem where granular materials interact with their environment or with each other. The rapid development of informatics enabled us to use DEM for solving mechanical problems arising in agricultural engineering, where most of the products can be modelled as granular assemblies. However, because of the large number of particles and time steps and the various micromechanical parameters which can really increase the computational time, it is still challenging to use this method [2].

2. The discrete element method

For modelling the mechanical behavior of the granular material, we used the academic version of EDEM 2.7 discrete element software. In the discrete element model the simulation evaluates the contact forces according to the “Hertz-Mindlin no slip” contact model: the material and interaction parameters have their effect on the normal- and tangential forces. These forces and moments acting between the interacting soil particles in the form of the following equations [3].

The normal force is

$$F_n = \frac{4}{3} E_0 \delta^{\frac{3}{2}} \sqrt{R_0} - 2 \sqrt{\frac{5}{6} \frac{\ln C_r}{\sqrt{\ln^2 C_r + \pi^2}}} \sqrt{2 E_0^4 \sqrt{R_0} \delta} \sqrt{m_0 v_{\text{rel}}}, \quad (1)$$

where $\frac{1}{E_0} = \frac{1-\nu_1^2}{E_1} + \frac{1-\nu_2^2}{E_2}$ is the equivalent Young modulus of the two interacting soil particles, δ is the overlap between these two soil particles. This normal overlap represents the normal deformation of a particle. The

normal overlap δ between two particles i and j at positions x_i and x_j (where x is the distance measured on the line connecting the centers of the two overlapping particles) with radii R_i and R_j is defined as: $\delta = R_i + R_j - (x_j - x_i)$.

$R_0 = \frac{R_1 R_2}{R_1 + R_2}$ is the equivalent radius, $m_0 = \frac{m_1 m_2}{m_1 + m_2}$ is the equivalent mass and v_{rel} is the normal component of the relative velocity of the soil particles.

The tangential force is

$$F_t = -8G_0 \sqrt{R_0} \delta \delta_t - 2 \sqrt{\frac{5}{6} \frac{\ln C_r}{\sqrt{\ln^2 C_r + \pi^2}}} \sqrt{2G_0^4 \sqrt{R_0} \delta} \sqrt{m_0} v_{\text{rel}}, \quad (2)$$

where $\frac{1}{G_0} = \frac{2-\nu_1}{G_1} + \frac{2-\nu_2}{G_2}$ is the equivalent shear modulus of the two interacting soil particles, δ_t is the tangential overlap between the two particles and v_{rel} is the tangential component of the relative velocity of the soil particles. The tangential overlap is the tangential displacement of the contact point up to the point at which the contact ends or the particle begins to roll or slip. The tangential overlap represents the tangential deformation of a particle. The tangential force is limited by Coulomb friction $\mu_s F_n$, where μ_s is the coefficient of static friction.

The moment from rolling friction is $M_r = -\mu_r F_n R_i \omega_i$, where R_i is the distance of the contact point from the center of the i -th soil particles and ω_i is the unit angular velocity vector, which is a dimensionless quantity representing only the direction of rotation of the i -th soil particle. μ_r is the coefficient of rolling friction. The tangential force also has moment on the particle: $M_t = F_t R_i$.

During the simulations, the linear- and angular momentum theorem is used to write the equation of motion for all the individual particles resulting multiple number of differential equations to be solved in a sufficiently large number of time steps. The used time step has a great impact on the stability of the numerical model. We selected for the simulation 25% of the Rayleigh-type time step:

$$\delta t = 0,25T_R = 0,25 \cdot (0,1631\nu + 0,8766)^{-1} \pi R \left(\frac{\rho_p}{G_p} \right)^{\frac{1}{2}} \quad (3)$$

It is important to consider that the quality of the obtainable solution could sensitively depend on the value of this time step used during the simulations. The same time step must be used during the calibration process of the discrete element model and during the simulations.

3. Materials and Methods: the angle of repose test

Finding the micromechanical parameters governing the above listed mechanical interactions is not a trivial task [4]. There is no robust method for DEM calibration, results are highly dependent on micromechanical parameters [5]. Because of this the usual way of finding these parameters is based on the simulation of the macromechanical behavior of the particle assembly. The parameters are modified until the micromechanical parameters used are resulting in the same macromechanical behavior in the current model than in the real life. Different techniques are applied for this, for example shear test [6]. [7] was suggested a combined friction model for calibration based on single particle behavior but from the application point of view the easiest solution is the calibration based on angle of repose test (Figure 1.). The most important property of this test, that there is no need for any special apparatus to do it, so it can be done easily and rapidly.

[8] showed how the results of a typical calibration test using a lifting cylinder for the angle of repose (AoR) test are invariant regarding the considered particle size and the dimensions of the test rig, however, the dimensions of the test rig become important for cohesive or elasto-plastic soils according to [9].

Three different techniques for forming conical piles were proposed by [10] using various slumping and pouring procedures to establish a simple calibration method. [11] created a modified draw down test which allows the generation of four experimental reference criteria in one test. Their criteria are the following: AoR test, shear angle test, mass flow rate measurement and the measurement of the discharged mass. We suppose that in our case the angle of repose test is sufficient for doing proper calibration.



Figure 1. Angle of repose test can be done easily and rapidly anywhere

3.1. Discrete element model of the angle of repose test

Material properties which were used in the simulations are shown in Table (1). We used the material properties of corn, because of our further objective is to find the micromechanical properties of corn particles, but this is not the goal of this work. The Poisson's ratios, density of steel, density of concrete and shear modulus of the particles came from literature [12] [13]. The density of particle had to be calculated from the total mass of grains and volume of the cylinder considering the particle shape and porosity of the material assembly. We modified the particle density until the desired bulk density has been reached. The shear modulus values of steel and concrete are the minimal values of the software because in this case the examined material is only the particle so there is minimal effect of these values to the examined results, but computational time is really sensitive to the shear modulus values [12] [13].

Table 1. Material properties used in the DEM simulation

	Material		
	Particle	Steel	Concrete
Poisson's ratio [-]	0.31	0.3	0.2
Shear modulus [Pa]	$3 \cdot 10^7$	10^6	10^6
Density [kg/m^3]	1180	7500	2400

The interaction properties between the particles and the other materials can be seen in Table (2). The values of coefficient of static friction came from literature [12], the coefficient of restitution and the coefficient of friction values are minimum values, in this case the effect of these values are minimal, but the computational time depends on these variables [14].

Table 2. Interaction properties between materials in DEM simulation

	Interaction		
	Particle - Particle	Particle - Steel	Particle - Concrete
Coefficient of restitution [-]	0.1	0.1	0.1
Coefficient of static friction [-]	0.2	0.2	0.53
Coefficient of rolling friction [-]	0.01	0.01	0.01

Particles were made from two spherical surfaces, the radius of one sphere was $R = 3.8$ mm. For the examination of the effect of the particle shape in simulations, the distance was varied between the centers of gravity of the two spheres from $d = 0$ mm which is a single sphere to the maximum $d_{max} = 7.6$ mm, in this case these spheres have contact only in one point. Different particle shapes can be seen in Figure 2.a.-c.

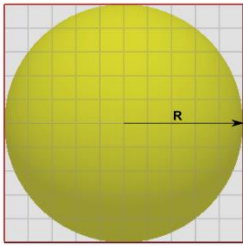


Figure 2.a. Spherical particle with $d = 0$ mm

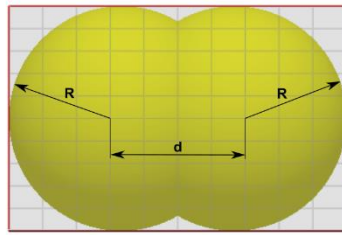


Figure 2.b. Particle with distance d between centers of gravity

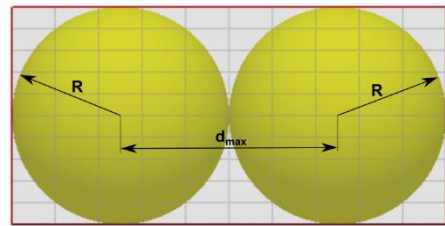


Figure 2.c. Particle with distance d_{max} between centers of gravity

The dimensions of the cylinder geometry can be seen in Figure 3. In simulations a single cylinder with the same $D = 0.2$ m diameter as the cylinder in the corn related measurements was used. The height of the cylinder in the measurements was $h = 0.25$ m and it was fully filled, so the height of the corn pile was the same. Because of settling down of the particles in the simulation, the height of the cylinder must be higher than in reality, it was $h = 0.75$ m. With this h height the h_{pile} was around the original pile height as during measurements. The surface's material was modeled as concrete, and the cylinder as steel.

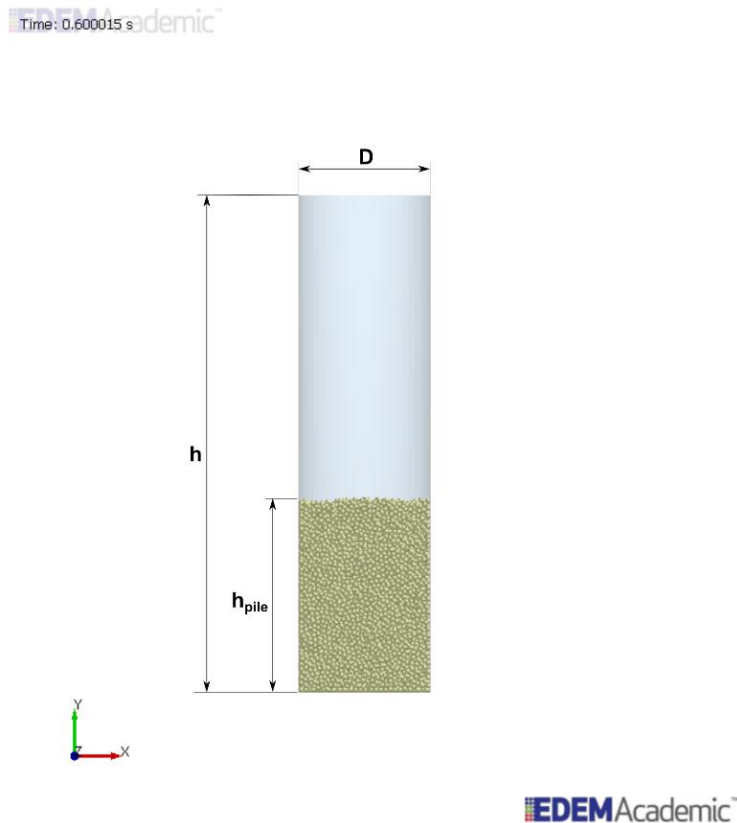


Figure 3. Dimensions of the cylinder in simulations

The number of particles and the mass of one particle was calculated by the software, so the total mass of grains was given. The position of every particle was also calculated in every time step, so when the pile reached the equilibrium state, which was at 0.6 s simulation time, the maximum coordinate y of the pile gave the height of the pile. From the geometrical properties the volume of the cylinder containing the bulk material could be calculated. From the total mass and the volume of the cylinder and the bulk density can be calculated, which is in this case $\rho = 1180 \frac{kg}{m^3}$.

3.2. Data analysis

As it was mentioned above, in simulations the distance d between the centers of gravity of two spheres was varied according to the examination of the effect of particle shape on the angle of repose. Distance d was increased with 1 mm steps from 0 mm to 7 mm, plus $d_{max} = 7.6$ mm case was also applied. 3 repetitions were made in every case.

Particles were settling down in the first 0.6 s, reached the equilibrium state, then the cylinder started moving upwards to direction y with constant velocity $0.11 \frac{m}{s}$. This velocity value was determined from our measurements. The simulation stopped after total time of 2.5 s, when the granular material pile reached the equilibrium state again. After reaching equilibrium state the angle of repose α was calculated from the maximal coordinates x , y and z (Figure 4.), excluding the particles being far away from the pile. The origin of the coordinate system was at the centerpoint of the circle which can be drawn around the pile on concrete floor.

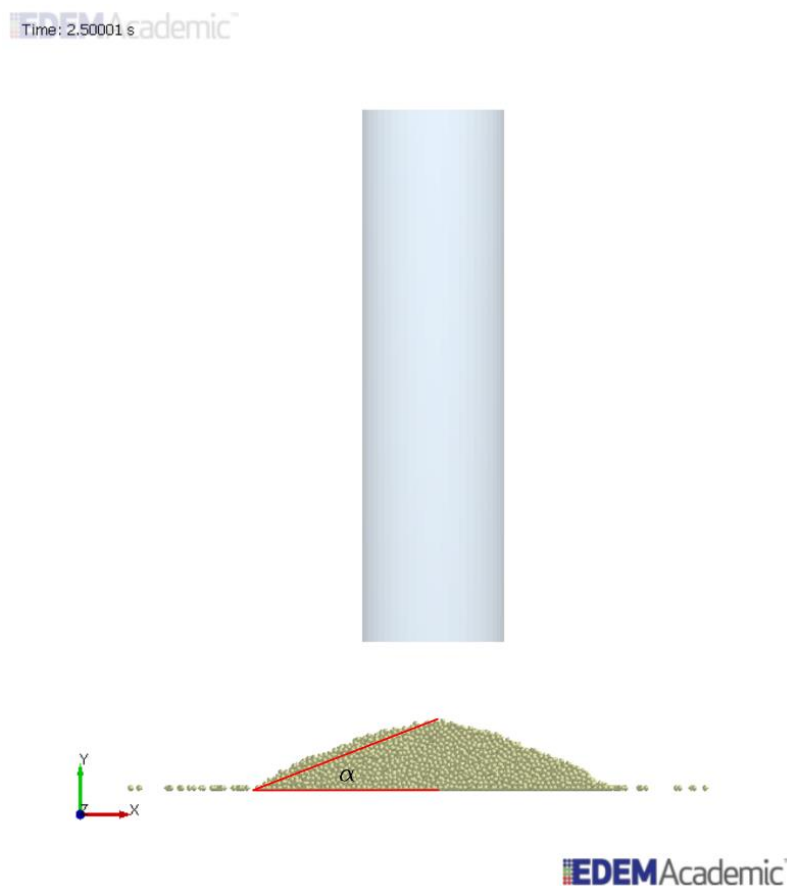


Figure 4. Angle of repose α of the pile

The software calculates the coordinates of centers of gravity of every particle in every time step and α was calculated from the x_{max} and y_{max} coordinates of the pile as the following:

$$\alpha_x = \tan^{-1} \frac{|y_{max}|}{|x_{max}|} \quad (4)$$

Because the pile in equilibrium state is not exactly circular, the angle α was calculated from z_{max} and y_{max} as well, similarly to the calculation above:

$$\alpha_z = \tan^{-1} \frac{|y_{max}|}{|z_{max}|} \quad (5)$$

For further calculations the average value of α_x and α_z was used. Table (3) contains the calculated values with all 3 repetitions.

Table 3. Calculated values of angle of repose with 3 repetitions in every cases

d [mm]	d/dmax [-]	α_x [°]	α_z [°]	$\alpha_{average}$ [°]
0	0	6.020	6.311	6.165
0	0	6.558	6.370	6.464
0	0	5.917	6.240	6.079
1	0.132	8.299	8.317	8.308
1	0.132	8.467	8.386	8.427
1	0.132	8.103	8.073	8.088
2	0.263	12.385	12.428	12.406
2	0.263	12.258	12.362	12.310
2	0.263	12.148	12.337	12.242
3	0.395	15.359	14.797	15.078
3	0.395	14.999	15.219	15.109
3	0.395	15.111	15.238	15.174
4	0.526	16.592	17.157	16.874
4	0.526	17.666	17.625	17.645
4	0.526	17.474	17.366	17.420
5	0.658	18.765	18.459	18.612
5	0.658	19.272	18.896	19.084
5	0.658	19.429	18.156	18.792
6	0.789	21.255	20.292	20.773
6	0.789	20.079	19.815	19.947
6	0.789	19.612	20.039	19.826
7	0.921	21.795	20.884	21.340
7	0.921	20.695	20.857	20.776
7	0.921	21.394	21.571	21.482
7.6	1.0	21.117	20.886	21.002
7.6	1.0	21.588	22.079	21.833
7.6	1.0	21.571	21.846	21.708

4. Results

In Figure 5, angle of repose α can be seen in function of $\frac{d}{d_{max}}$ which is a dimensionless value varying between 0 and 1.

The diagram shows a trend which has maximum at $\frac{d}{d_{max}} = 1$. A quadratic polynomial function was applied to data points, the equation of the polynomial function is:

$$\alpha = -12.214 \left(\frac{d}{d_{max}} \right)^2 + 28.052 \left(\frac{d}{d_{max}} \right) + 5.7117 \quad (6)$$

The value of coefficient of determination is $R^2 = 0.9928$ which means a good fitting in this case. According to these data, where the angle of repose at $\frac{d}{d_{max}} = 0$ (this means one sphere) is around 6° and at $\frac{d}{d_{max}} = 1$ is more then 20° , it can be said that the simulation is really sensitive to the shape of particles, that's why using a particle shape which is similar to a real particle shape is important.

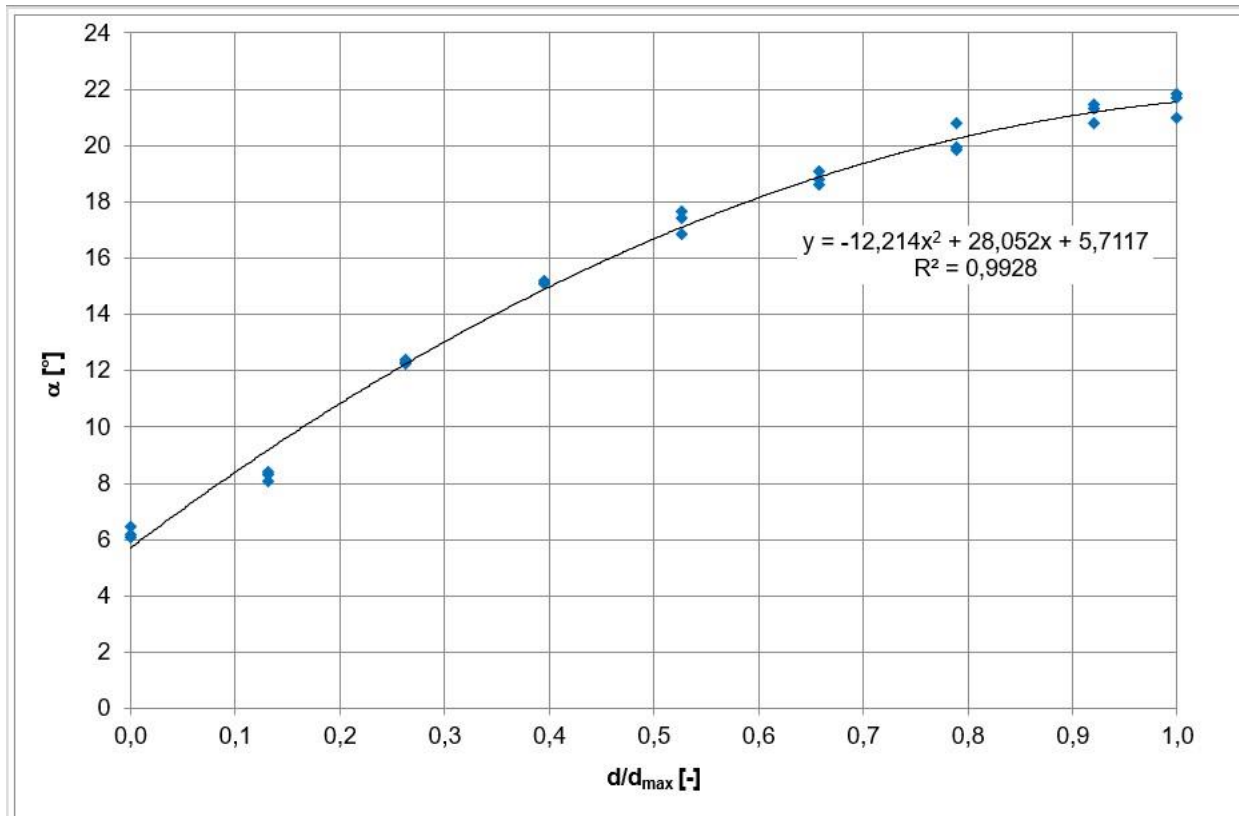


Figure 5. Angle of repose α in function of d/d_{max} dimensionless value

5. Conclusions

The angle of repose measurement is an easy way for finding the data needed to determine the micromechanical parameters of agricultural materials. It is maybe not the best and most accurate measurement, but it can be done anywhere, easily. This makes it the ideal method for calibration measurement. As we have seen in the preceding sections, the discrete element model behavior highly depends on the particle shape. Using the simplest possible non-spherical particle (clump of two spheres) we demonstrated that the angle of repose depends on the asphericity of the particles according to a quadratic function written in the previous section. We suppose that this property is caused by the particles stuck to each other. This result means that during the calibration of agricultural granular material's discrete element models, the geometrical shape of the particles has an important effect on the modelled mechanical behavior.

Acknowledgement

Thanks to KFI_16-1-2016-0198 "Procedural and equipment development for energy and closed loop for waste recovery crop management and machine system to develop from harvest to storage and / or further processing technologies " research and development project and thanks to RAIL SAFE Ltd. and Toldi-Agroszolg. Ltd. consortium as project owner for assisting in the performance of experiments.

References

- [1] **Cundall, P.A. and Strack, O.D.L.** (1979) A discrete numerical model for granular assemblies. *Geotechnique*, 29(1), 47-65.
- [2] **Mio, H., Akashi, M., Shimosaka, A., Shirakawa, Y., Hidaka, J. and Matsuzaki, S.** (2009) Speed-up of computing time for numerical analysis of particle charging process by using discrete element method. *Chemical Engineering Science*, 64, 1019-1026.

- [3] **Keppler I., Hudoba Z., Oldal I., Csatar A., Fenyvesi L.** (2015) Discrete element modeling of vibrating tillage tools. *Engineering Computations*, 32(2), 308-328.
- [4] **Coetzee, C.J.** (2017) Review: calibration of the discrete element method. *Powder Technology*, 310, 104-142.
- [5] **Asaf, Z., Rubinstein, D. and Shmulevich, I.** (2007) Determination of discrete element model parameters required for soil tillage. *Soil & Tillage Research*, 92(1-2), 227-242.
- [6] **Keppler I., Safranyik F., Oldal I.** (2016) Shear test as calibration experiment for DEM simulations: a sensitivity study, *Engineering Computations*, Volume 33, Issue 3, pp. 742 – 758.
- [7] **Syed, Z., Tekeste, M. and White, D.** (2017) A coupled sliding and rolling friction model for DEM calibration. *Journal of Terramechanics*, 72, 9-20.
- [8] **Roessler, T. and Katterfeld, A.** (2018) Scaling of the angle of repose test and its influence on the calibration of DEM parameters using upscaled particles. *Powder Technology*, 330, 58-66.
- [9] **Mohajeri, M.J., Helmons, R.L.J., van Rhee, C. and Schott, D.L.** (2020) A hybrid particle-geometric scaling approach for elasto-plastic adhesive DEM contact models. *Powder Technology*, 369, 72-87.
- [10] **Grima, A.P. and Wypych, P.W.** (2011) Discrete element simulations of granular pile formation element models. *Engineering Computations*, 28, 314-339.
- [11] **Roessler, T., Richter, C., Katterfeld, A. and Will, F.** (2019), Development of a standard calibration procedure for the DEM parameters of cohesionless bulk materials – part I: solving the problem of ambiguous parameter combinations. *Powder Technology*, 343, 803-812.
- [12] **M. Moya, P.J. Aguado, F. Ayuga** (2013) Mechanical properties of some granular agricultural materials used in silo design. *International Agrophysics*, 27, 181-193.
- [13] **Oldal I., Safranyik F., Keppler I.** (2017) Reducing computational time of cohesionless discrete simulations based on particle clusters. *Engineering Computations*, Volume 34, Issue 2, pp.
- [14] **Simons, T.A.H., Weiler, R., Strege, S., Bensmann, S., Schilling, M. and Kwade, A.** (2015) A ring shear tester as calibration experiment for DEM simulations in agitated mixers – a sensitivity study. *Procedia Engineering*, 102(1), 741-748.

INTRODUCTION TO 3D PRINTING: TECHNIQUES, MATERIALS AND AGRICULTURAL APPLICATIONS

Author(s):

R. F. Faidallah¹, Z. Szakal², I. Oldal²

Affiliation:

¹ Doctoral School of Mechanical Engineering – Hungarian University of Agriculture and Life Sciences, 2100 Gödöllő, Páter Károly u. 1., Hungary;

² Institute of Mechanical Engineering - Hungarian University of Agriculture and Life Sciences, 2100 Gödöllő, Páter Károly u. 1., Hungary;

Email address:

Faidallah.Rawabe.Fatima.2@phd.uni-mate.hu; szakal.zoltan@uni-mate.hu; oldal.istvan@uni-mate.hu

Abstract: The Production of complex products is easily possible with the help of additive manufacturing. By using additive manufacturing products may be mass-produced. Compared to traditional subtractive manufacturing, Additive manufacturing is advantageous in short design cycles, suitable for manufacturing complex structures, and high material utilization. Polymers and composites are frequently used in AM technologies, which have evolved into a variety of industrial and emerging applications. Among the many materials currently used in 3D printing are ceramics, metals, polymers, and concrete. ABS and PLA thermoplastics are the most often used materials for agricultural 3D printing since they are easy to print and relatively cheap. This article provides an overview of 3D printing technologies, materials, and applications in agriculture.

Keywords: additive manufacturing, technologies, materials, agricultural, 3D printing techniques

1. Introduction

Three-dimensional printing is a buzzword in the material manufacturing world of materials manufacturing, and it has lately been the focus of the investigation by materials scientists. This technology has grown rapidly in recent years and is expected to revolutionize manufacturing sectors by enabling the development of next-generation high-performance materials. Additive manufacturing (AM) could be defined as "the process of joining materials to produce parts from 3D model data" Often layer upon layer, as opposed to formative and subtractive manufacturing methods. The AM process fuses, cools, and solidifies to create 3D geometries without adopting complex molds [1].

Additive manufacturing has been advantageous at short design cycles, suitable for manufacturing complex structures, and high material utilization compared to traditional subtractive manufacturing. Therefore, additive manufacturing has been widely used in manufacturing parts and devices for aerospace [2], aviation [3], automobiles [4], medical devices [5], construction [6], clothing [7], and so on. This technology creates objects by adding materials to reduce waste while reaching satisfactory geometric accuracy [8]. It is begun with a meshed 3D computer model that could be created by acquired image data or structures built in Solidworks or computer-aided design (CAD) software. An STL (Surface Tessellation Language) file is commonly created, Figure 1. the process of 3d printed product. These three technologies combined together made possible the printing of three-dimensional objects sent to the 3D printing machine[9, 10]. Speed, direct data translation, management of complicated geometry, high precision, environmental benefits, and cost-effectiveness are just a few of its features.

The main methods of AM: additive manufacturing of powders by selective laser sintering (SLS) [12], liquid binding in three-dimensional printing (3DP) [13], as well as inkjet printing, contour

crafting, stereolithography [14], laminated object manufacturing (LOM) [15] and the most common method of 3D printing that mainly uses polymer filaments is known as modeling (FDM)[16].

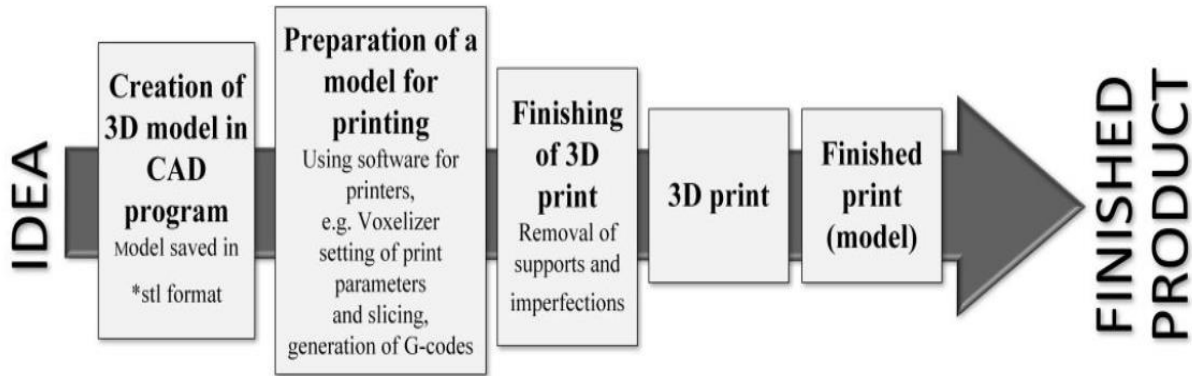


Figure 1. The process of 3d printed product [11]

Additive manufacturing become more prevalent in industrial applications that require high performance, like rapid prototyping, rapid manufacturing, rapid tooling [17–21], advanced electronics [22], water filtration, and desalination [21, 23], medical applications [24], and others. In agriculture, 3D printing is mainly useful for manufacturing agricultural equipment [25] and spare parts [26] without greatly affecting their quality. There are various materials and printing technologies for 3D printing. One of the most popular 3D printing technologies used in agriculture is Fused Deposition Modeling (FDM) because it offers consumer-grade materials/filaments like polylactic acid (PLA) thermoplastic and acrylonitrile butadiene styrene (ABS) [17]. The reason why 3D printers are very common in all kinds of industries is obvious because this technology offers distinct advantages Figures 2. shows the percentages of disciplines ranging from motor vehicles to medicine, from academic work to many others.

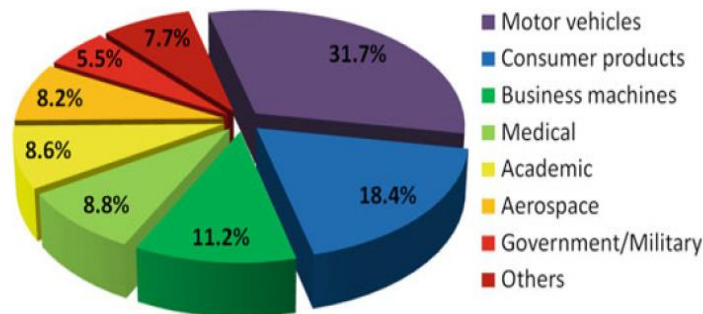


Figure 2. The range of 3D printing used by discipline [27].

2. Methods of 3D printing technologies

Additive manufacturing (AM) methods were developed to meet the demand for printing complex structures at high resolution, Figure 3. Rapid prototyping, the ability to print large structures, the reduction of printing defects, and the improvement of mechanical properties are one of the key factors that have been driven the development of AM technologies [28].

2.1 Selective Laser Sintering

Selective laser Sintering (SLS) is a method that employs a laser as the source for layer-by-layer sintering of powder into a single object [1]. The processes of sintering and melting (SLS/SLM) are identical. The configuration of SLS employing a CO₂ laser is shown in Figure 4. Because the laser is the source of the

binding, light rays are not permitted inside the chamber during printing [30]. The powder fills in the vat for layer spreading. The platform then moves in the z axis, spreading the powder across the next layer for sintering. The procedure is repeated till the item is finished. Metal powders are utilized in this process to make a component that may be used as a finished product [1, 30]. Electron Beam Melting (EBM) uses an electron beam source as energy to melt layers of material utilizing a vacuum chamber and a heated platform, similar to the electron beam. For better surface hardness and strength, use cyanoacrylate or epoxy resin in Figure 5.

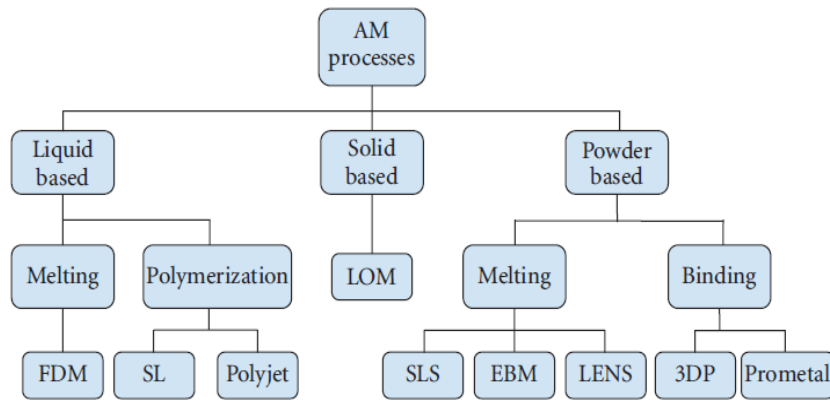


Figure 3. Three Dimension printing processes.

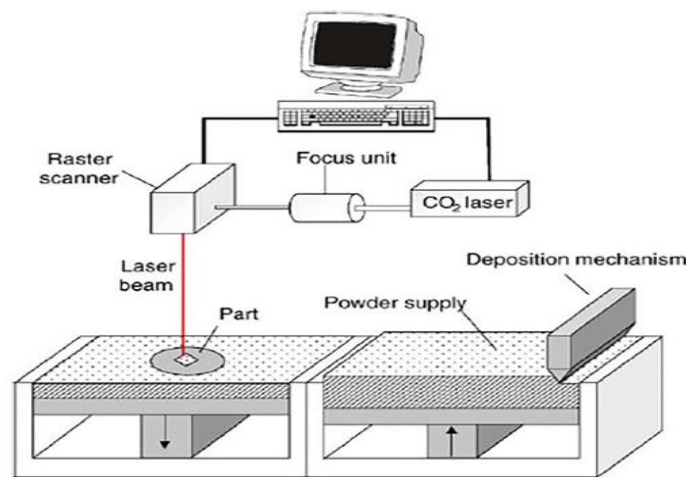


Figure 4. Selective Laser Sintering (SLS) layout

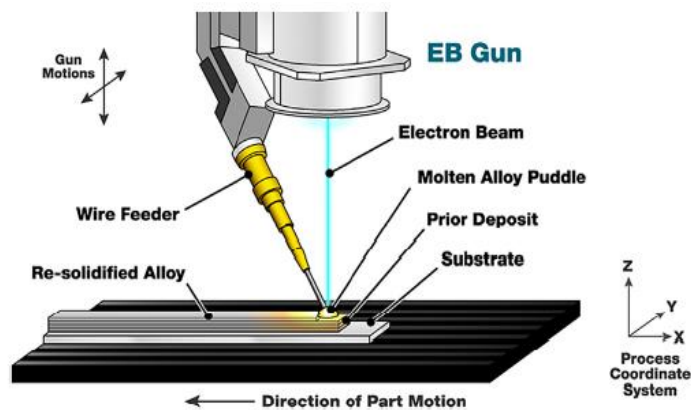


Figure 5. The nozzle of Electron Beam Melting (EBM)

2.2 Stereolithography (SLA)

A stereolithography Apparatus is built layers on resin layers by using light projectors or scanning lasers [31]. The resins which are used here are photopolymers cured by light [32]. Every layer is created by drawing light or laser on the resin surface on the construction platform (Figure 6.). Once the layer is built, the platform moves immersion into the resin and a coating is used to align the resin layer with the layer thickness in the input parameters [33]. The major limitation in this process is the size of the objects created. The process is performed in a light-proof room because the resin is light sensitive. If the support area is increased, the deposition of the resin layer might create an uneven layer. This process is used in dental applications and smaller parts such as molding gold ornaments, etc.[34] Casting resin could also be used for the production of dental parts. Direct end-use components for dental purposes can also be manufactured using the SLS technique.

2.3 Laminated Object Manufacturing

Laminated Object Manufacturing (LOM) is a process which is combines additive and subtractive techniques to build up a part layer by layer shown in Figure 7. In this process, the materials are in the form of sheets. The layers have been bonded together using pressure and heat, as well as a thermal adhesive coating. A laser of carbon dioxide cuts the material into the shape of the individual layers using the information from the 3D model which is created by the CAD and STL files. The advantages of this process are the low cost, no need for post-processing or supporting structures, no deformation or phase changes during the process, and the ability to produce large parts. The disadvantages are the low surface sharpness, the directionality of the materials in terms of machinability and mechanical properties, and the difficulty of building complex internal cavities. This method can be used for models made of paper, metal, and composite [9, 35].

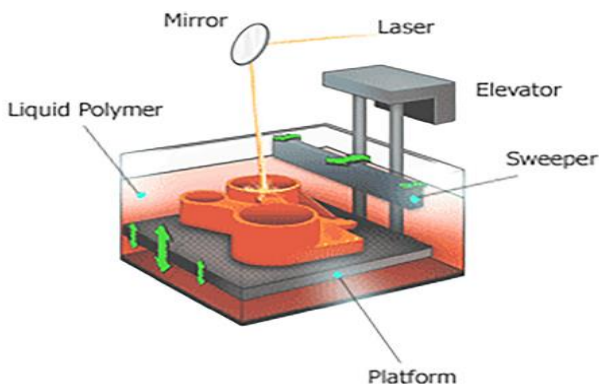


Figure 6. Stereolithography

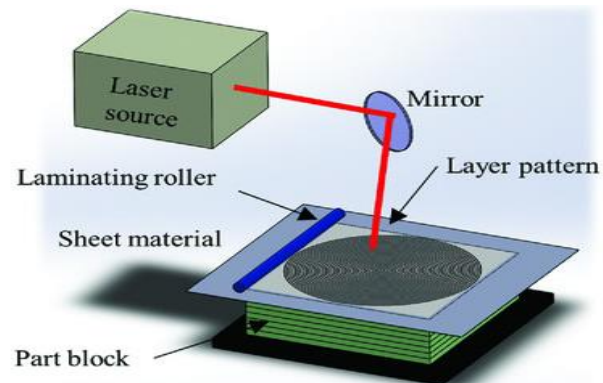


Figure 7. Laminated Object Manufacturing (LOM)

2.4 Inkjet printing and contour crafting (IJP)

The liquid resin is passed through a micro nozzle to create a thin layer on the platform. The extruder head's movement occurs in the contour created by the shape of the part during cutting. Curing of the resin is done in the air for some resins, but mostly often the resin printed objects are held in UV curing for better cure and stiffness [36].

2.5 Binder jetting

It is a process and technology that uses powder-based binders and materials. A liquid binder (adhesive) is placed in a thin layer of powder particles like ceramics, metal, composites, or sand to build the parts. An object is made layer by layer while the binder is placed in a powder bed to form a solid object [36]. The

binder is responsible for holding the powder layer together [36]. Materials used in binder jetting include, silica, metal, ceramics, sand, and polymers in the granular form [37].

2.6 Directed energy deposition

Directed energy deposition is the most complex printing process often used to add additional material to or repair existing components [38]. Directed energy deposition allows the grain structure to be highly controlled and the good quality of the object to be achieved. This process is similar in principle to materials extrusion but here the nozzle is not fixed to a specific axis and may move in multiple directions. In addition, this process could be used for ceramics and polymers but is usually used for metals and metal-based hybrids in the form of wire or powder. An example of this technology is laser engineered net shaping (LENS) and laser deposition [38]. Laser deposition is an emerging technology and may be used to fabricate or repair parts that are in millimetres to meter range. Laser deposition technology is gaining traction in the transportation, aerospace, tooling, and oil and gas industries because it offers scalability and multiple capabilities in a single system [36]. Meanwhile, the laser LENS can use thermal energy for melting during casting and the parts are subsequently finished [39].

2.7 Fused Deposition Modeling (FDM)

Fused filament fabrication (FFF) or Fusion deposition modelling (FDM) is an old method for manufacturing parts in the AM process (Figure 8.). In this process, the source material is filaments made of various thermoset plastics [40]. Some materials are biodegradable polymers (PLA), which are used as key elements in scaffold structures [41, 42]. Extruder nozzles of various diameters are used to melt the filament in a semi-solid condition and make it flow on the platform [43]. Most often, the extruder moves in the x and y directions reading the g-code which is created by the slicing software. On some machines, the extruder moves in the z-direction, on others the platform does. For some materials, the platform must be heated to improve the adhesion and prevent warping [43]. Filaments with higher melting points are difficult in part production. When complex structures are created the support structure is formed. These support materials can be made of the same material or different materials. For some designs, the support materials can be easily removed, but when it comes to complex structures, removing the support materials presents some difficulties. Ultimaker has developed a water-soluble support material that leaves no trace in the supporting parts and creates a clear part. Dynamic structures may be easily created with this type of support material. The accuracy of the part that had been created depends on the movement of the extruder, the temperature, the speed, and the flow rate of the material during the nozzle. The FDM is widely used for creating anatomical models in dentistry and surgical exercises [44]. Table 1. Summary of materials, application, advantages, and drawbacks of the main additive manufacturing methods.

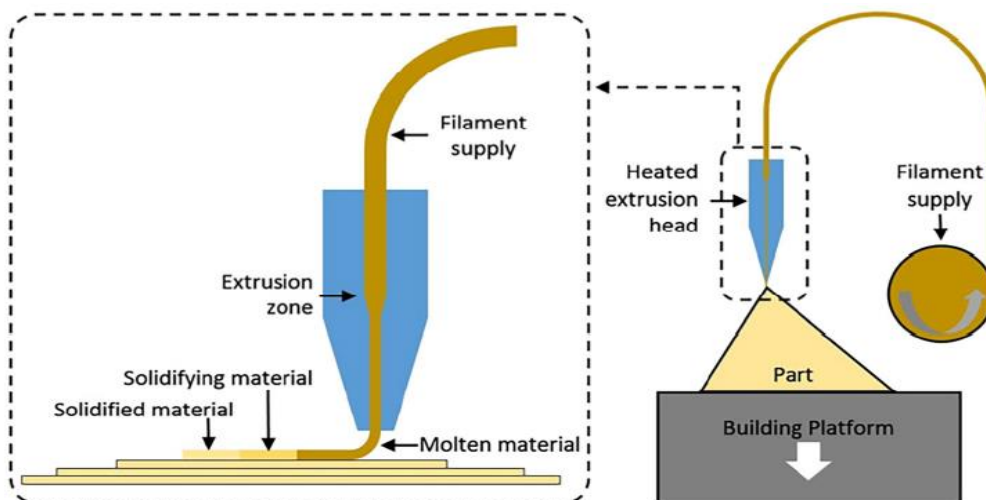


Figure 8. Fusion Deposition Modelling (FDM).

Table 1. Summary of materials, application, advantages, and drawbacks of the main additive manufacturing methods [45, 46].

Method	Description	Materials	Applications	Benefits	Drawbacks	Resolution range (µm)
Inkjet Binder Jetting (IBJ)	Drop-on-demand Binder	Ceramic, Powder of metals, concrete Sand, and soil	Structures Buildings Biomedical Large	Quick printing Ability to print large structures	Lack of adhesion between layers Layer-by-layer finish. Maintaining workability Coarse-resolution	Inkjet: 5–200 µm Contour crafting: 25–40mm [32]
Laminated object manufacture	Builds parts by Cutting sheets of material and assembling them together in layers	Ceramics Polymer composites Metal rolls Paper Metal-filled tapes	Electronics Paper manufacturing Foundry industries Smart structures	Low cost Reduced manufacturing and tooling time A vast range of materials Very good for manufacturing of larger structures	Limitation in manufacturing of complex shapes Inferior surface dimensional accuracy And quality	Depends on the thickness of laminates
Stereolithography	UV induced curing Laser scanning and	A resin with photo-active monomers	Biomedical Prototyping	High-quality Fine resolution	Slow printing Very limited materials Expensive	10 µm [13]
Selective Laser Sintering (SLS)	Heat and Laser scanning induced sintering	ceramics Plastic; metals;	Aerospace Biomedical Lightweight Electronics structures (lattices)	High-quality Fine resolution	Expensive Slow printing	80-250 µm [13]
Direct energy deposition	Builds parts By directing thermal energy to fuse materials when applied to a substrate.	Metals and alloys in the form of powder or wire Ceramics and polymers	Aerospace Retrofitting Repair Cladding Biomedical	Excellent for repair and retrofitting Reduced mechanical properties are Controlled microstructure Accurate composition control manufacturing time and cost Excellent	Low surface Need for a dense Low accuracy quality Limitation in printing complex shapes with fine details support structure	250 µm [23]
Fused deposition modeling	Creates objects by Extrusion material through a nozzle to build layers	Polymer; composites; cement; aggregates	3D curve printing, Aggregate, Rapid prototyping advanced composite parts	High speed Simplicity Low cost	Limited materials (only thermoplastics) Weak mechanical properties Layer-by-layer finish	50-200 µm [13]

3. Materials that are used in 3D printing

While engineers have focused on improving equipment function and AM methods, applications of various 3D printing technologies evolved on developing the best 3D printing materials through scientific research. For 3D printing of polymers, thermomechanical properties, reactivity (or stability), stimulability, and hybrid materials are important factors. Practical considerations emphasized durability, price, strength, frequency, and safety to animals, humans, and the environment. To date, various polymeric materials such as thermoplastic materials including acrylonitrile butadiene styrene (ABS), polylactic acid (PLA), polyethylene terephthalate glycol (PETG), and polyether ether ketone (PEEK), have been widely used. Thermosets and elastomeric materials for 3D printing are usually made from better-formulated starting materials such as acrylates. These materials can be used in different forms, such as liquid resins, filaments, powders, etc. The following discussions focus on the common and widely known polymer materials used for agricultural 3D printing and do not claim to be exhaustive.

3.1 Polylactic Acid

PLA (Polylactic acid) [45, 46] is a biodegradable thermoplastic polymer compound. It's a non-toxic, ecologically friendly aliphatic polyester made from lactic acid (derived from animals and plants) that's used to make films, textiles, and bottles. PLA has excellent mechanical qualities and, because of its biodegradability, can be used to replace petroleum-based polymers [47]. PLA has quite a high melting and boiling point than nylons and ABS, which is one of its greatest benefits in 3D printing [48]. PLA is very useful in medical technologies due to its compatibility. Also, it is a good material for disposable food packaging because of its biodegradability [49]. Previous works [17, 49, 50] have detailed in detail the significant physical features including thermal and mechanical of PLA material. PLA has low heat resistance and brittleness, properties that limit its potential applications compared to ABS [51]. However, its biodegradable property is an important reason why it can be used in numerous biomedical applications such as drug delivery microspheres, tissue engineering, and bone fixation [52]. The chemical structure of PLA can be found elsewhere [53].

3.2 Acrylonitrile Butadiene Styrene (ABS)

ABS is a commonly used thermoplastic substance in 3D printing, especially for FDM. Acrylonitrile, which offers chemical resistance and impact resistance, Butadiene, which provides toughness and impact resistance, and Styrene, which provides rigidity and ease of manufacturing, are the three components of ABS [54]. It is a material that is amorphous, rigid, hard, and abrasion-resistant [55]. ABS, like other polymer materials, melts when heated and solidifies when cooled. Because it can be reshaped or remodelled at a certain temperature, it is an excellent polymer for FDM [56]. In previous works [17, 54, 57], several research groups described the material ABS's other physical features (mechanical, thermal, and so on). When ABS is used, hazardous fumes are released during printing, a well-ventilated area, and requiring proper handling [57]. Some examples of 3D printing applications of the material ABS are wheel covers, dashboards, and car body parts. It could also be used for the body of devices such as vacuum cleaners, telephone sets, and cameras. It can also be used for medical equipment [58].

3.3 Nylon or Polyamide

Polyamide (PA), sometimes known as nylon, has grown in importance in 3D printing. Although the printed material has extraordinary elasticity, high tensile strength, and excellent tribological properties, it is moisture sensitive [59]. This material is available in powdered or filament form and is based on 3D printing processes such as multi-jet fusion (MJF), FDM, and SLS.

PA can be further classified depending on their chemical composition, particularly the number of carbon atoms (n). PA6, PA11, and PA12 are the most prevalent PA (n) on the market, and they're used in FDM. PA6 is the most widely available chemical. It has a lot of elasticity and can withstand a lot of wear and tear. Nylon, on the other hand, must be printed on a heated plate (about 80°C) to minimize adhesion problems and moisture absorption in the environment, which might compromise print quality. The extrusion temperature should be between 220-250°C [60] depending on the kind of nylon. Other advantages of using PA in the

medical field include biocompatibility with human tissue, robust mechanical properties, chemical stability, high toughness, excellent wear, and sliding properties. These are the reasons why PA is used not only in engineering and OEM manufacturing but also in biomedical applications [61].

3.4 Recycled 3d Filaments

Plastic recycling technologies are not new to research, but the raw materials for 3d printing are not yet made from recycled plastic. There is research in the field of Development of 3D Printing Raw Materials from Plastic Waste. More research is being done on the recycling of plastics to make new raw materials suitable for 3D printing from waste [68, 69, 70]. [68], [69], [70].

The PET is recycled quite frequently and has the number "1" as its recycling symbol, and after drying PET prepared for extrusion, then material is shredded and dried, its ready to be extruded. The 'Next filament extruder' was used for the extrusion of PET (shredded format), with 3 different diameters of shredded material and constant range of temperature heater and speed of fan speed, the measurement can be ready after 3 or maximum 5 tests. Recent research points the way towards chemical recycling methods with lower energy requirements, compatibilization of mixed plastic wastes to avoid the need for sorting, and expanding recycling technologies to traditionally non-recyclable polymers. They mentioned the recycling technologies from which they concluded that mechanical recycling is the only widely adopted technology for large-scale treatment of plastic solid waste. The main steps were the removal of organic residue through washing, followed by shredding, melting, and remoulding of the polymer, which is often blended with virgin plastic of the same type to produce a material with suitable properties for manufacturing.

4. 3D Printing applications in agriculture

4.1 Printing technology and materials

FDM is the most widely utilized printing method for producing different agricultural implements and equipment. Agricultural equipment such as sprinklers and hose manifolds for irrigation [62], spare parts for machinery such as corn augers [63] and gears [64], and seed application equipment are all made from thermoplastics, particularly PLA and ABS. [65]. Farmers can also make customized tools from PLA, such as a fruit picker and shovel, because the material is biodegradable and recyclable [62]. Although these thermoplastics differ slightly in properties such as heat resistance and stiffness, their (low) cost and ease of use in 3D printing make them the most commonly used filaments. Table 1 highlights the application, material, and 3D printing method which is used in the field of agriculture.

4.2 Urban farming

While there are many numerous innovations for optimizing bulk harvesting, 3D printing can provide a simple mechanism for picking up high-hanging fruit without the use of ladders. The 3D-printed parts of the tool may be assembled with conventionally manufactured components such as the wooden handle, screws, and spring to create the three claw fruit picker and 3D printed corn shellers are shown in Figure 9,10 [62]. PLA (Polylactic acid) proves useful in the material composition of parts produced by fused deposition modelling because it is biodegradable and recyclable. This eliminates unnecessary waste generated by conventional manufacturing and thus promotes sustainability.



Figure 9. 3D printed fruit picker [63]



Figure 10. 3D printed corn-shellers [63]

4.3 Irrigation and water management

The adapter/garden hose manifold shown in Figure 11. [62] is an example of water management and irrigation equipment that may be created using 3D printing. This add-on device's design might be altered to allow water to flow in several directions from a garden hose. The most popular material for 3D printing items and components is thermoplastic, which may be highly beneficial in agricultural water distribution systems since it can replace pricey, original parts. PLA thermoplastic is used as a printing medium in this application due to fused deposition modelling.

The 3D-printed spigot shown in Figure 12. was made specifically for a 5-gallon bucket [62]. It is made from the thermoplastic PLA using FDM technology. Additive Manufacturing, can be used to customize the size and dimensions of such a tool with a unique design and attachments like a contour that fits the specific water container. The technology enables efficient production and cost-effectiveness and of these parts.

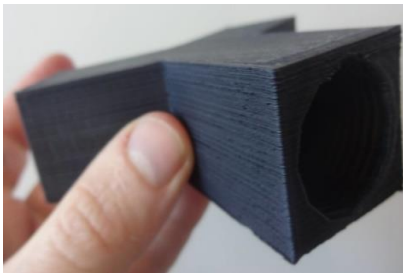


Figure 11. 3D printed garden hose splitter [66]



Figure 12. 3D printed spigot [66]

Table 2. 3D printing techniques, materials, and application used for 3D printing in agriculture [62].

3D Printed Part	3D Printing Technique	Material/Filament	Application	Reference
<i>Shovel and handle</i>	FDM	PLA	Urban Farming	[62]
<i>Fruit picker</i>	FDM	PLA	Urban Farming	[62]
<i>Sprinkler</i>	FDM	ABS	Irrigation	[66]
<i>Hose splitter</i>	FDM	PLA	Irrigation	[62]
<i>Corn Auger</i>	FDM	PLA	Spare Part	[63]
<i>Gear</i>	FDM	Polymeric material	Spare Part	[64]
<i>Spigot</i>	FDM	PLA	Water Management	[62]
<i>Packer bottom</i>	FDM	ABS	Testing Equipment	[65]

5. Conclusion

3D printing is now used in many different fields. From manual labour to making machines that help us fabricating the products we consume and the parts which have practical applications. Additive manufacturing allows us to take our thoughts from the digital to the tangible also this technology allows us to save time and capital that we would have to spend on conventional manufacturing methods, which often involve lengthy and complicated processes. 3D printing can foster entrepreneurship among young people by allowing them to design and print their own models and potentially use of the technology as a business. Such businesses can also lead to collaboration between professional designers, entrepreneurs, and especially farmers, who are the main beneficiaries of additive manufacturing in agriculture. Research and development could be conducted to further increase the efficiency and quality of manufacturing and to find new materials that could be used as alternatives to common 3D printing materials such as thermoplastics [67].

With the advent of large-format 3D printers, large parts of at least 1 cubic meter, can now be produced, further expanding the applications of 3D printing. This paper showed some use cases of 3D printing in

agriculture. Specifically, the different materials used in 3D printing parts and the different printing technologies were discussed.

References

- [1] **Technologies ACF on AM, Terminology ACF on AMTSF 91** (2012) Standard terminology for additive manufacturing technologies. Astm International
- [2] **Joshi S. C., Sheikh A. A.** (2015) 3D printing in aerospace and its long-term sustainability. *Virtual Phys Prototyp* 10:175–185
- [3] **Murr L. E.** (2016) Frontiers of 3D Printing/Additive Manufacturing: from Human Organs to Aircraft Fabrication†. *J Mater Sci Technol* 32:987–995
- [4] **Korger M., Bergschneider J., Lutz M., Mahltig B., Finsterbusch K., Rabe M.** (2016) Possible Applications of 3D Printing Technology on Textile Substrates. *IOP Conf Ser Mater Sci Eng* 141:012011
- [5] **Revilla-León M., Özcan M.** (2019) Additive Manufacturing Technologies Used for Processing Polymers: Current Status and Potential Application in Prosthetic Dentistry: Polymer Additive Manufacturing for Prosthodontics. *J Prosthodont* 28:146–158
- [6] **Buchanan C., Gardner L.** (2019) Metal 3D printing in construction: A review of methods, research, applications, opportunities and challenges. *Eng Struct* 180:332–348
- [7] **Jasminka K., Josipa Š.** (2018) 3D print additive technology as a form of textile material substitute in clothing design – interdisciplinary approach in designing corsets and fashion accessories. *Ind Textila* 69:190–196
- [8] **Levy G. N., Schindel R., Kruth J. P.** (2003) Rapid Manufacturing and Rapid Tooling with Layer Manufacturing (LM) Technologies, State of the Art And Future Perspectives. *Cirp Ann* 52:589–609
- [9] **Cooper K.** (2001) Rapid Prototyping Technology. CRC Press, 0 Aufl.
- [10] **Kruth J. P.** (1991) Material Increment Manufacturing by Rapid Prototyping Techniques. *CIRP Ann* 40:603–614
- [11] **Bryll K., Piesowicz E., Szymański P., Ślaczka W., Pijanowski M.** (2018) Polymer composite manufacturing by FDM 3D printing technology. *MATEC Web of Conferences*. EDP Sciences, Bd. 237 02006
- [12] **Slavko D., Matic K.** (2010) Selective laser sintering of composite materials technologies. *Annals of DAAAM & Proceedings*, Bd. 21
- [13] **Liu C., Huang N., Xu F., Tong J., Chen Z., Gui X., Fu Y., Lao C.** (2018) 3D Printing Technologies for Flexible Tactile Sensors toward Wearable Electronics and Electronic Skin. *Polymers* 10:629
- [14] **Wang J., Goyanes A., Gaisford S., Basit A. W.** (2016) Stereolithographic (SLA) 3D printing of oral modified-release dosage forms. *Int J Pharm* 503:207–212
- [15] **Ahn D., Kweon J.-H., Choi J., Lee S.** (2012) Quantification of surface roughness of parts processed by laminated object manufacturing. *J Mater Process Technol* 212:339–346
- [16] **Turner B. N., Strong R., Gold S. A.** (2014) A review of melt extrusion additive manufacturing processes: I. Process design and modeling. *Rapid Prototyp J* 20:192–204
- [17] **Dizon J. R. C., Espera Jr A. H., Chen Q., Advincula R. C.** (2018) Mechanical characterization of 3D-printed polymers. *Addit Manuf* 20:44–67
- [18] **Diego J.R., Martinez D. W. C., Robles G. S., Dizon J. R. C.** (2021) Development of smartphone-controlled hand and arm exoskeleton for persons with disability. *Open Eng* 11:161–170
- [19] **Dizon J. R. C., Gache C. C. L., Cascolan H. M. S., Cancino L. T., Advincula R. C.** (2021) Post-processing of 3D-printed polymers. *Technologies* 9:61
- [20] **Valino A. D., Dizon J. R. C., Espera A. H., Chen Q., Messman J., Advincula R. C.** (2019) Advances in 3D printing of thermoplastic polymer composites and nanocomposites. *Prog Polym Sci* 98:101162
- [21] **Dong Y., Fan S.-Q., Shen Y., Yang J.-X., Yan P., Chen Y.-P., Li J., Guo J.-S., Duan X.-M., Fang F.** (2015) A novel bio-carrier fabricated using 3D printing technique for wastewater treatment. *Sci Rep* 5:1–10
- [22] **Espera A. H., Dizon J. R. C., Chen Q., Advincula R. C.** (2019) 3D-printing and advanced manufacturing for electronics. *Prog Addit Manuf* 1–23
- [23] **Tijing L., Dizon J. R., Cruz Jr. G.** (2021) 3D-Printed Absorbers for Solar-Driven Interfacial Water Evaporation: A Mini-Review. *Adv Sustain Sci Eng Technol* 3:0210103

- [24] **Advincula R. C., Dizon J. R. C., Chen Q., Niu I., Chung J., Kilpatrick L., Newman R.** (2020) Additive manufacturing for COVID-19: devices, materials, prospects, and challenges. *MRS Commun* 10:413
- [25] **Pearce J.** (2013) Applications of open source 3-D printing on small farms. *Org Farming* 1:19–35
- [26] **Podchasov E. O.** (2021) Design and Technological Features of 3D-Printing. *work* 5:9
- [27] **Cotteleer D. M. J.** (o. J.) 3D opportunity: Additive manufacturing paths to performance, innovation, and growth 23
- [28] **Ngo T. D., Kashani A., Imbalzano G., Nguyen K. T. Q., Hui D.** (2018) Additive manufacturing (3D printing): A review of materials, methods, applications and challenges. *Compos Part B Eng* 143:172–196
- [29] **Taheri H., Shoaib M. R. B. M., Koester L. W., Bigelow T. A., Collins P. C., Bond L. J.** (2017) Powder-based additive manufacturing-a review of types of defects, generation mechanisms, detection, property evaluation and metrology. *Int J Addit Subtractive Mater Manuf* 1:172–209
- [30] **Liu Y., Wang W., Zhang L.-C.** (2017) Additive manufacturing techniques and their biomedical applications. *Fam Med Community Health* 5:286–298
- [31] **Castoro M., Kumpaty S.** (2013) Impact of laser power and build orientation on the mechanical properties of selectively laser sintered parts. *Proceedings of The National Conference on Undergraduate Research (NCUR)*. University of Wisconsin La Crosse, WI
- [32] **Kang J., Shangguan H., Deng C., Hu Y., Yi J., Wang X., Zhang X., Huang T.** (2018) Additive manufacturing-driven mold design for castings. *Addit Manuf* 22:472–478
- [33] **Nandi C., Caspi A., Grossman D., Tatlock Z.** (2017) Programming language tools and techniques for 3D printing. 2nd Summit on Advances in Programming Languages (SNAPL 2017). Schloss Dagstuhl-Leibniz-Zentrum fuer Informatik
- [34] **Araya-Calvo M., López-Gómez I., Chamberlain-Simon N., León-Salazar J. L., Guillén-Girón T., Corrales-Cordero J. S., Sánchez-Brenes O.** (2018) Evaluation of compressive and flexural properties of continuous fiber fabrication additive manufacturing technology. *Addit Manuf* 22:157–164
- [35] **Noorani R.** (2006) *Rapid prototyping: principles and applications*. John Wiley & Sons Incorporated
- [36] **Shahrubudin N., Lee T. C., Ramlan R.** (2019) An Overview on 3D Printing Technology: Technological, Materials, and Applications. *Procedia Manuf* 35:1286–1296
- [37] **Gibson I., Rosen D., Stucker B., Khorasani M.** (2021) *Additive manufacturing technologies*. Springer: Cham, Switzerland, Third edition
- [38] **Tofail S. A. M., Koumoulos E. P., Bandyopadhyay A., Bose S., O'Donoghue L., Charitidis C.** (2018) Additive manufacturing: scientific and technological challenges, market uptake and opportunities. *Mater Today* 21:22–37
- [39] **Dilberoglu U. M., Gharehpapagh B., Yaman U., Dolen M.** (2017) The Role of Additive Manufacturing in the Era of Industry 4.0. *Procedia Manuf* 11:545–554
- [40] **Duda T., Raghavan L. V.** (2016) 3D metal printing technology. *IFAC-Pap* 49:103–110
- [41] **Syvanen T., Nyrhila O., Kotila J.** (2009) Metal powder for use in an additive method for the production of three-dimensional objects and method using such metal powder. *Google Patents*
- [42] **Brown S. L., Pierson H. A.** (2018) Digital design integrity for additive manufacturing: examining reliability issues in the digital preproduction process. *Int J Rapid Manuf* 7:43–58
- [43] **Osswald T. A., Puentes J., Kattinger J.** (2018) Fused filament fabrication melting model. *Addit Manuf* 22:51–59
- [44] **Mostafa N., Syed H. M., Igor S., Andrew G.** (2009) A study of melt flow analysis of an ABS-Iron composite in fused deposition modelling process. *Tsinghua Sci Technol* 14:29–37
- [45] **Harris A. M., Lee E. C.** (2008) Improving mechanical performance of injection molded PLA by controlling crystallinity. *J Appl Polym Sci* 107:2246–2255
- [46] **Benwood C., Anstey A., Andrzejewski J., Misra M., Mohanty A. K.** (2018) Improving the Impact Strength and Heat Resistance of 3D Printed Models: Structure, Property, and Processing Correlations during Fused Deposition Modeling (FDM) of Poly(Lactic Acid). *ACS Omega* 3:4400–4411
- [47] **Yang Z., Peng H., Wang W., Liu T.** (2010) Crystallization behavior of poly(ϵ -caprolactone)/layered double hydroxide nanocomposites. *J Appl Polym Sci* NA-NA

- [48] **Wittbrodt B., Pearce J. M.** (2015) The effects of PLA color on material properties of 3-D printed components. *Addit Manuf* 8:110–116
- [49] **Avérous L.** (2008) *Polylactic Acid: Synthesis, Properties and Applications. Monomers, Polymers and Composites from Renewable Resources.* Elsevier, 433–450
- [50] **Tymrak B. M., Kreiger M., Pearce J. M.** (2014) Mechanical properties of components fabricated with open-source 3-D printers under realistic environmental conditions. *Mater Des* 58:242–246
- [51] **Yang T.-C.** (2018) Effect of Extrusion Temperature on the Physico-Mechanical Properties of Unidirectional Wood Fiber-Reinforced Polylactic Acid Composite (WFRPC) Components Using Fused Deposition Modeling. *Polymers* 10:976
- [52] **Lopes M. S., Jardini A. L., Filho R. M.** (2012) Poly (Lactic Acid) Production for Tissue Engineering Applications. *Procedia Eng* 42:1402–1413
- [53] **Casalini T., Rossi F., Castrovinci A., Perale G.** (2019) A Perspective on Polylactic Acid-Based Polymers Use for Nanoparticles Synthesis and Applications. *Front Bioeng Biotechnol* 7:259
- [54] **Zhang H., Cai L., Golub M., Zhang Y., Yang X., Schlarman K., Zhang J.** (2018) Tensile, Creep, and Fatigue Behaviors of 3D-Printed Acrylonitrile Butadiene Styrene. *J Mater Eng Perform* 27:57–62
- [55] **Sumithra H., Sidda Reddy B.** (2018) A review on tribological behaviour of natural reinforced composites. *J Reinf Plast Compos* 37:349–353
- [56] **Selvamani S. K., Samykano M., Subramaniam S. R., Ngui W. K., Kadirgama K., Kanagaraj G., Idris M. S.** (2019) 3D printing: Overview of ABS evolvement. *Gehalten auf der Proceedings of the 3rd International Conference on Automotive Innovation Green Energy Vehicle: AIGEV 2018, Kuantan, Malaysia, 020041*
- [57] **Ayrilmis N., Kariz M., Kwon J. H., Kitek Kuzman M.** (2019) Effect of printing layer thickness on water absorption and mechanical properties of 3D-printed wood/PLA composite materials. *Int J Adv Manuf Technol* 102:2195–2200
- [58] **Begum S. A., Rane A. V., Kanny K.** (2020) Applications of compatibilized polymer blends in automobile industry. *Compatibilization of Polymer Blends.* Elsevier, 563–593
- [59] **Patil A., Patel A., Purohit R.** (2017) An overview of Polymeric Materials for Automotive Applications. *Mater Today Proc* 4:3807–3815
- [60] **Fu X., Zhang X., Huang Z.** (2021) Axial crushing of Nylon and Al/Nylon hybrid tubes by FDM 3D printing. *Compos Struct* 256:113055
- [61] **Tuan Rahim T. N. A., Abdullah A. M., Md Akil H., Mohamad D., Rajion Z. A.** (2015) Preparation and characterization of a newly developed polyamide composite utilising an affordable 3D printer. *J Reinf Plast Compos* 34:1628–1638
- [62] **Pearce J. M.** (2015) Applications of Open Source 3-D Printing on Small Farms. *Org Farming* 1:19–35
- [63] **Admin** (o. J.) 3D Printing in Agriculture | How 3D Printer uses for Agriculture (Zugriff vom 30.01.2022). <https://garuda3d.com/3d-printing-in-agriculture>
- [64] **Lukaszewski K., Buchwald T., Wichniarek R.** (2021) The FDM Technique in Processes of Prototyping Spare Parts for Servicing and Repairing Agricultural Machines: A General Outline. *Int J Appl Mech Eng* 26:145–155
- [65] **3D Printing Helps Test Crop Seeding System** - 3DPrint.com | The Voice of 3D Printing / Additive Manufacturing (o. J.) (Zugriff vom 30.01.2022). <https://3dprint.com/48469/3d-printing-groundbreaking/>
- [66] **Farm Tech** (o. J.) (Zugriff vom 30.01.2022). <https://proximitydesigns.org/service/farm-tech/>
- [67] **Exploring the potential of 3D printing for agriculture** (o. J.) (Zugriff vom 30.01.2022). <https://www.cta.int/en/blog/all/article/exploring-the-potential-of-3d-printing-for-agriculture-sid0e875bb2c-478a-4577-975b-a8197d441ef3>
- [68] **Oussai A., Bártfai Z., Kátai L.** (2021); Development of 3D Printing Raw Materials from Plastic Waste. A Case Study on Recycled Polyethylene Terephthalate; *APPLIED SCIENCES-BASEL* 11 : 16 Paper: 7338 , 10 p.
- [69] **Oussai A., Katali L., Bártfai Z.** (2020); Development Of 3d Printing Raw Materials From Plastic Waste, *Hungarian Agricultural Engineering*: 37 pp. 34-40. , 7 p.
- [70] **Oussai A., Bártfai Z., Kátai L.,** (2022); A Small-Scale Recycling technology: Proposal of Plastic waste recycling Technic, *American Journal Of Engineering Research* 11 : 1 pp. 36-41. , 6 p.

TESTING AXIAL FLOW SOLAR CHIMNEY TURBINE USING WIND TUNNEL

Author:

W. M. A.-Elmagid^{1,2}

Affiliation:

¹ Institute of Technology - Hungarian University of Agriculture and Life Sciences, 2100 Gödöllő, Péter Károly u. 1., Hungary;

² Dept. of Mech. Power Engineering, Faculty of Energy Engineering, Aswan University, Sahary, P.O. Box 81525, Aswan, Egypt;

Email address:

w.abdelmaged@aswu.edu.eg

Abstract: The solar chimney power plant (SCPP) is a modernistic and promising technology, which utilizes the combination of solar heating and chimney effect for producing electricity. Solar collector, updraft tower and air turbine are the main components of a solar chimney unit, however, the turbine plays a royal role because it converts the kinetic energy of the heating air into useful mechanical energy. In this study, I measured the power, flow rate, rotational speed and pressure drop of the designed and industrial turbines within the wind tunnel, and the power coefficient of the turbines are calculated by measured values. The turbine was designed according to the blade element theory modified to consider the surrounding duct. we measured the electric power, flow rate and pressure drop of the turbine, and the power coefficient of the turbine is calculated by measured values. Testing of the designed and industrial turbine within wind tunnel shows that the highest power coefficient of the designed turbine is 0.45, while the highest power coefficient of the industrial turbine is 0.32. The designed turbine produces 28.89% higher than the industrial one.

Keywords: axial turbine, wind tunnel measurement, solar chimney power plant, turbine of SCPP

1. Introduction

The energy system in the entire world is depending on fossil fuel and this fuel has harsh effects on the human environment. Finding alternative sources is an essential issue nowadays, so many researchers focus to develop renewable energy as a way of solving energy issues. The solar chimney power plant is a renewable source, which heats the ambient air by solar radiation inside the solar collector. The updraft tower is located in the center of the collector and increases the kinetic energy of the hot air according to a chimney effect principle, as shown Figure 1. The air turbine is the most important component, it produces beneficial mechanical power by converting the kinetic energy of the hot air and controls the airflow inside the SCPP system that effect on the other system components.

In 1976, M. Simon showed the solar chimney has reasonable economic feasibility for production of the SCPP. Haaf et al. [1] was continuing Simon's work in 1979 by developing the first pilot prototype of SCPP in Manzanares, Spain, which was designed peak output of 50 kW, whereas in fact, the measured output was 36 kW [2]. This pilot plant was testing from the year 1982 to 1989. The most important finding of the prototype is the solar chimney concept has enough technically viable and operated reliably for electricity production. In 2002, Gannon and von Backström [3] redesign the turbine of the Manzanares prototype by using free vortex design, their configuration is a single-stage blade rotor with inlet guide vane. They carried out the experimental test to evaluate the proposed turbine. They conclude the proposed design has a total-to-static efficiency of 77-80% and a total-to-total efficiency of 85-90% [4].

On the other hand, researcher used other theory to design solar chimney turbine. Y Zhou et al. [5] used Wilson theory to propose design for solar chimney with vertical collector. The wind tunnel test was carried

out to optimize the number of blades turbine and tip speed ratio of their design. Tingzhen et al [6] designed the wind turbine for MW-graded solar chimney power plant system and investigated their turbine by computational fluid dynamic (CFD). To validate the theoretical results, the CFD simulation model was compared with the experimental results of the Manzanares prototype using similar dimensions.

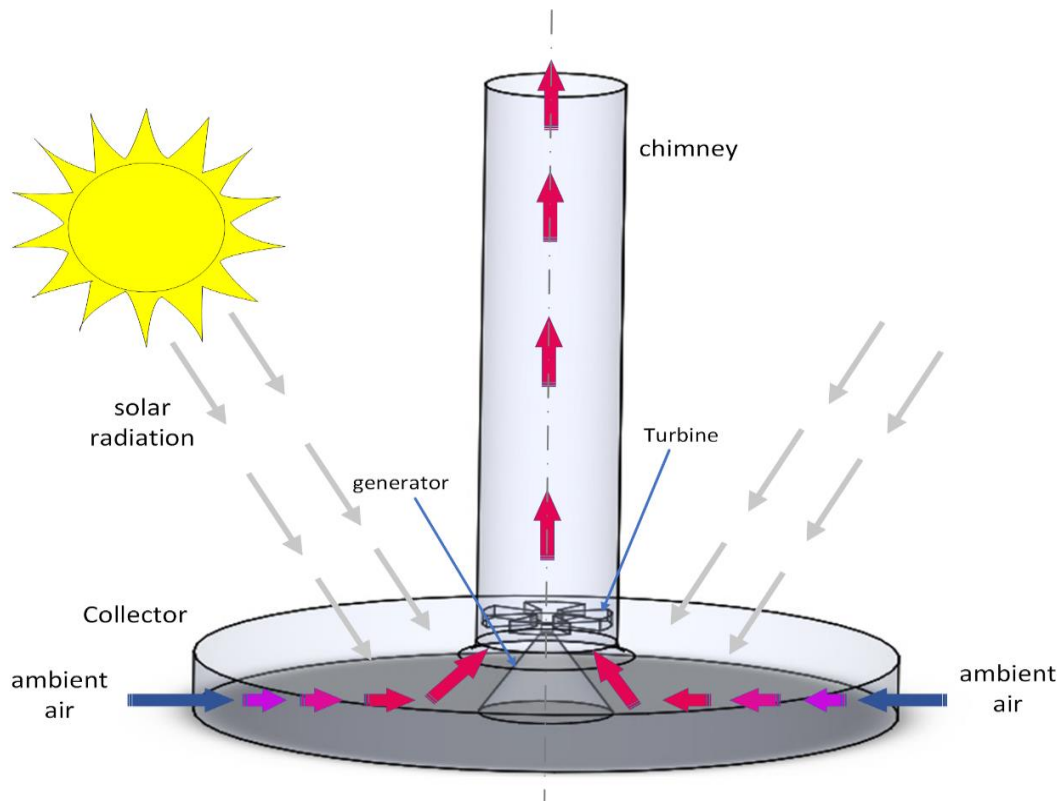


Figure 1. Schematic diagram of SCPP

Many studies proposed approaches of a solar chimney turbine and all of them aim to maximize the output power of SCPP system. Denantes and Bilgen [7] presented two counter vertical rotor turbines approached with/without inlet guide vanes and compared the performance of the presented configuration to a single turbine. Fluri and von Backström [8] presented many solar chimney turbine approaches; horizontal turbine, single vertical and counter vertical with/ without inlet guide vanes. Their conclusion is a vertical single turbine has the lowest efficiency but the widest efficiency range. Both of studies [7] and [8] used the mathematical model to demonstrate their results.

Lipnicki et al. [9] solved momentum, mass, and energy conservation equations of airflow inside a solar chimney system and used dimensionless numbers to describe the heat transfer phenomenon of a solar chimney system, then they compared the theoretical and experimental results. Pasumarthi and Sherif [10] also used the mathematical model to study effect of various parameters on the performance of SCPP. To validate theoretical these results, they carried out the experiment work and compared it against theoretical results [11]. Muhammed and Atrooshi [12] studied the collector and chimney area by modeling the heat and transport relations, they aimed to optimize dimensions for a solar chimney plant. Ismail et al. [13] improve both flow field and heat transfer characteristics of a collector of an SCPP using passive flow control, approaches have been numerically examined. Another configuration to improve the heat transfer inside collector is presented by Fu [14], who proposed a partial inclined and convergent collector design to enhance energy conversion efficiency. Nasraoui et al. [15] studied the effect of the chimney shape on the SCPP performance by testing different shapes numerically and experimentally.

Solar chimney system has a capability of cooperation the other renewable system for increasing profitable. Ahmed and Hussein [16] presented and tested the hybrid system of a solar chimney and PV panel to find the best configuration, which achieves the maximum available output power. Aurybi et al. [17] increased the output power of SCPP by adding thermal enhancing channels inside the collector. This proposed change

increases the kinetic energy of the air, because of increasing the exit temperature of the collector especially at night time. Zuo et al. [18] proposed the integration solar chimney system and solar desalination technology and Zuo et al. [19] evaluated the performance of combination of a solar chimney power plant, seawater desalination and waste heat with/ without a wind supercharging.

In this study, I manufactured the solar chimney turbine by the 3D printing technology. The blade calculation was according to the Blade element theory (BET) as shown in ref [20] by author. Tests of the turbine are carried out on a wind tunnel of 1m diameter and 8 m length. I measured the electrical output power, pressure difference around the turbine and airflow rate to calculate dimensionless parameters.

2. Descriptions of the apparatus

Experimental works provide an accurate and realistic performance of the physical system; however, it is costly because of requiring more infrastructure. Therefore, we consider the experiment is an essential part of any research work. A wind tunnel is usually used for testing turbomachines because it saves the criteria of the operation condition during testing by strictly controlling inflow conditions. The blades and hub are a main construction of the conventional axial flow turbine; however, the blade shape has the essential influence of the capability to capture the energy from the air flow.

The rig of the experiment should allow for a detailed investigation of the turbine performance and satisfy the design objectives listed above. In this study, we chose the wind tunnel technique to test the solar chimney turbine, a wind tunnel is usually used for testing turbomachines because it saves the criteria of the operation condition during testing by strictly controlling inflow conditions. The blades and hub are a main construction of the conventional axial flow turbine; the blade consists of the aerofoils that interact with the hot air and convert the power in the air to mechanical power. The geometry and dimensions of the blades are determined by characteristics flow of SCPP to make it an optimum. 3D printing is used to manufacture blades of turbine prototype according to calculations of BET theory.

The tested prototype comprises the four-blade turbine rotor, which connects to the electrical generator that working as the load of the turbine. The hub is the part that transmits all the power and loads from the blades to the generator shaft. I designed the hub as two parts that makes it can change the angle of the blades, and easy to manufacture and assemble by 8 bolts. Figure 2. shows the prototype hub, which manufactured of polyethylene.

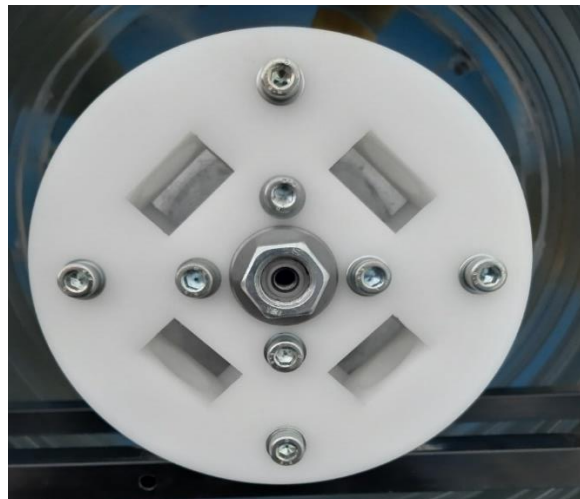


Figure 2. The hub of the tested turbine

The experiment is carried out in the energy laboratory, Hungarian University of Agriculture and Life Sciences (MATE) at Gödöllő campus. I used the wind tunnel, 8 m of length and 1 m of the square/circle cross-section, as shown Figure 3. Its first block from the inlet side has the laminar basket for damping the inference of surrounding. The draft fan connects with the suitable inverter, the inverter saves a proper control of the rotational speed of the fan, consequence, providing the control of the airflow velocity.



Figure 3. The wind tunnel at Hungarian University of Agriculture and Life Sciences (MATE) at Gödöllő campus

3. Measurement strategy

To evaluate the performance of the solar chimney turbine from the experimental rig, certain physical properties have to be measured, then, the dimensionless variables have to be determined from this measured quantity. The Physics quantity as:

- Airflow velocity, v_{in} .
- Pressure drops around turbine, $\Delta p_{tur,st}$.
- DC Voltage, V .
- DC Current, I .
- Outside Air temperature and humidity.
- Reference pressure.
- Rotational speed of the turbine.

Figure 4 shows the schematic and layout of the wind tunnel testing for the designed turbine. After fixation the rotor of the turbine on the generator shaft and the prob of the sensors as shown in Figure 4, the procedure of the solar chimney turbine will be carried out by following the next steps:

- 1- Turn on the fan on the low speed and check the sensors reading on the laptop screen.
- 2- Adjust the fan on the required speed and waiting for few minutes to achieve steady state operation.
- 3- Change excitation voltage of the generator
- 4- Start recording the data logger and manual reading (electric power, voltage, and current) for about 15 minutes
- 5- Stop the fan and prepare to the next reading
- 6- Repeat the above steps with a new speed

4. The sensors of the measurements

Many sensors were used in this work, all sensors connect to the data logger of ALMEMO 2590-9, which has 8 channels for sensors, and two channels for commination computer or other data logger. ALMEMO Control 5.20 software is used on the computer system to read the recorded value, then making it presentable. Figure 5 shows the location of the sensors inside the wind tunnel the more details about each sensor as following:

- *Anemometer*

One of the main parameters that affects the performance of the turbine is the inlet air velocity. FVAD 15-H series hot-wire anemometer instrument was used to measure the air velocity then the air mass flow can be

calculated by multiplying with the cross-section area and the air outlet density. The measuring range is 0.3 to 40 m/s. The anemometer works with ALMEMO 2590-9 Data logger. The accuracy is $\pm 2\%$ with mentioned working range. The air flow rate had been measured 2.5m from the inlet of the wind tunnel as shown in Figure 5.

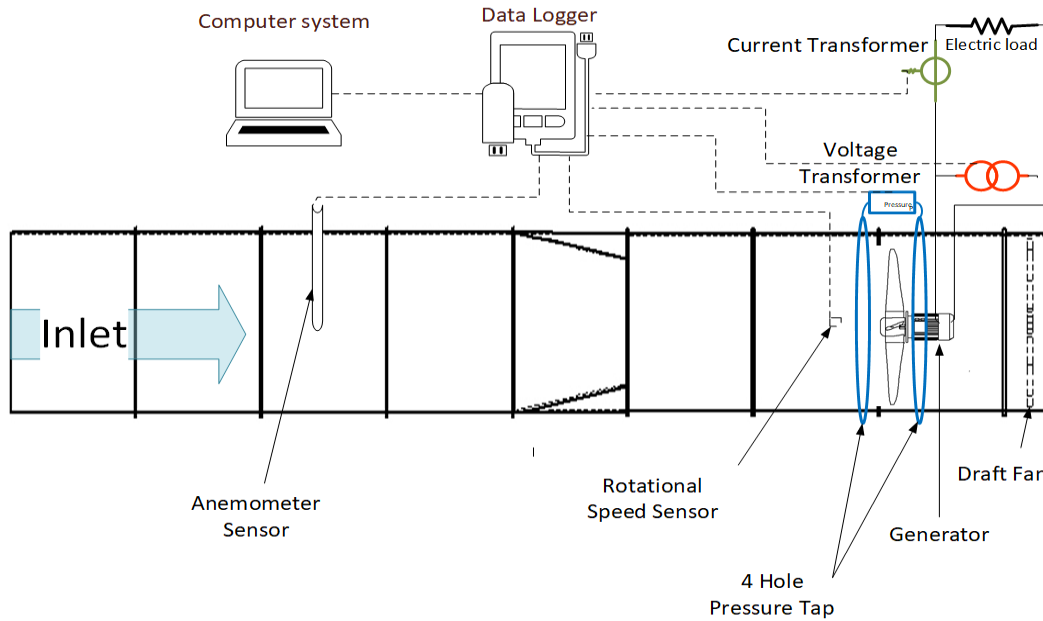


Figure 4. Schematic diagram of testing the turbine within wind tunnel

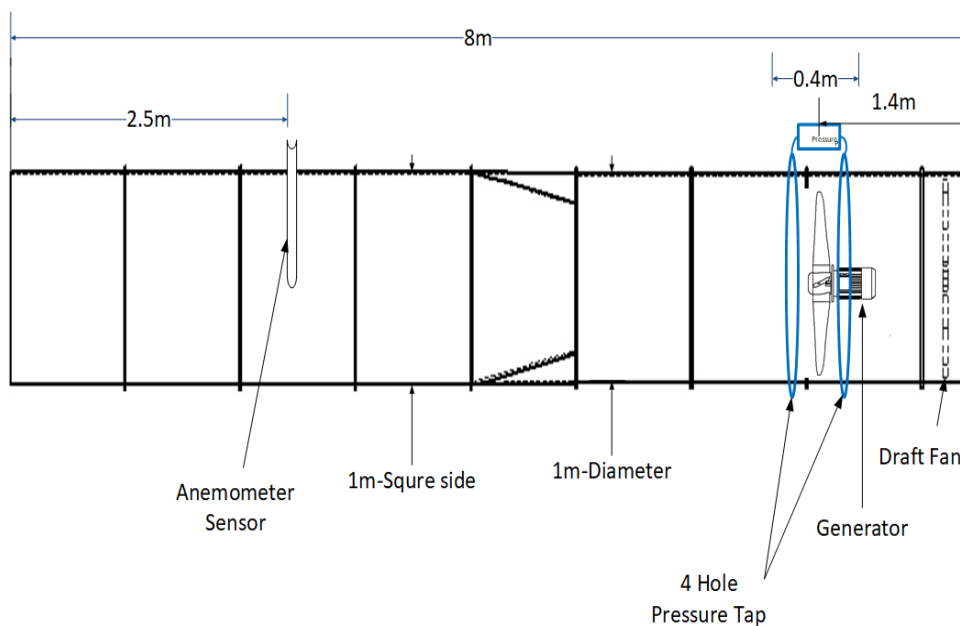


Figure 5. Locations of the sensors on the wind tunnel

- *Pressure gauge*

The effect of the turbine on the airflow reveals by the pressure drop of it, the pressure difference around the turbine indicates to us; the quantity of power that the turbine can absorb from the airflow. An FDA 602 S1K / S6K Differential pressure is used to measure the pressure drop around the turbine, it has Max. common mode pressure 700 mbar within -10 to +60 °C, 10 to 90% RH, and its dimension is 74 x 20 x 8.8 mm. Figure

6 shows the pressure sensor, which also can work with ALMEMO 2590-9 Data logger and its Accuracy is $\pm 0.5\%$ of final value in range zero to positive final value.



Figure 6. Differential pressure sensor

4. Results

Wind tunnel testing provides an accurate performance of the physics system, but they do it under the very strict operating conditions to ensure the stability of the system. This condition and stability assist in the systems investigation and going deeply in some point. I tested two turbines; the industrial fan rotor that was manufactured by MULTI WING and model of MWCZF2505041, and the second one is the turbine designed according to our calculation, which was manufactured by 3D printing technology. The geometry of the experimented elements is shown in Figure 7 as; Figure 7-a show the designed blade and Figure 7-b show the industrial one.



a. Designed blade



b. Industrial blade

Figure 7. Geometry of the experimented blade

The electrical load of the turbine is the generator, changing the excitation to change the torque against turbine torque. Figure 8. shows the different excitation of the generator for the industrial turbine. The change of the excitation has a minor effect on the rotational speed of the turbine because the turbine works at the near its designed tip speed ratio. The generator construction puts its limit on the excitation power.

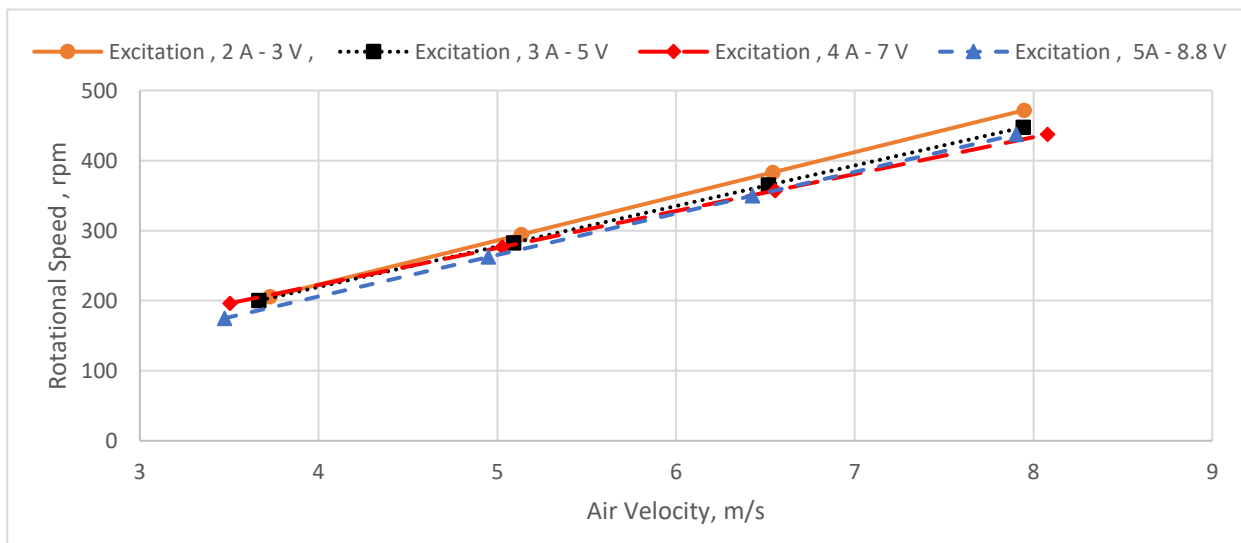


Figure 8. The rotational speed of the industrial turbine at the different excitation power

The generator shows the same behaviour on the designed turbine, as shows in Figure 9. The turbine has the higher rotational speed on the 8 m/s as design point while I calculated my design at 5.5 Tip speed ratio. The designed turbine achieved higher rotational speed than the industrial one at low air velocity (5-8 m/s), that give the designed turbine advantages to work at this range of air velocity.

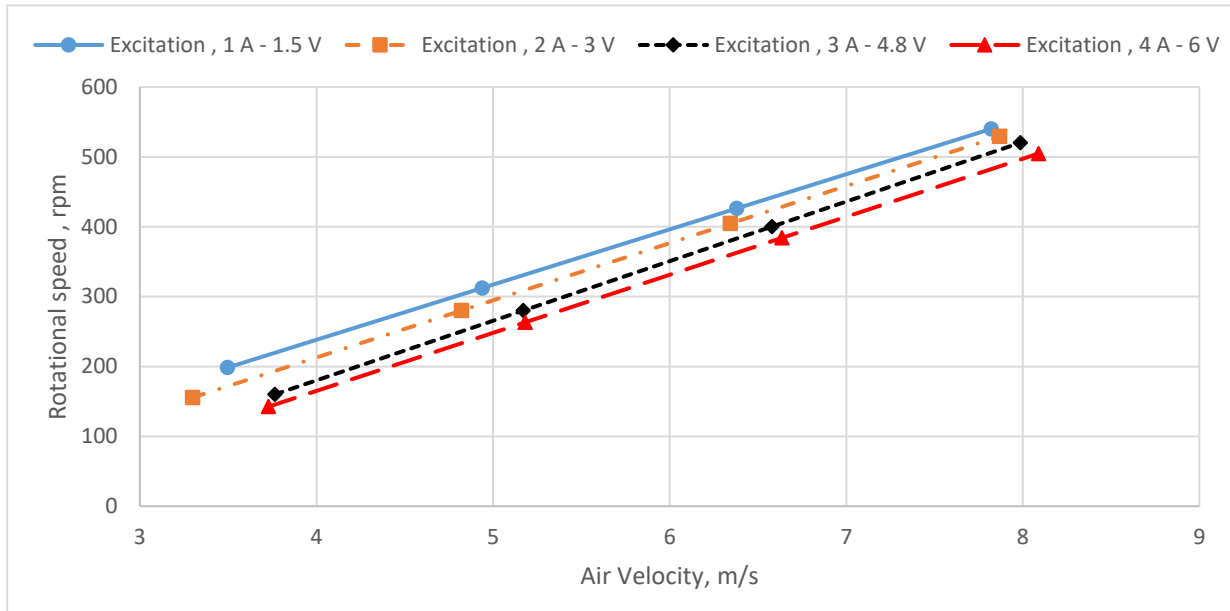


Figure 9. the rotational speed of the designed turbine at the different excitation power

Figure 10 shows the pressure drop by the turbine pressure drop has a dominant influence on performing the SCP, indicates what energy is absorbed by the turbine at excitation of generator by 2 A - 3 V. The pressure drops increases with increasing the inlet velocity because more energy is available for the turbine by the airflow. Generally, the pressure drop of the designed turbine is higher than the industrial turbine by 1.5 times approximately at all points. The designed turbine achieved 65.08 Pa of the pressure drop, while the industrial turbine achieved 43.93 Pa at the inlet velocity of 15 m/s.

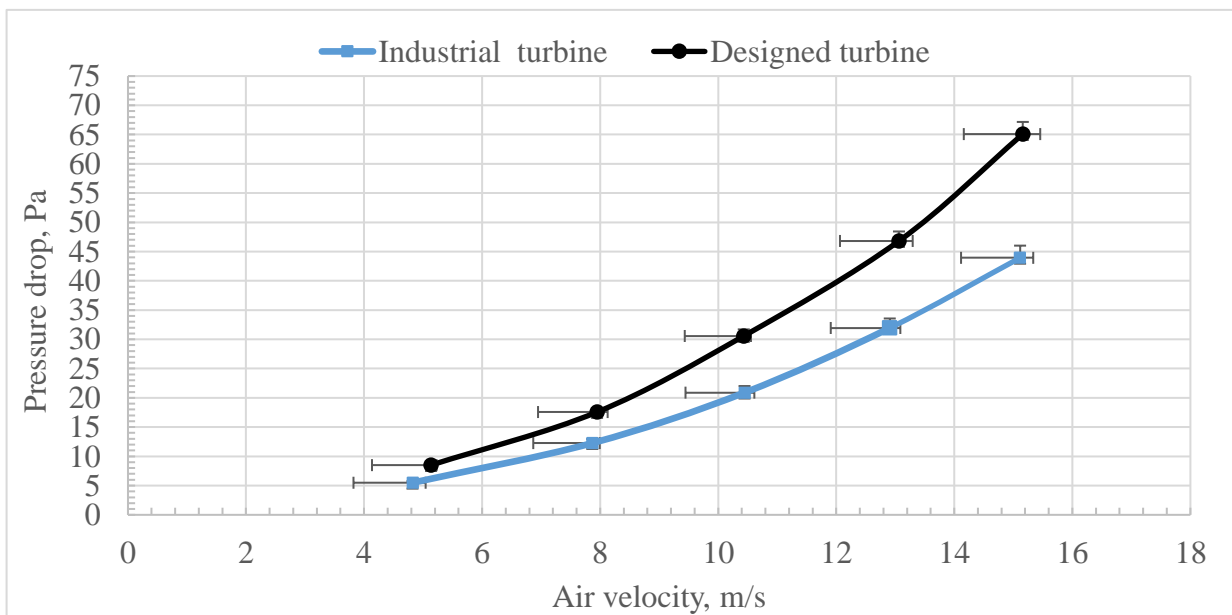


Figure 10. Pressure drop around the turbine

Output power is the major purpose of the system, the turbine produces power that is proportional to inlet fluid power. In the case of the shrouded turbine, fluid power is a combination of the kinetic energy of airflow and pressure energy. Figure 11. shows the power of the turbine according to the inlet velocity of the airflow at excitation of generator by 2 A - 3 V. The designed turbine achieved more power than the industrial one. The designed turbine comprises 4 blades, and the industrial turbine comprises 3 blades, the designed turbine produces 520 W, and the industrial turbine provides 380 at 15 m/s inlet velocity. Thus, the designed turbine produces 26.92 % higher than the industrial one as average increase on all points.

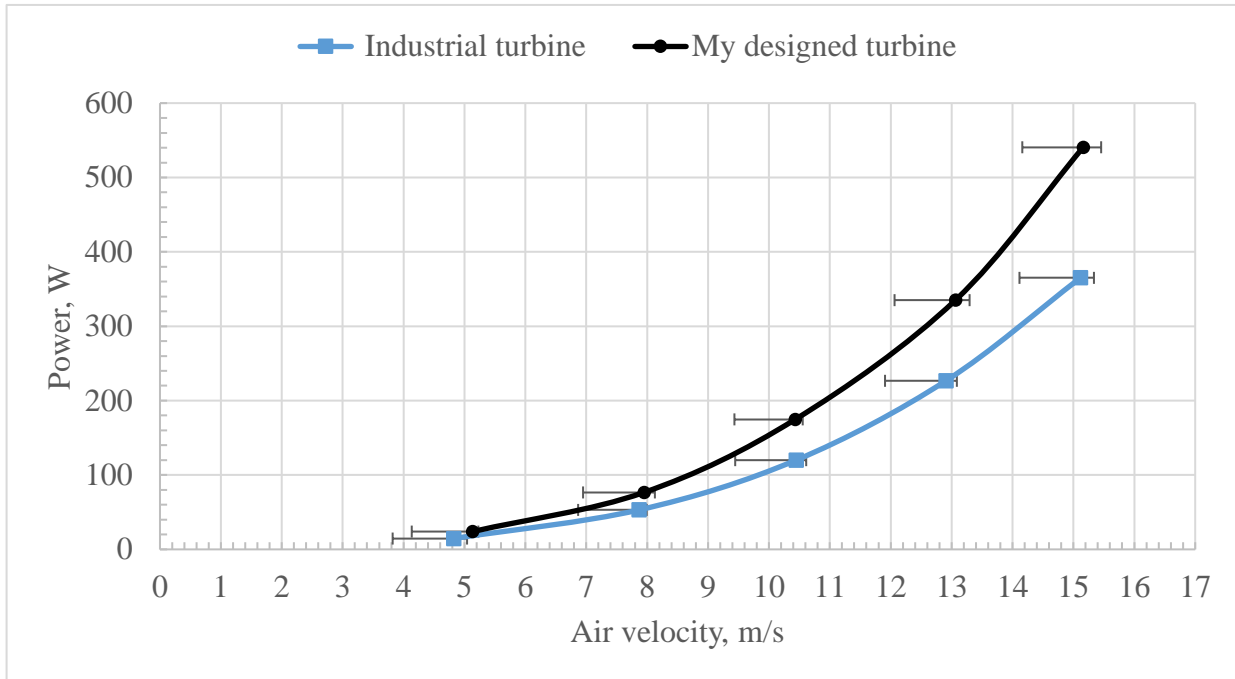


Figure 11. Power of the turbine vs. the inlet velocity

5. Conclusions

Wind tunnel testing provides an accurate performance of the physics system. The experiment is in the energy laboratory, Hungarian University of Agriculture and Life Sciences (MATE) at Gödöllő campus. I tested two turbines; an industrial fan rotor that was manufactured by MULTI WING and model of MWCZF2505041, and a turbine designed according to my calculations and manufactured by 3D printing technology. we measured the power, flow rate, rotational speed and pressure drop of the designed and industrial turbines within the wind tunnel, and the power coefficient of the turbines are calculated by measured values.

The turbine designed by me achieved more power than the industrial one. The designed turbine comprises 4 blades, and the industrial turbine comprises 3 blades. The turbine designed by me produced 520, and the industrial turbine provided 380 W at 15 m/s inlet velocity. Thus, my designed turbine produced near to 12% higher power than the industrial one on all points of measurement.

Power coefficient and tip speed ratio variables have to be determined from the measured quantity, as shown in Table 1.. Figure 12. shows the power coefficient that achieved according to tip speed ratio. The highest power coefficient of the designed turbine is 0.45 achieved at a 5 tip speed ratio, while it was designed at 5.5 tip speed ratio. The highest power coefficient of the industrial turbine is 0.32 achieved at a 3.3 tip speed ratio. The designed turbine achieved power coefficient 1.4 times (approximately) higher than the other turbine.

Table 1. Sample of the experimental data

My Designed turbine				
Inlet Velocity (m/s)	Rotational speed (rpm)	Outlet Power (W)	Power Coefficient	Tip Speed ratio
4.949637112	476.9230769	23.33086675	0.44540822	5.045144391
7.902899913	823.0769231	75.96867313	0.3563055	5.453214313
10.56070584	612.3076923	173.0338108	0.34009446	3.035815624
13.03536116	727.6923077	320.791605	0.33527504	2.922963135
15.38203959	878.4615385	536.8006359	0.34144336	2.990249657
16.66507328	1026.153846	767.3410202	0.38380812	3.224065615
Industrial turbine				
Inlet Velocity (m/s)	Rotational speed (rpm)	Outlet Power (W)	Power Coefficient	Tip speed ratio
5.170658438	280	17.64671834	0.29551112	2.835376943
7.984517832	520	54.18487745	0.24642198	3.409991299
10.45852021	735.3846154	122.2511203	0.24739422	3.681653585
12.74871903	916.9230769	219.740332	0.24550343	3.76586698
15.13228875	1123.076923	360.1664686	0.24062284	3.88600635

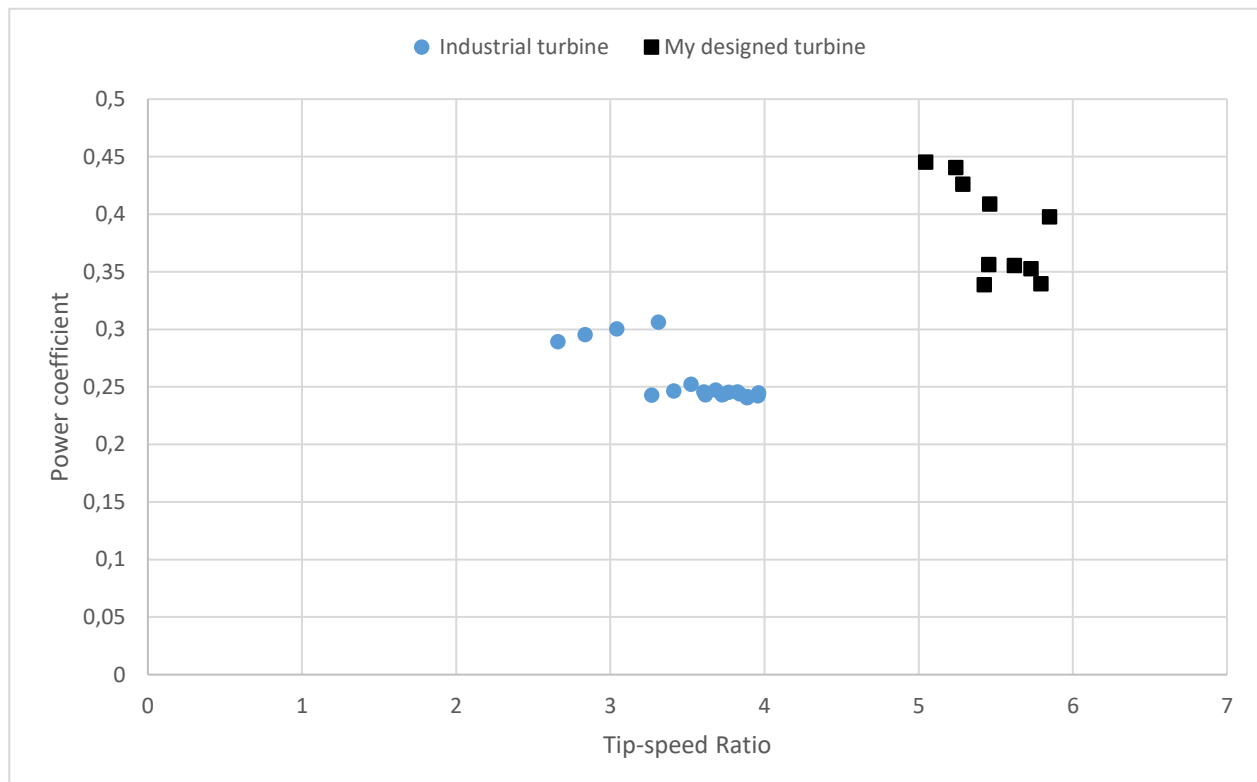


Figure 12. Power coefficient of the tested turbines

References

- [1] **W. Haaf, K. Friedrich, G. Mayr and J. Schlaich**, "Solar chimneys; Part I: Principle and construction of the pilot plant in Manzanares," *International Journal of Solar Energy*, no. 2, p. 3–20, 1983.
- [2] **W. Haaf**, "Solar chimneys; Part II: Preliminary test results from the Manzanares pilot plant," *International Journal of Solar Energy*, vol. 2, no. 2, pp. 141-161, 1984.
- [3] **Anthony J. Gannon and Theodor W. von Backström**, "Solar chimney turbine: Part 1 of 2 — Design," *ASME Solar 2002: International Solar Energy Conference*, pp. 335-341, 15–20 June 2002.
- [4] **Anthony J. Gannon and Theodor W. von Backström**, "Solar chimney turbine: Part 2 of 2 — Experimental Results," *ASME Solar 2002: International Solar Energy Conference*, pp. 343-349, 15–20 June 2002.
- [5] **Y Zhou, B Gao, H R Dong and K Hao**, "Design for the turbine of solar chimney power plant system with vertical collector," *IOP Conf. Series: Earth and Environmental Science*, vol. 40, no. 012085, 2016.
- [6] **Ming Tingzhen, Liu Wei, Xu Guoling, Xiong Yanbin, Guan Xuhu and Pan Yuan**, "Numerical simulation of the solar chimney power plant systems coupled with turbine," *Renewable Energy*, vol. 33, no. 5, pp. 897-905, May 2008.
- [7] **F. Denantes and E. Bilgen**, "Counter-rotating turbines for solar chimney," *Renewable Energy*, vol. 31, p. 1873–1891, 2006.
- [8] **T.P. Fluri and T.W. von Backström**, "Comparison of modelling approaches and layouts for solar chimney turbines," *Solar Energy*, vol. 82, p. 239–246, 2008.
- [9] **Zygmunt Lipnicki, Marta Gortych, Anna Staszczuk, Tadeusz Kuczyński and Piotr Grabas**, "Analytical and experimental investigation of the solar chimney system," *Energies*, vol. 12, no. 11, p. 2060, 2019.
- [10] **N. Pasumarthi and S. A. Sherif**, "Experimental and theoretical performance of a demonstration solar chimney model—Part I: mathematical model development," *International Journal of Energy Research*, vol. 22, no. 3, pp. 277-288, December 1998.
- [11] **N. Pasumarthi and S. A. Sherif**, "Experimental and theoretical performance of a demonstration solar chimney model—Part II: experimental and theoretical results and economic analysis," *International Journal of Energy Research*, vol. 22, no. 5, pp. 443-461, December 1998.
- [12] **Hardi A. Muhammed and Soorkeu A. Atrooshi**, "Modeling solar chimney for geometry optimization," *Renewable Energy*, vol. 138, pp. 212-223, August 2019.
- [13] **Alaa Ismail, Abd-Allah El-Marhoumy, A. M. Hamed and A. M. T. A. Eldein Hussin**, "Numerical modeling for a solar chimney," *Journal Of Al-Azhar University Engineering Sector*, vol. 14, no. 50, pp. 87-98, Jun 2019.
- [14] **Shijun Fu**, "An enhanced heat collector design and numerical simulation for solar chimney power plant," *IOP Conference Series: Materials Science and Engineering*, vol. 631, no. 042022, 2019.
- [15] **Haythem Nasraoui, Zied Driss and Hedi Kchaou**, "Effect of the chimney design on the thermal characteristics in solar chimney power plant," *Journal of Thermal Analysis and Calorimetry*, p. 1–12, November 2019.
- [16] **Omer Khalil Ahmed and Abdullah Sabah Hussein**, "New design of solar chimney (case study)," *Case Studies in Thermal Engineering*, vol. 11, pp. 105-112, March 2018.
- [17] **Mohammed A. Aurybi, S.I. Gilani, Hussain H. Al-Kayiem and Ali A. Ismaeel**, "Mathematical evaluation of solar chimney power plant collector, integrated with external heat source for non-interrupted power generation," *Sustainable Energy Technologies and Assessments*, vol. 30, pp. 59-67, December 2018.
- [18] **Lu Zuo, Ling Ding, Yue Yuan, Zihan Liu, Ning Qu and Pengzhan Dai**, "Research progress on integrated solar chimney system for freshwater production," *Global Energy Interconnection*, vol. 2, no. 3, pp. 214-223, June 2019.
- [19] **Lu Zuo, Zihan Liu, Ling Ding, Ning Qu, Pengzhan Dai, Bofeng Xu and Yue Yuan**, "Performance analysis of a wind supercharging solar chimney power plant combined with thermal plant for power

and freshwater generation," *Energy Conversion and Management*, Vols. In Press, Corrected Proof, November 2019.

- [20] **Elmagid W. M. A., Keppler I. and Molnar I.**, "Efficient Axial Flow Turbine for Solar Chimney," *J. Thermal Sci. Eng. Appl*, vol. 12, no. 3, p. 031012 (12 pages), Jun 2020.
- [21] **E. Babbie**, *The practice of social research*, 13th ed., USA Belmont: Wadsworth, Cengage Learning, 2013.
- [22] **M. Burawoy**, "The extended case method," *Sociological Theory*, pp. 4-33, 17 12 2002 .

ASSESEMENT AND MODELLING OF INDUSTRIAL-SCALE SOLAR THERMAL SYSTEM APPLICATION IN HUNGARY

Author(s):

R. Ghabour¹, P. Korzenszky²

Affiliation:

¹ Doctoral School of Mechanical Engineering – Hungarian University of Agriculture and Life Sciences, 2100 Gödöllő, Páter Károly u. 1., Hungary;

² Institute of Technology - Hungarian University of Agriculture and Life Sciences, 2100 Gödöllő, Páter Károly u. 1., Hungary;

Email address:

Ghabour.Rajab@phd.uni-mate.hu; Korzenszky.Peter.Emod@uni-mate.hu

Abstract: With approximately 1.2% growth annually, the industrial sector accounts for 54% of the total consumed energy globally. Most of those facilities use fossil fuels to generate their needs. Renewable energies, mainly solar energy, can play a major role in meeting the global policies of reducing carbon dioxide emissions. Presently, Hungarian researchers exploit more energy from renewable energies such as solar sources, wind, and biomass. Knowing that reducing the carbon emission level is a general tendency in Hungary. This article presents an extensive analysis of the solar thermal system in the central European climate, especially in Hungary. The scope of this study is the low-to-medium heat generation in industries such as pharmaceutical, pulp & paper textile, food processing and beverages. Through all the applications, the heat is consumed in hot water form. Integrating solar thermal technology in the industrial sector depends mainly on solar radiation, conventional fuel prices, available installation area, and the complexity level of integrating the solar system with the existing process. Furthermore, more challenges show up during the integration of economic difficulties. This article analyses the feasibility of providing industrial hot water for small-to-medium enterprises (SMEs) in different Hungarian counties. The analysis was performed using T*Sol 5.5 software, and metrological data were obtained by MeteoSyn built-in software. Results indicate that the most suitable region for integrating solar thermal energy was Szeged, Szolnok, and Kecskemet, which supplied 54.89%, 54.16%, and 54.03% of the total heat load for the studied case, respectively. This result accounts for 849.57, 840.25 and 839.27 kWh/m² of specific generated heat of the solar system. In addition, it results in points that the annual carbon dioxide saved amount is up to 4,442.3 kg and 2,100.7 m³ annual amount of natural gas. In conclusion, Hungary has a potentially attractive market for solar thermal systems to provide industrial hot water for small and medium-sized factories.

Keywords: buffer tank, solar heat, flowrate, heat process, solar thermal system

1. Introduction

Using conventional energy generation technologies to cover the increase of the energy demand worldwide results in health, pollution, and environmental issues [1]. Also, it is reported that the availability of conventional fossil fuels is decreasing in the coming years [2]. Furthermore, process heat in industry accounts for 35% of the final consumed energy worldwide, and it reaches up to 48% in Malaysia, 70% in China, and 29% in Europe [3,4]. At the same time, 60% of this energy is consumed at a temperature between 30°C to 250°C [5]. And 71% of this demand is in a heat form [6]. Generally, the process heat temperature used in industry is below 400°C. It is also noted that 80% of the used energy in industry is powered by natural gas and fossil fuel products. More than 30% of the industrial demand is due to the petrochemical and food industries. However, the share of solar energy in these sectors is nearly zero [7]. Up to 2020, not less than 95 solar thermal plants have been installed worldwide in the food industry, with a total capacity of 41 MW_{th} [8].

The thermal conversion efficiency of solar radiation is much higher than the electrical conversion. This is due to the photon's low conversion efficiency and absorption. So, heat energy is preferred for various applications in the process industries. And thus, solar thermal technology is one of the most attractive solutions for producing heat process thermal energy. Hence, there is a massive opportunity to replace conventional sources with solar thermal systems. Important industrial applications where solar thermal energy can play a major role are serialisation, pasteurisation, washing, cooling, drying, dyeing, and distillation [9]. There were many efforts to analyse the potential of using solar thermal energy in industry. Jarimi et al. [10] explored the heat storage technologies and designs used for solar thermal energy storage. Also, they explored the heat recovery methods to restore industrial waste heat. Evangelisti et al [11], conducted a comprehensive review study on solar thermal collectors and their potential use in industry. Schoeneberger et al. [12], summarised the policy recommendations and modelling approaches for solar heat for industrial processes. In conclusion, most of those researchers are restricted to a particular location and related to either applications of a certain solar energy system for a specific industrial process or performance analysis of a solar thermal system for a certain industrial process. Thus, there are gaps related to technological aspects and the understanding of the industrial energy requirements.

Hungary is a central European country in the middle of the Carpathian Basin, with a relatively flat surface surrounded by high mountains. Compared to other European countries, Hungary has favourable weather conditions for using solar energy. The average annual sunshine hours are between 1,900 – 2,200, while the average total incident radiation is 1,300 kWh/m² as in Figure 1. So, the southern and middle regions of the country are suitable areas to utilise solar energy for domestic hot water and process heat. The solar energy theoretical potential is 1838 PJ, and the actual potential is between 4-10 PJ.

Many paper and pulp mill factories in Hungary convert woods into paper form. And the global average consumption per capita is around 95 kg per year [13]. The maximum process temperature requirement in the pulp and papers industry is 200°C, while the average temperature range is between 127°C and 175°C [14], where 8 tons of steam are required for processing one ton of pulp. Usually, the recovery boiler alone produces the needed steam for this process. ETC collectors can be used for processes such as bleaching, drying, and washing as a solution for integrating solar thermal energy. And to overcome the natural fluctuation of solar energy, a buffer tank may be considered.

Also, the textile industry considering the production of new clothes and the subsequent manufacturer or design of all processes and EU countries alone accounts for 64% of the clothing consumption. The textile manufacturing process can be divided into spinning, weaving, and finishing. The required energy in terms of hot water or steam is used for weaving, yarning, bleaching, curing and drying. The required temperature in textile industry varies between 40°C to 120°C [15]. Generally, all processes require heat temperature below 100°C except for yarn conditioning. As a solution for integrating solar energy, the ETC collector can generate the required temperature up to 120°C and be mounted on the roof of the building. Therefore, ETC solar system is the best option to meet the textile heat demand. Similar to the pulp and paper industry, using auxiliary heaters or buffer tanks will minimise the effect of solar fluctuation.

Most notably in Hungary, the food processing and beverage industry are highly fragmented and comprises of many sub-segments like milk, meat fruit, grains products, packaged food and drinks [16]. Most of that food and drinks have cooking, sterilisation, washing vessels, drying, and chilling processes. The heat required for this industry can be harvested from solar thermal systems. All food and beverage processes have a process temperature between 60°C and 120°C except for drying, which can reach up to 180°C [17]. Two main processes are involved in the dairy industry: i. heat treatment ensures the milk's safety, and ii. derivatives products like butter, cheese, and milk powder. Dairy processes like pasteurisation, sterilisation, drying and cleaning require heat energy. This industry consumes substantial heat energy and electricity for heat processes and storage [18], and in addition to utilizing solar energy, the use of heat pumps also has significant savings potential [19].

Nevertheless, all processes can be done using heat temperature below 120°C. ETC solar system is the best option for dairy industry applications. While in the case of enormous heat demand and available land, a linear Fresnel reflector (LFR) solar system is a better solution. Also, an auxiliary heat source and buffer tank can help avoid fluctuation during the rising season or prolonged cloudy weather. It is also important to mention that the temperature range and the load profile are the most critical factor. For example, dairy factories sometimes shut down during the cold season due to the low market demand and raw material availability [20]. It gives the advantage to shift the load profile towards sunny seasons and thus, increase the solar fraction.

The pharmaceutical industry includes many processes that consume both electrical and thermal energy. Usually, the thermal energy is produced gas-fired boilers for meeting the requirements of the steam and hot water, which range between 55°C and 120°C. Most thermal processes require low heat demand, which can be achieved easily by non-concentrating solar thermal systems like FPC, ETC. Generally, ETC collectors are considered the most suitable solar system to provide the required heat up to 120°C. Finally, the automotive industry is the fastest-growing globally [21]. Most of the processes are mechanical and uses electricity for operating.

In contrast, few processes consume a significant amount of thermal energy like painting, metal casting, and pre-treatment. Generally, it is produced using conventional methods to produce hot water [22]. At the painting process, hot air is needed at a temperature between 80°C to 100°C, while hot water is needed at only 40°C [23]. As an integrating solution, ETC solar system is the most suitable solution for providing hot water at around 100°C.

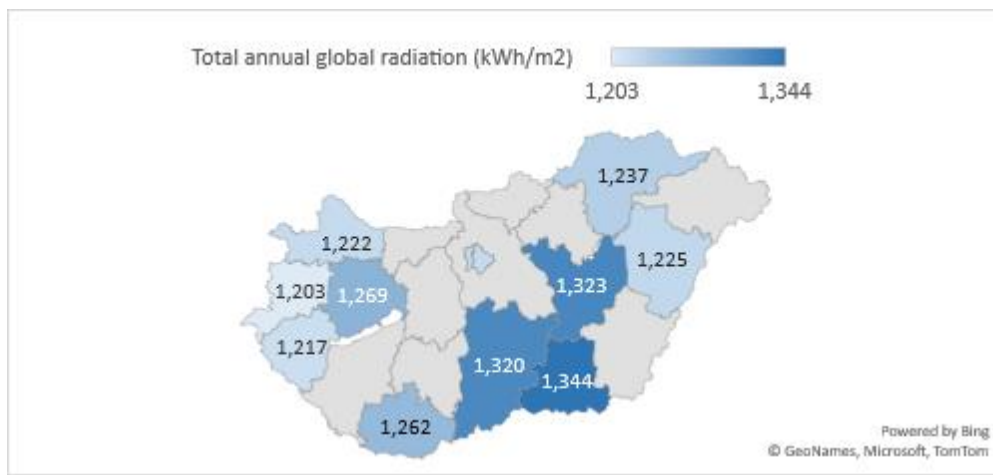


Figure 1. Annual global radiation in Hungary.

While the currently installed systems are about 0.1 PJ with around 70,000 m² surface area, Hungary has no database available on the actual installed solar capacity; therefore, all efforts made are only estimates [24]. In 2021, the adequate potential of solar energy had been identified by more than 2,000 MW. On the contrary, solar thermal energy is far beyond the electrical one and the most common collector in Hungary is the flat-plate collector (FPC). However, the demand for other types like evacuated tube collectors (ETC) has recently increased. In Hungary, industrial solar production began with small steps, and the installed capacities are hard to measure economically. Using solar energy has the highest positive effects of creating new jobs among all other types of renewable energies. According to the Hungarian solar energy association, installing 449 MW results in 1,500-1,600 new jobs all around the country. This capacity would provide around 1.1% of the total electricity demand in 2020. Another advantage is that installed solar systems are decentralised, reducing power distribution losses. Energy generation of renewable energy sources in Hungary has increased by approximately 30% over the last two decades. At the same time, the solar heat for industrial processes (SHIP) continued to its steady growth during 2020, with at least 74 new plants primarily in Germany, Mexico, and China.

Hungary has around 1980 hours of annual sunshine while July is the sunniest month with 279 hours and December is the lowest with only 51 hours. The average annual sunshine is quite close to Austrian data, with about 1925 hours per year. But Austria is among the best countries in Europe to utilise solar energy (fifth place in 2019) while Hungary stands at the bottom of the list (21st place over 27). It is also noted that all neighbour countries have a higher share of renewable energies in their gross final energy consumption, e.g., Croatia 28.5%, Romania 24.3%, Slovenia 21.7%, Bulgaria 21.6%, and Slovakia 16.9% while Hungary is only 12.6%. This data motivates researchers to search for a genuine reason and show decision-makers potential, especially since Hungary is a solid industrial country and a well-known destination for multinational companies.

The most recent reported efficiency of the production of low-temperature solar systems for the flat-plate collector (FPC) and the evacuated tube collector (ETC) is in the range of 15-40% while for medium

temperature generation in the range of 50-60% [25]. The nominal achieved temperature by the FPC, and the ETC is 85°C and 125°C, while the average cost per square meter is 180 \$/m² for both collector types [13].

The present article aims to map researchers' generated knowledge in solar thermal technologies and the actual industrial applications. It also proposes a general help to investors and decision-makers to find the generated solar energy corresponding to each location in Hungary. The procedures developed in this article assume that the solar system's integration is a design modification or a retrofit dilemma. Therefore, an existing industrial process is assumed to integrate the solar thermal system.

2. Methodology

The SHIP system comprises ETCs, an integrated heat exchanger in the buffer tank, and the heat process section as in Figure 2. In the primary loop, the water flows in the pipes using an active circulation pump in a closed loop. The flow rate of the primary loop is 50 litres per hour, and the fluid is a mixture of glycol and water of 30% volumetric percentage to avoid freezing and bursting during low-temperature conditions. The demand at the factory is constant from 6:00 AM – 5:00 PM at assumed constant load on weekdays except for Saturday and Sunday. The average daily consumption for all cases is 115 kWh, and the resulting annual energy requirement is 29.89 MWh. The assumed maximum hourly requirements are not more than 10 kWh, which means a small factory like food processing or packaging. The process heat needed at 75°C nominal supply temperature and 60°C minimum outlet temperature. The collector field consists of 16 ETC with 34.24 m² gross area. The manufacturer is B. Schweizer Energie AG, and the type is Swisspipe 2 with an 87.8% conversion factor as in Table 1. The collector field faces the south at 0° azimuth angle and 72° inclination angle lengthwise. The buffer tank has 1,900 litres, and it has stratified return with a redirection valve and buffer tank bypass. Finally, the boiler is a gas-fired Riello Unit SL 48 S ECO with a 53.1 kW nominal output. All data were analysed using T*Sol software, a thermal solution program developed by Valentine software GmbH, Germany. This software is used for optimising and designing solar thermal systems dynamically. The results can be calculated over an annual cycle for several systems like domestic hot water, heating support, and process heating system. The studied Hungarian locations were chosen all around the country to have a full-scale assessment as in Table 2.

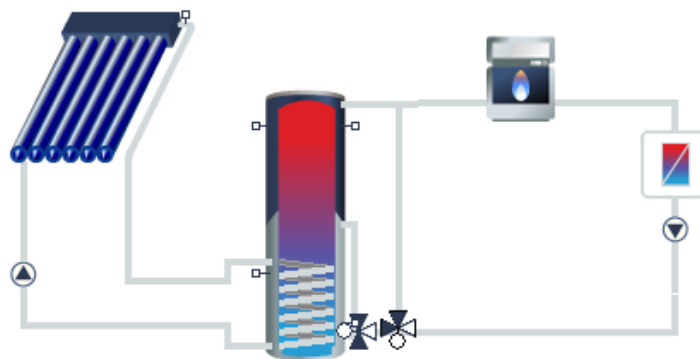


Figure 2. Process heating system with a buffer tank and continuous flow heater.

Table 1. ETC collector specifications.

Collector	Characteristics	Value
Evacuated-tube collector (ETC)	Absorber area	1.31 m ²
	Optical efficiency (a ₀)	87.8 %
	Heat loss coefficient (a ₁)	1.43 W/m ² k
	Heat loss coefficient (a ₂)	0.0038 W/m ² k ²

Table 2. The studied Hungarian stations.

Station	Latitude	Longitude	Total annual global radiation (kWh/m ²)	Mean outside temperature °C	Diffuse radiation percentage (%)
Budapest	47.5°	19.0°	1,222.4	11.4	53.6
Miskolc	48.1°	20.8°	1,236.7	10.4	52.1
Veszprém	47.1°	17.9°	1,268.8	10.6	52.1
Debrecen	47.5°	21.6°	1,225.3	10.9	52.9
Szeged	46.3°	20.1°	1,344.4	11.5	49.5
Pécs	46.0°	18.2°	1,261.8	11.6	52.9
Zalaegerszeg	46.9°	16.8°	1,217.1	10.7	53.8
Szombathely	47.3°	16.6°	1,202.8	10.5	53.7
Sopron	47.7°	16.6°	1,228.9	10.9	52.4
Győr	47.7°	17.7°	1,222.0	11.1	52.5
Kecskemét	46.9°	19.7°	1,320.0	11.4	50.3
Szolnok	47.2°	20.2°	1,323.0	11.6	49.6

3. Results and Discussion

The analysis results in 12 studied stations are as in Table 3. According to the results, it is noted that Szeged, Szolnok, and Kecskemét have the highest solar fraction with 54.89%, 54.16%, and 54.03%, respectively. All power stations produce good yields per annum by supplying between 745-850 kWh/m²/year. It is also noted that the system efficiency is around 60% for all stations.

Table 3. The analysis results.

Station	Specific irradiation collector active surface area	Specific energy delivered by collector loop	The energy delivered by the collector	Solar contribution	Energy from auxiliary heating	Total solar fraction of process heat	System efficiency
	kWh/m ²	kWh/m ²	kWh	kWh	kWh	%	%
Zalaegerszeg	1,160.31	745.48	15,625	14,392	15,492	48.16	59.18
Debrecen	1,176.50	757.24	15,872	14,640	15,255	48.97	59.37
Budapest	1,187.09	761.89	15,969	14,719	15,184	49.22	59.15
Szombathely	1,187.51	757.36	15,874	14,592	15,315	48.79	58.62
Győr	1,222.01	765.98	16,055	14,788	15,103	49.47	59.31
Sopron	1,190.69	757.81	15,884	14,592	15,305	48.81	58.47
Pécs	1,194.00	762.11	15,974	14,701	15,185	49.19	58.74
Miskolc	1,204.64	773.18	16,206	14,925	14,988	49.89	59.11
Veszprém	1,227.54	790.65	16,572	15,270	14,614	51.1	59.35
Szolnok	1,299.60	840.25	17,612	16,196	13,707	54.16	59.46
Kecskemét	1,301.20	839.27	17,591	16,169	13,758	54.03	59.29
Szeged	1,302.02	849.57	17,807	16,417	13,493	54.89	60.16

A robust negative correlation is found by plotting the correlation between the total annual global radiation and the diffusive radiation. It means that as high is the diffusive radiation, low is the total annual global radiation, as shown in Figure 3a. Also, the diffusive radiation is negatively correlated with the solar fraction. It means as high is the diffusive radiation as low is the solar fraction as in Figure 3b. It is a logical result since the solar fraction is strongly correlated with the annual global radiation in Figure 3c.

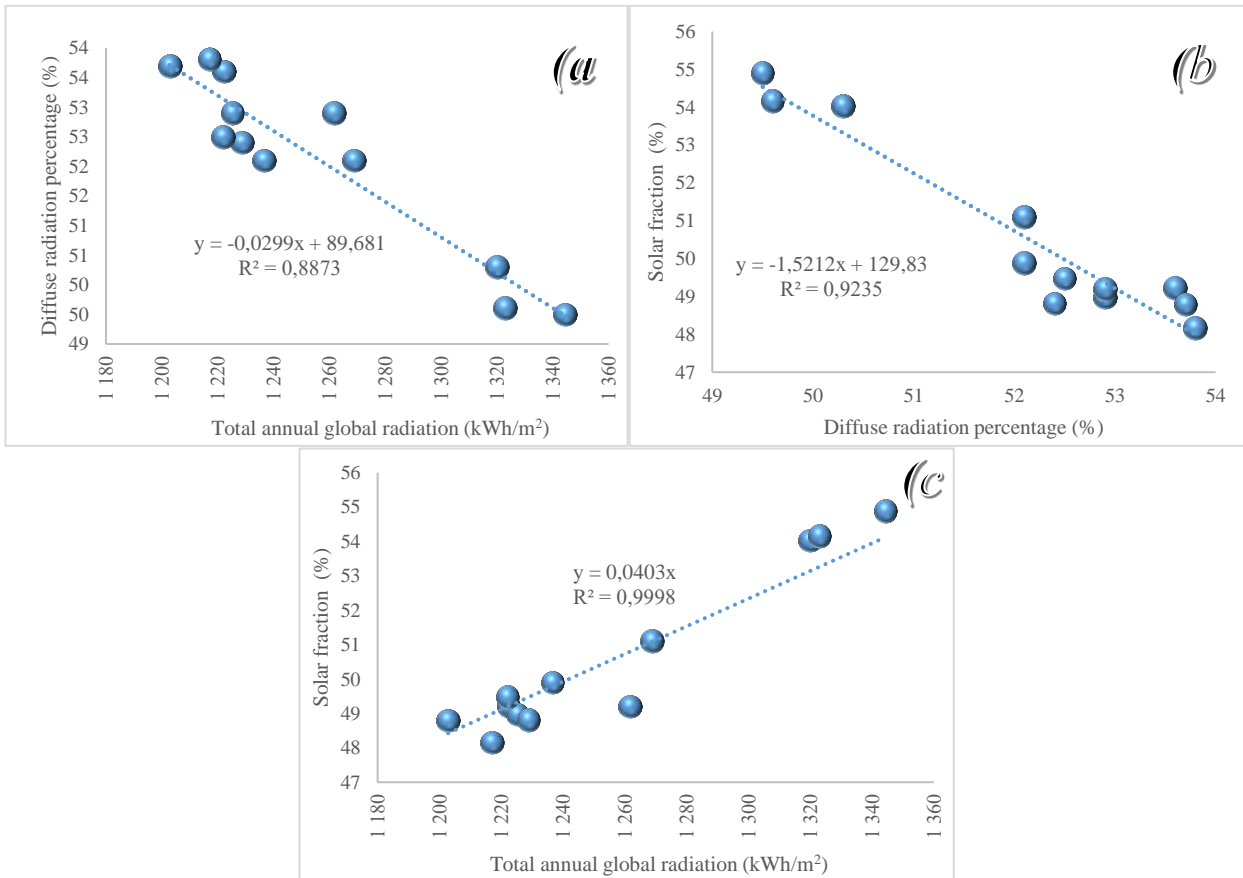


Figure 3. a) Correlation between annual global radiation with diffusive radiation percentage. b) Correlation between diffusive radiation and solar fraction. c) Correlation between annual global radiation and solar fraction.

The solar fraction map shows that Szeged, Szolnok, and Kecskemet, which accounts for the lowest diffuse radiation with 49.5%, 49.6%, and 50.3%, have the highest solar fraction with the highest 54.89%, 54.16% and 54.03%, respectively. To understand the potential, each square meter of the collector field can generate a certain amount of energy per year. Suppose we consider the average Hungarian annual radiation on a horizontal surface as around 1280 kWh/m². In that case, the plotted map in Figure 4 shows us the highest potential regions for utilising the solar thermal system. The specific highest potential is around 840 kWh/m²/year for Szeged, Szolnok and Kecskemet.

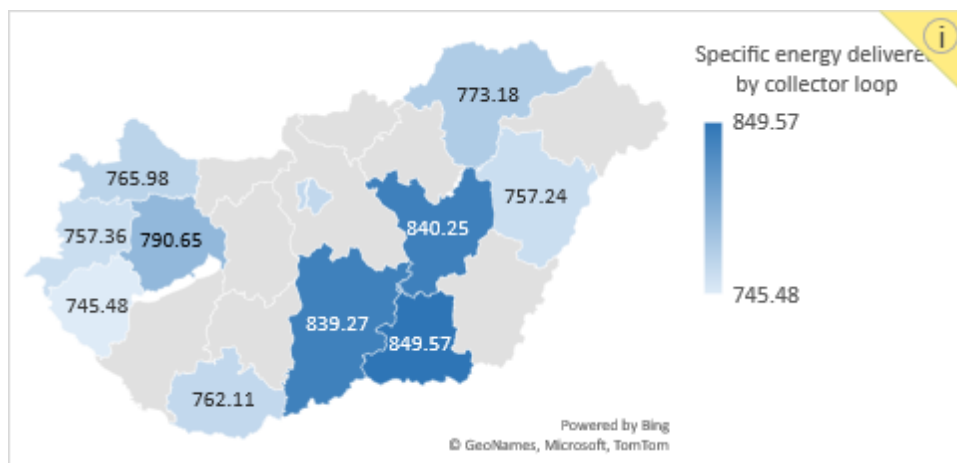


Figure 4. The specific solar generation per square meter collector area.

Comparing the specific energy delivered by the collector loop between pioneer European countries at approximately the same latitude as Budapest, Hungary is proper to compare it with Vienna, Austria and München, Germany. Vienna and München have global solar radiation of 1212.048 kWh/m² and 1156.022 kWh/m², respectively. It results in 751.59 kWh/m² and 698.467 kWh/m² specific energy delivered by the collector loop. By comparing those values with the specific collector energy in Budapest 757.24 kWh/m², it is found that Budapest has a higher potential than Vienna and München. Nevertheless, Austria and Germany are far better than Hungary utilising solar energy. It happens due to main reasons, like the late joining of Hungary to the EU compared to Austria and Germany, national renewable energy strategies, incentive subsidiary projects, and national decision-makers [26]. Without a subsidy, it was reported that no payback would be reached during the lifetime of the solar system, which shows the importance of the governmental subsidy [27].

4. Conclusions

Important factors decide the solar augmentation for a specific industrial heat process within the existing process. Food & beverage, textile, rice mill, leather, automotive, and pharmaceutical industries offer low-temperature solar utilisation and are available widely in Hungary. To improve the process efficiency and reduce the installation costs, an extensive technical assessment analysis should be done before integrating the solar collectors within the industrial heat process. This assessment should study the potential solar thermal system and its applications to various heat processes. According to the literature, no comprehensive work has been conducted to find the optimal location in Hungary for SHIP use.

Further, the simulation supply of heat is required for the heat process in industrial factories, which is another innovation of this article. The results show that each studied location can supply a partial amount of the required solar heat. Therefore, this article uses T*Sol 5.5 software to investigate the potential of using the solar thermal system in Hungary. Assessment analysis of 12 different locations under the Hungarian meteorological conditions was conducted for presumed industrial processes with daily and annual hot water demand. For low temperature below 120°C applications, evacuated-tube collectors ETC showed good yields with not less than 745 kWh/m² per year and around 840 kWh/m²/year at three locations Szeged, Szolnok, and Kecskemét. Those results were higher than pioneer users of solar thermal energy in the EU, such as Germany and Austria. The results presented in this study can be beneficial for industrial manufacturers and decision-makers who look for clean energy sources to minimise greenhouse gases and reduce their operating costs.

Acknowledgement

This work was supported by the Stipendium Hungaricum Programme and by the Mechanical Engineering Doctoral School, Hungarian University of Agriculture and Life Sciences, Gödöllő, Hungary.

References

- [1] **Rabaia, M.K.H., Abdelkareem, M.A., Sayed, E.T., Elsaid, K., Chae, K.J., Wilberforce, T., et al.** (2021). Environmental impacts of solar energy systems: A review. *Science of the Total Environment*, vol. 754 p. 141989, DOI:10.1016/j.scitotenv.2020.141989.
- [2] **Covert, T., Greenstone, M., Knittel, C.R.** (2016). Will we ever stop using fossil fuels? *Journal of Economic Perspectives*, vol. 30 no. 1, p. 117–138, DOI:10.1257/jep.30.1.117.
- [3] **Sharma, A.K., Sharma, C., Mullick, S.C., Kandpal, T.C.** (2017). Solar industrial process heating: A review. *Renewable and Sustainable Energy Reviews*, vol. 78 no. December 2016, p. 124–137, DOI:10.1016/j.rser.2017.04.079.
- [4] **Bolognese, M., Viesi, D., Bartali, R., Crema, L.** (2020). Modeling study for low-carbon industrial processes integrating solar thermal technologies. A case study in the Italian Alps: The Felicetti Pasta Factory. *Solar Energy*, vol. 208 no. January, p. 548–558, DOI:10.1016/j.solener.2020.07.091.
- [5] **Lizárraga-Morazán, J.R., Martínez-Rodríguez, G., Fuentes-Silva, A.L., Picón-Núñez, M.** (2021). Selection of solar collector network design for industrial applications subject to economic and operation criteria. *Energy and Environment*, vol. 32 no. 8, p. 1504–1523, DOI:10.1177/0958305x20927375.
- [6] **Barberis, S., Peccianti, F., Castellino, L., Bolognesi, T.** (2020). integration of Solar Heat in Industrial Process – Preliminary evaluation. vol. 1 no. 792276, p. 3–7,.

- [7] **Fuller, R.J.** (2011). Solar industrial process heating in Australia e Past and current status. *Renewable Energy*, vol. 36 no. 1, p. 216–221, DOI:10.1016/j.renene.2010.06.023.
- [8] **Ismail, M.I., Yunus, N.A., Hashim, H.** (2021). Integration of solar heating systems for low-temperature heat demand in food processing industry – A review. *Renewable and Sustainable Energy Reviews*, vol. 147 no. January, p. 111192, DOI:10.1016/j.rser.2021.111192.
- [9] **Taibi, E., Gielen, D., Bazilian, M.** (2012). The potential for renewable energy in industrial applications. *Renewable and Sustainable Energy Reviews*, vol. 16 no. 1, p. 735–744, DOI:10.1016/j.rser.2011.08.039.
- [10] **Jarimi, H., Aydin, D., Yanan, Z., Ozankaya, G., Chen, X., Riffat, S.** (2019). Review on the recent progress of thermochemical materials and processes for solar thermal energy storage and industrial waste heat recovery. *International Journal of Low-Carbon Technologies*, vol. 14 no. 1, p. 44–69, DOI:10.1093/ijlct/cty052.
- [11] **Evangelisti, L., De Lieto Vollaro, R., Asdrubali, F.** (2019). Latest advances on solar thermal collectors: A comprehensive review. *Renewable and Sustainable Energy Reviews*, vol. 114 no. August, p. 109318, DOI:10.1016/j.rser.2019.109318.
- [12] **Schoeneberger, C.A., McMillan, C.A., Kurup, P., Akar, S., Margolis, R., Masanet, E.** (2020). Solar for industrial process heat: A review of technologies, analysis approaches, and potential applications in the United States. *Energy*, vol. 206 p. 118083, DOI:10.1016/j.energy.2020.118083.
- [13] **Kumar, L., Hasanuzzaman, M., Rahim, N.A.** (2019). Global advancement of solar thermal energy technologies for industrial process heat and its future prospects : A review. *Energy Conversion and Management*, vol. 195 no. February, p. 885–908, DOI:doi.org/10.1016/j.enconman.2019.05.081.
- [14] **Ravi Kumar, K., Krishna Chaitanya, N.V.V., Sendhil Kumar, N.** (2021). Solar thermal energy technologies and its applications for process heating and power generation – A review. *Journal of Cleaner Production*, vol. 282 p. 125296, DOI:10.1016/j.jclepro.2020.125296.
- [15] **Ashokkumar, Y.D.L.** (2013). A CASE STUDY A Study on Energy Conservation in Textile Industry. vol. 94 no. May, p. 53–60, DOI:10.1007/s40031-013-0040-5.
- [16] **Ghabour, R., Korzenszky, P.** (2022). Linear Model of DHW System Using Response Surface Method Approach. *Tehnicki Vjesnik - Technical Gazette*, vol. 29 no. 1, p. 201–205, DOI:10.17559/tv-20201128095138.
- [17] **Kabir, E., Kumar, P., Kumar, S., Adelodun, A.A., Kim, K.H.** (2018). Solar energy: Potential and future prospects. *Renewable and Sustainable Energy Reviews*, vol. 82 no. September 2016, p. 894–900, DOI:10.1016/j.rser.2017.09.094.
- [18] **Ghabour, R., Josimović, L., Korzenszky, P.** (2021). Two Analytical Methods for Optimising Solar Process Heat System Used in a Pasteurising Plant. *Applied Engineering Letters : Journal of Engineering and Applied Sciences*, vol. 6 no. 4, p. 166–174, DOI:10.18485/aeletters.2021.6.4.4.
- [19] **Hermanucz, P., Gácsi, G.** (2018). Risks of refrigerants in food industry. *Researched Risk Factors of Food Chain*, pp. 97-101, Szent István Egyetemi Kiadó, Gödöllő, Hungary
- [20] **Baniassadi, A., Momen, M., Amidpour, M.** (2015). A new method for optimization of Solar Heat Integration and solar fraction targeting in low temperature process industries. *Energy*, vol. 90 no. July, p. 1674–1681, DOI:10.1016/j.energy.2015.06.128.
- [21] **Mayyas, A., Qattawi, A., Omar, M., Shan, D.** (2012). Design for sustainability in automotive industry : A comprehensive review. *Renewable and Sustainable Energy Reviews*, vol. 16 no. 4, p. 1845–1862, DOI:10.1016/j.rser.2012.01.012.
- [22] **Giampieri, A., Ling-chin, J., Ma, Z., Smallbone, A., Roskilly, A.P.** (2020). A review of the current automotive manufacturing practice from an energy perspective. vol. 261 no. July 2019.
- [23] **Zahler, C., Iglauer, O.** (2012). Solar process heat for sustainable automobile manufacturing. vol. 30 p. 775–782, DOI:10.1016/j.egypro.2012.11.088.
- [24] **Bursík, M., Chalupa, Š., Doležal, J., Gajewska, I., Karaba, J., et al.** (2020). Renewables in National Energy and Climate Plans of Visegrad countries Challenging the low ambition. .
- [25] **Zheng, H.** (2017). *Solar Concentrating Directly to Drive Desalination Technologies*. Elsevier, .
- [26] **Ghabour, R., Korzenszky, P.** (2021). Technical and non-technical difficulties in solar heat for industrial process. *ACTA TECHNICA CORVINIENSIS – Bulletin of Engineering*, vol. 3 no. July – September, p. 11–18,.
- [27] **Karki, S., Haapala, K.R., Fronk, B.M.** (2019). Technical and economic feasibility of solar flat-plate collector thermal energy systems for small and medium manufacturers. *Applied Energy*, vol. 254 no. March, p. 113649, DOI:10.1016/j.apenergy.2019.113649.

GENERATING COLD ENERGY USING WASTE HEAT FROM A PYROLYSIS GENERATOR (CHP)

Author(s):

V. Madar¹, N. Schrempf², A. Betovics², L. Toth²

Affiliation:

¹ Pyrowatt Kft., 6120 Kiskunmajsa, Vágóhíd utca 91. Hungary;

² Institute of Technology - Hungarian University of Agriculture and Life Sciences, 2100 Gödöllő, Páter Károly u. 1., Hungary;

Email address:

madar.viktor@pyrowatt.hu, Schrempf.Norbert.Attila@uni-mate.hu, Toth.Laszlo.emeritus@uni-mate.hu

Abstract: Pyrolysis of wastes and agricultural by-products was addressed in the study. During the energetical utilization of biomasses, the pyrolysis power plant produces electricity and heat, so we examined the possibilities of using the generated waste heat. This waste heat can be used at the place of generation, to produce the so-called "cold energy", which can meet the energy demand of cold stores.

Keywords: biomass, pyrolysis, gas generator, waste heat, cold energy

1. Introduction

In this article, we present a special use of the energy obtained during the pyrolysis of biomass, which is less discussed and known among consumers. More research institutes and companies are involved in the pyrolysis of various wastes and agricultural main and by-products than in the exploitation for energy purposes, considering that in some respects, the so-called circular farming can take place. Throughout the process, heat and electricity are generated, but as an intermediate product from biomass, to improve the structure of agricultural soils, stable so-called biochar [1] can be produced, that has a positive effect. RAIL SAFE LTD. [2] and CSŐMONTAGE LTD. [3] have been engaged in the development, design and manufacture of pyrolysis generators for several years [4-9]. Small power plants with gas generators of 5, 30, 50 and 100 kW are already available. A number of authors and analysts have pointed out that these generators can be used economically if the obtained electricity and heat are used entirely. There are also many woody and cellulose-rich (Fig. 1 and 2) main and by-products [10] available in Hungary, which have an attractive carbon and energy content. Thereby, this solution can be applied to decentralized energy production as well, as there are legal possibilities for electricity feed-in, and thermal energy can be used in situ for several purposes.



Figure 1. Wood chips and pellets



Figure 2. Herbaceous material, e.g. straw pellets

We talk about a system that recycles waste heat at a higher temperature to produce “cold energy”, that allows fruits, vegetables and other foods to be stored permanently. These systems are able to provide the cold energy supply needed for cold stores with the waste heat of their operation.

2. Material and Method

2.1. Expectations to fuels

For the operation of the planned equipment, various biomasses arising in agriculture are suitable, but deteriorated rail sleepers are raw material as well.

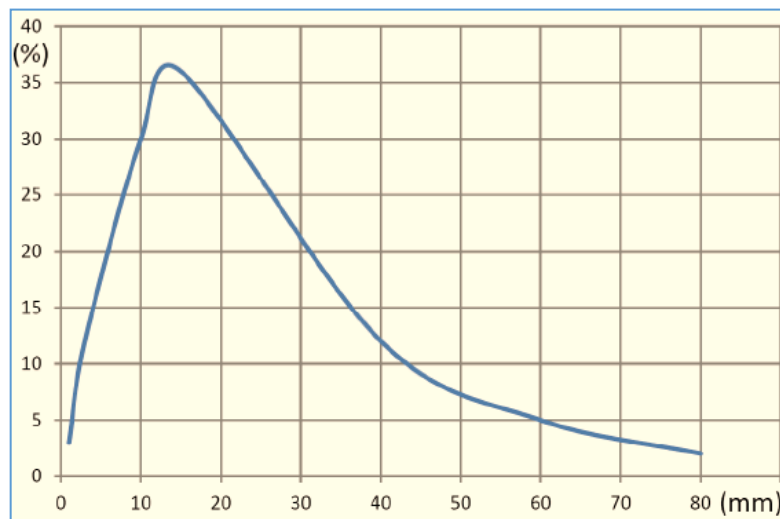
Important factors for proper operation [11]:

- degree of shooting of substances (Table 1, Fig. 3),
- moisture content and
- energy content but
- the amount of minerals may also be decisive.

Table 1. Wood chips according to size (according to ÖNORM M7133)

Wood chips	Dimensions allowed				Allowed extremes max.	
	max. 4%	max. 20%	60-100%	max. 20%		
Category	Chips' size [mm]				Cross-section [cm ²]	Length [cm]
G30	<1,0	1-2,8	2,8-16	>16,0	3	8,5
G50	<1,0	1-5,6	5,6-31,5	>31,5	5	12
G100*	<1,0	1-11,2	11,2-63	>63,5	10	25

* - Not recommended.



Size ranges (mm)	<1	1 - 3	3-10	10-15	15-40	40-60	>80
Hardwood chips (%)	3	12	30	36	12	5	2

Figure 3. The distribution curve characteristic of hardwood chips

After delivery, substances must be dried to a moisture content of 18-20% before pyrolysis [12]. The equipment is suitable for this, as the heat demand of drying from heat demolition and energy conversion (gas engine electric generator), while heat is generated in exotherm processes. This is suitable and cheap for the high-temperature waste heat generated by the gas engine. It is more economical to get raw material with a low moisture content, and only the need for cutting to the right size can mean extra energy. The specifications of the test material are listed in Table 2.

Table 2 Characteristics of the test material

Denomination	Elemental composition					Moisture content	Calorific value (on dry matter basis)
	N	C	S	H	Cl		
	(%)						
Hardwood	0,10	42,83	0,07	6,29	0,00	12,73	16,86

If we decide to use herbaceous plants, it is best to pellet the materials, as pyrolysis is more efficient in a compressed form in a fixed bed system and the operation of the equipment is more problem-free.

2.1. The equipment established

The complete equipment can be placed in a separate plant hall (Fig. 4), which also contains the units required for pre-storage, drying and cutting. The material can be transferred directly from the storage and drying units to the equipment. The feed into the gas generator is provided by a pneumatical sluice. Controlling the sluice is important because decomposition requires a certain oxygen-poor environment.

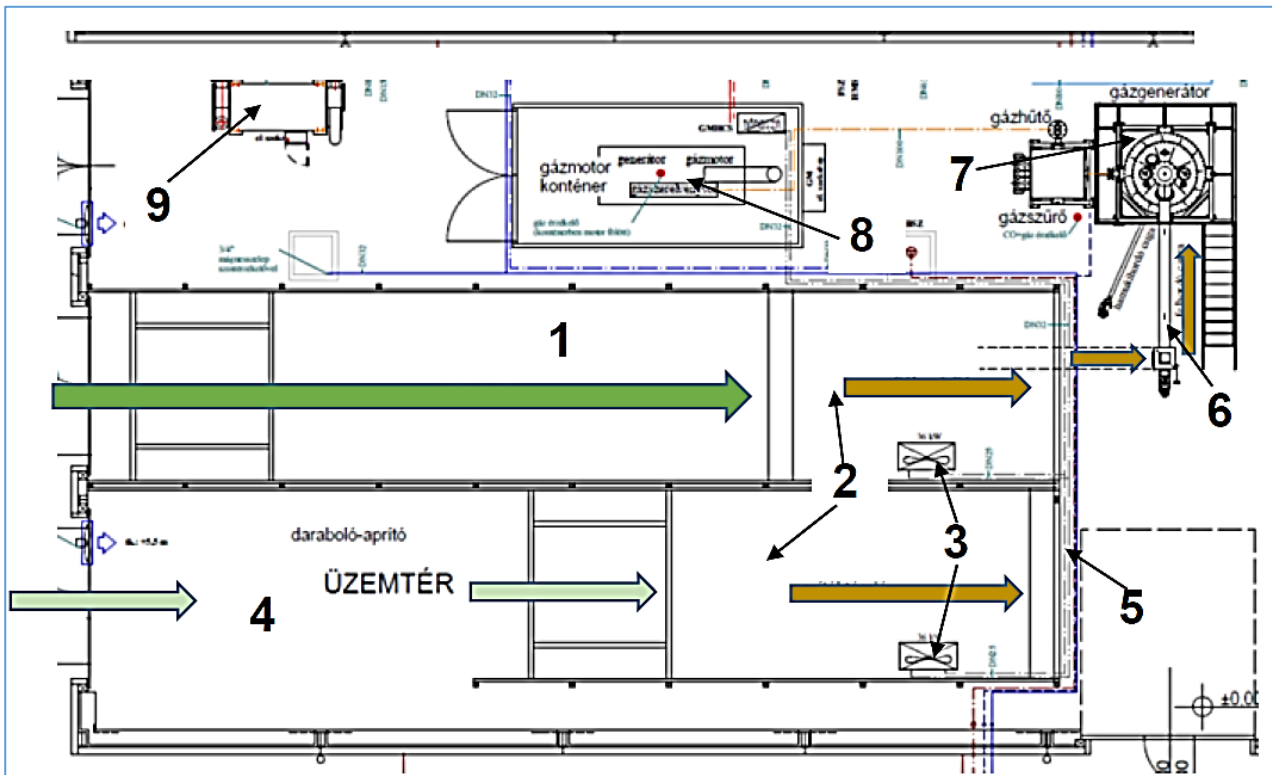


Figure 4. Layout of the complex facility in the building and the connection to the cooling system

Signs in fig. 4:

1. large storage (that can be folded by car)
2. drying areas
3. heaters
4. space reserved for cutting and shredding
5. transverse transport
6. delivery of the material to the reactor space
7. the reactor with its various components
8. motor and electric generator
9. absorption refrigeration equipment

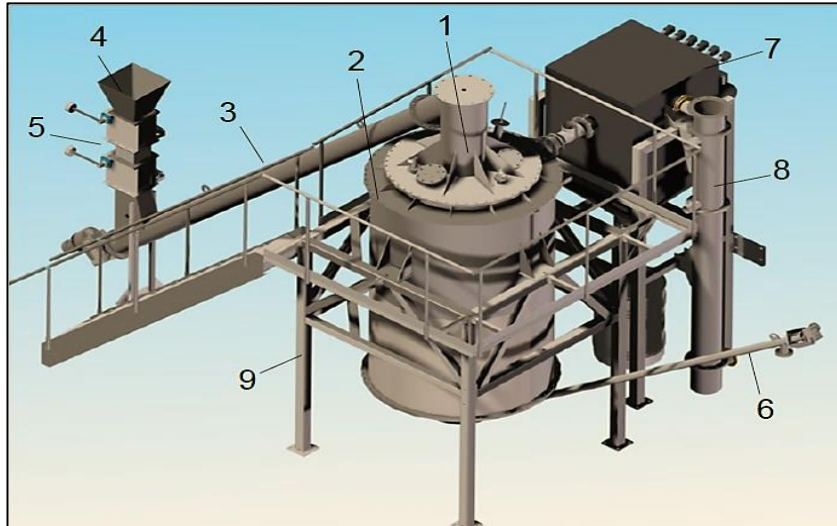


Figure 5. The generator body and the elements involved in the decomposition

Signs in fig. 5:

1. generator body with feed port
2. generator body and insulation
3. fuel delivery pipe
4. fuel inlet
5. sluice system
6. ash discharge and propulsion
7. gas filter and its units
8. heat exchanger
9. frame structure of the system

The generator (Fig. 5) belongs to the so-called fixed bed (Fig. 6) types [13], which represents a simple structure compared to screw or fluid bed designs. The material first enters the drying space, which ignites at the bottom and begins to glow at higher temperatures [14]. This and the next combustion chamber are also called oxidation zone, where gases and coal are produced by adding the optimal amount of air [15]. In the lower part of this layer, resp. in the next space is the reduction zone where the tar harmful to the gas engine decomposes (into combustible gases).

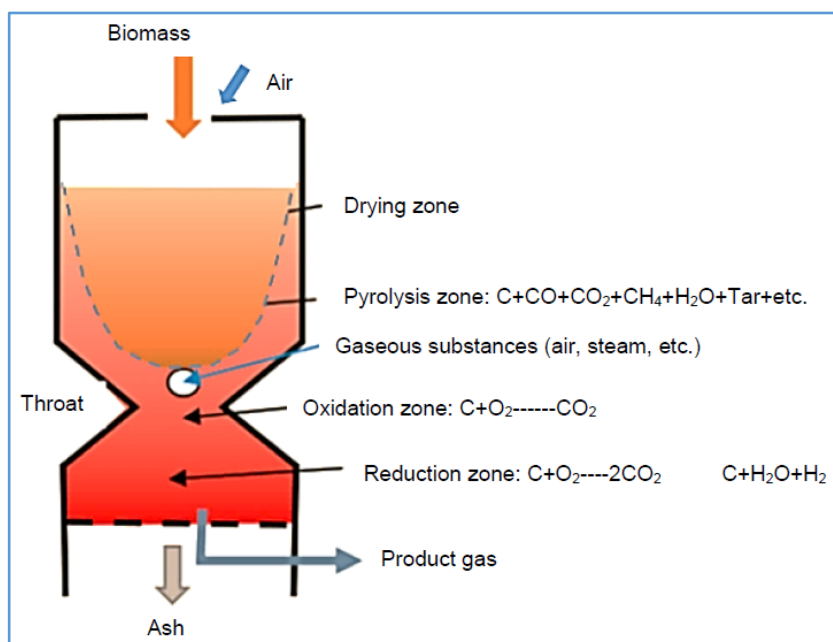


Figure 6. Theoretical operation of the bottom-drain fixed bed system

With the right temperature and air ratio, tar can be eliminated [16, 17]. Typically, the residual material contains 25-35% carbon and 1-2% minerals in the ash. The temperature of biomass stored outdoors is usually the same as the ambient temperature. It is higher in summer and lower in transition and winter time. Its moisture content is also variable, as it absorbs water from the air during the transition period.

The basic goal is the biomass entering the reactor to have a constant temperature and moisture content. We can only achieve this by fulfilling a pre-drying before the reactor. The heat generated in the reactor is used for this purpose: by passing the high temperature gas leaving the reactor into a heat exchanger.

The other side of this heat exchanger is supplied with drying air at a temperature suitable for the environment, which has been warmed up to 100-120°C in the heat exchanger. The temperature of the gas leaving the reactor is about 650-750°C. Due to the low temperature on the opposite side, the gas enters the second heat exchanger with a significant temperature loss, against which the air entering the reactor is preheated on its side (Fig. 7).

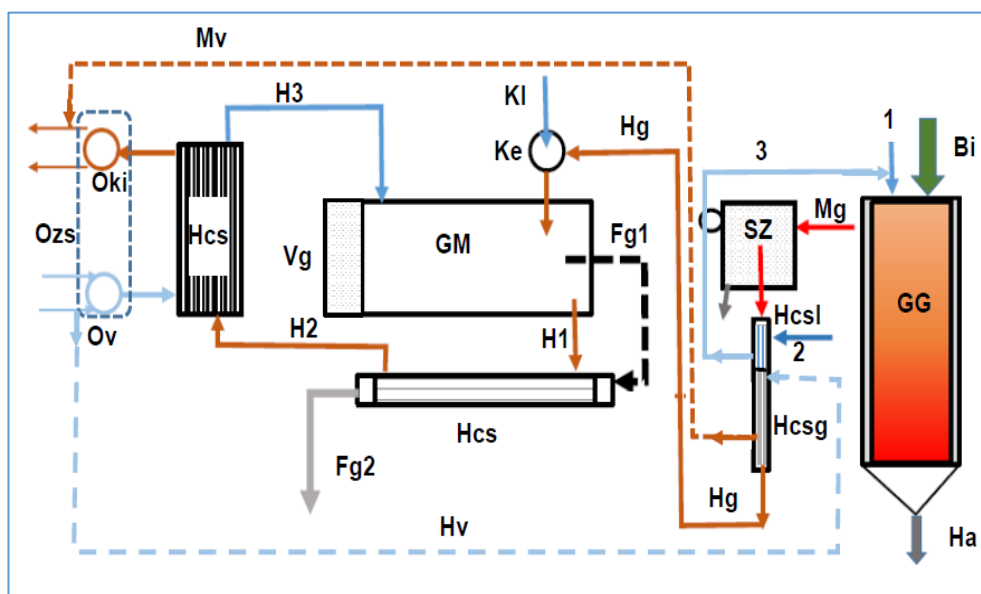


Figure 7. Schematic diagram of the system

Signs in the figure:

Sign	Denomination	Sign	Denomination
Bi	Biomass addition	Ke	Adding gas and air to the engine
KI	Ambient air	Fg1	Flue gas from the engine
GG	Gas generator	Hcs	Batch Heat Exchanger
Ha	Ash and residual coal	H1	Engine cover coolant
Mg	Hot gas	KI	External combustion air
SZ	Filter house and filters	Fg2	Cooled flue gas
Hcsg	Gas / water heat exchanger	Vg	Electric generator
Mv	Hot water	H1	Engine outlet coolant
Hcsl	Gas / air heat exchanger	H2	Heated coolant
1	External air	H3	Cooled coolant
2	External air inlet	Hcs	Laminar exchanger
3	Warm added air	Ozs	Output manifold connectors for dryer heater and absorption cooler
GM	Gas engine	Oki	Divider output
Hg	Cooled gas	Obe	Divider input

An important question is whether the material flows through the drying zone by gravity or vibration is required. When granular material is filled into the tank, the pressure at the bottom of the tank initially increases similarly to the hydrostatic pressure of liquids. However, with the amount of added material, the interaction between the sidewall and the grains increases, and the friction on the sidewall and between the grains as well. In addition to the gravity resulting from the height of the material column, the equilibrium of the set is determined by the compressive and frictional forces among particles. But due to irregular shape, tensions and entrapments can also occur.

In this case, the gas flowing between particles, which causes them to move, but the shredding knife at the bottom of the reduction space also plays a role in, which also has a force in the vertical direction (resulting in mechanical movement). In terms of static condition, a run-off occurs when the thrust is greater than the friction.

Model measurements with carbon particles (~ 1-8 mm) show that the drainage intensity is stable in the cone range of 40-60°, which is advantageous for the consistent operation of the system (Fig. 8).

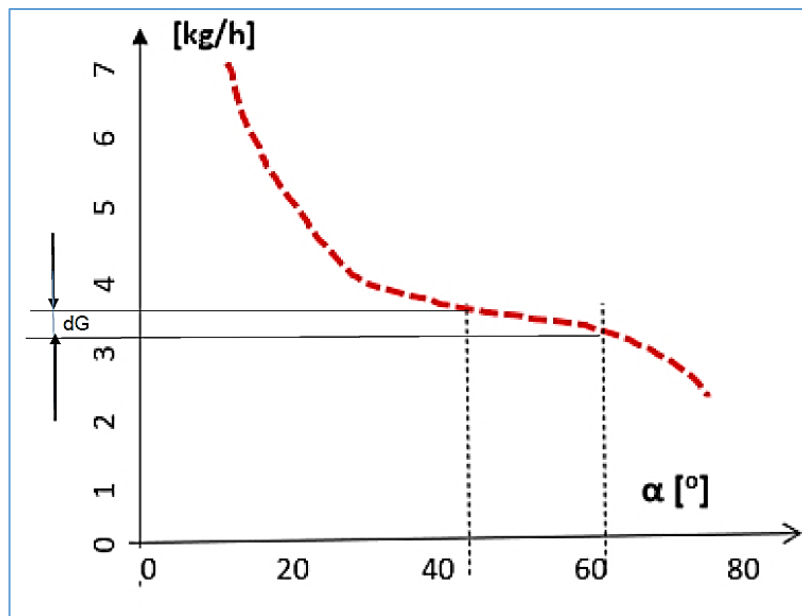


Figure 8. Mass flow as a function of α

If the value of α is smaller, the thrust will be larger, so the flow will be faster.

The scraper structure at the bottom of the reduction zone helps to remove ash and dust residues (it also prevents the lump residue from sticking together), but the gas also leaves the system on this surface and the perforated side wall. The gas flows to the dust separator and then to the bundle heat exchanger and then to the engine's mixing unit. So, the engine gets the right quality, dust and tar free gas, but the right mixture for ignition and combustion enters the engine by mixing air.

The filter unit is made of ceramic, which has excellent filtration properties, a long service life and can be easily cleaned by reverse flow air supply.

The amount of heat escaping through the exhaust of the engine heats a bundled heat exchanger [8], on the opposite side of which the engine outlet cooling water flows and further heats to the plate heat exchanger. There, the heat is released back into the engine compartment. On the outlet and inlet manifolds on the other side of this heat exchanger, a liquid of ~ 90°C supplies heat to the evaporator of the absorption cooler, and if necessary, to the heaters connected to the dryer. The intake air of the engine is heated by one part of a heat exchanger on the other side, which is a tubular but two-part heat exchanger, by warm gases. In the other part of the heat exchanger, the gas is further cooled, namely at the inlet of the plate heat exchanger, by the fluid of the return branch, which then opens into the outlet part of the manifold. The thermal energy content of the product gas is also used with these.

The spark-ignition gas engine (Fig. 9) drives the electric generator at synchronous speed, which supplies energy to the mains through a nearby transformer.

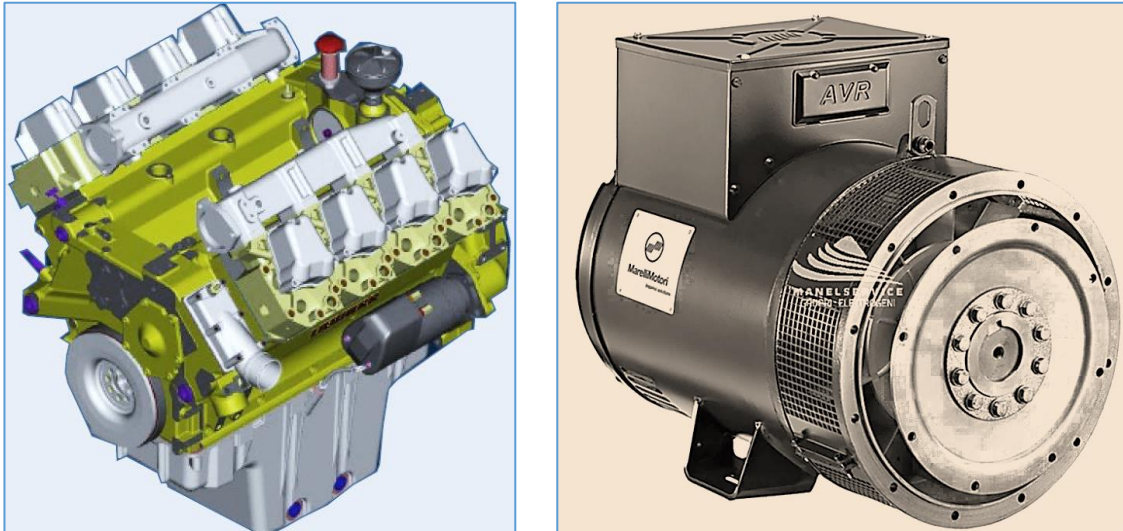


Figure 9. The spark-ignition 8-cylinder gas engine and the connected electric generator

After all, the waste heat of the system (55-60% of the total fed) can be used for cooling, or for drying fuel with a higher moisture content, for public utility purposes and for residential heat supply, depending on the needs and situations that arise.

An external air-based cooler is used to cool the absorber of the equipment.

The system can be considered a complicated assembly and the operation requires high accuracy, so the operation of the entire complex is automated.

The V1040 OPLC is a programmable logic controller with a built-in operator panel. The operator panel's 10.4" colour touch screen has function keys and a virtual alphanumeric keypad. The virtual keyboard will pop up automatically when required by the application, e.g. for data entry.

After all, control and management are made up of three systems. The **first unit** monitors and controls the pyrolysis equipment. This includes pre-drying, feedstock feed, air inlet, ash scraper operation, and temperature zone monitoring (Fig. 10).

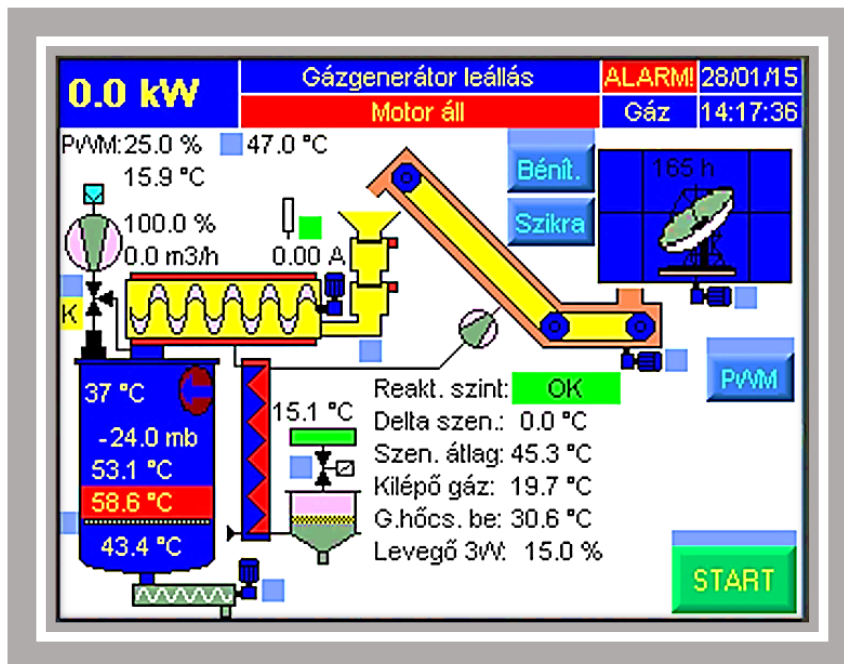


Figure 10. The operation and the operating parameters of the gas generator interface for monitoring and control

It monitors the operating parameters, controls the gas generator and tracks all process-related temperatures as well as pressure values etc.

The second unit monitors the operation of the motor (Fig. 11) and the interaction with the electric generator. It adjusts the gas/air mixing ratio to get the engine running at its best efficiency.

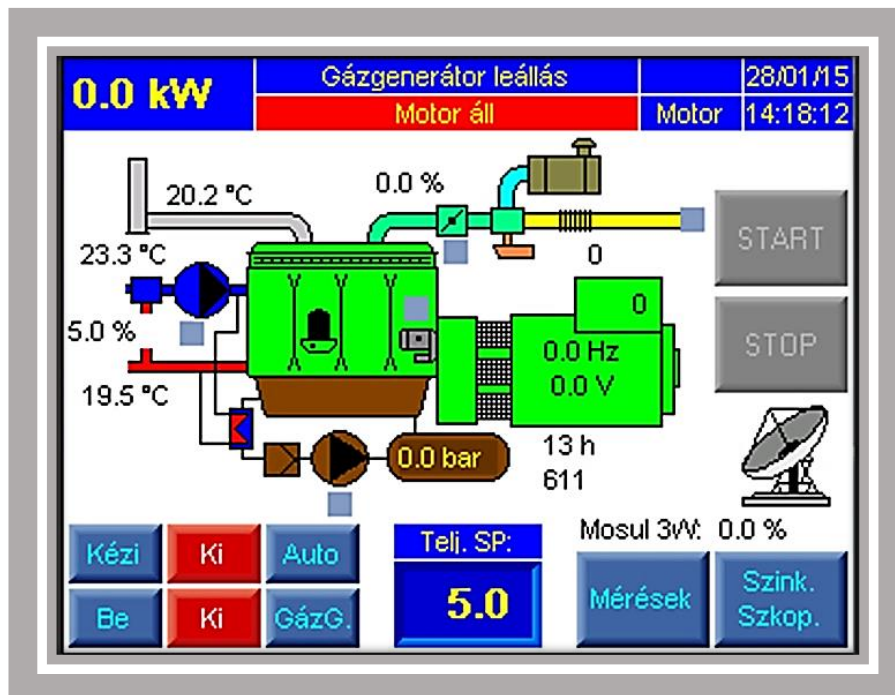


Figure 11. Operating characteristics of gas engine and electric generator

This screen shows the operation and operating parameters of the gas engine generator and the interfaces of the intervention options (touch buttons):

- The engine cannot be started until the gas generator parameters are correct.
- You can specify the desired power after start-up.
- Necessary controls for setting the motor mode.
- Engine speed, oil pressure and coolant temperature can be checked continuously.

The third system is based on the data and operational base of the two mentioned units, but it mainly cooperates with the electricity network, the base is provided by the network. After all, the system operates according to the strict needs of the network, subordinating the operation of the complex to it. If a malfunction detected by the controller, the main supply is cut off and the gas is burned by a logger placed outdoors. This eliminates the need to stop and restart the pyrolysis generator.

3. Result and Discussion

3.1. Characteristics of testing

Equipment designed for electrical power $100 \text{ kW}_{\text{max}}$

- Hardwood chips with a moisture content of 20%
- 13 MJ/kg calorific value

Table 3 shows the material used and the flow rate, table 4 describes the gas composition, table 5 introduces the characteristics of the energy produced and at last table 6 shows the occurring temperatures and other related characteristics.

Table 3. The material used

Fuel	Material flow (kg/h)
Wet wood	124
Moisture from the air	20
Air mass flow	239

Table 4. Gas composition

Gas composition	On wet basis (%)
CO	14.3
CO ₂	11.6
CH ₄	1.8
H ₂	18.5

Table 5. Energy characteristics

Characteristics	Energy (kW)	Heat energy (%)
Heat energy (input)	477	100
Energy in charcoal (residual)	17.8	3.7
Heat loss	18	3.8

Table 6. Temperatures and other characteristics

Related characteristics	On wet basis
Fuel moisture content (%)	20
Initial temperature of fuel (°C)	25
Outside and inlet air temperature (°C)	25
Hot gas temperature (°C)	600
Gasification temperature (°C)	850
The energy content of the gas (MJ/Nm ³)	5.1
Cold gas efficiency (%)	70.1
Ash (%)	1.9

CHP performance characteristics:

- $\eta_e = 0.23-0.26$: 108-121 kW_e
- Usable heat output: 350-365 kW
- 1 kWh of electricity can be produced from ~ 0.97-1.1 kg of wood chips.

The energy introduced into the wood but not utilized for drying and preheating the fuel, and includes the heat transferred by the components to the environment. These are: mainly with heat transfer and exhaust gas $\Sigma \sim 850$ MJ.

In this system, usable heat capacity is also used to produce cold energy for a cold store. In practice, it provides the input energy demand of the absorption chiller.

3.2. The absorption cooling system

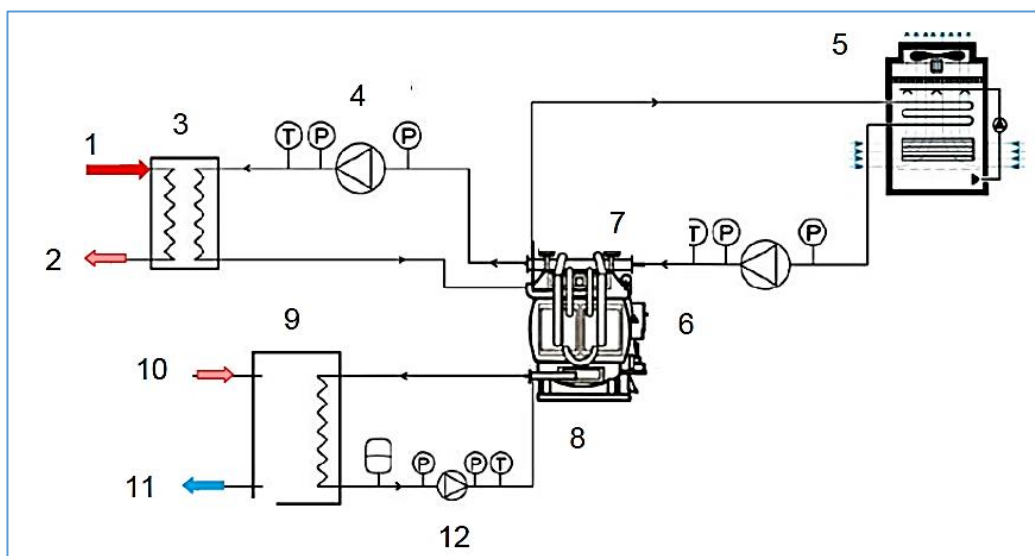


Figure 12. Cold power generation and system

Signs in fig. 12:

1. incoming heat energy to the distributor from a gas engine and a gas generator
2. return branch of divisor
3. plate heat exchanger
4. heating circuit elements
5. external air cooler to cool the absorber
6. absorption heat pump
7. cold energy circuit from the heat pump evaporator
8. cold energy circuit from the evaporator
9. heat exchanger of the cold store
10. return branch of the cold store
11. forward branch of the cold store
12. cooling circuit inlet fittings

The control of the CHP system described above is connected to the chiller, which is physically independent of its operation, namely it monitors the cold energy demand on the secondary side and intervenes according to its needs (Figure 12). If neither hot nor cold energy is needed, the thermal energy is released to the air through the air coolers.

In absorption refrigerators (Figure 13), instead of a compressor, in an absorption-desorption circuit, the working medium absorbs the vapor of the heat transfer medium at low pressure, increases the pressure of the solution to the upper pressure level, and then evaporates the heat transfer medium from the solution at the upper pressure level. So, they are also found in absorption machines: the evaporator, the condenser and the expansion valve. The mechanical compressor is replaced by a thermo-compressor (absorber + expeller) (Figure 13).

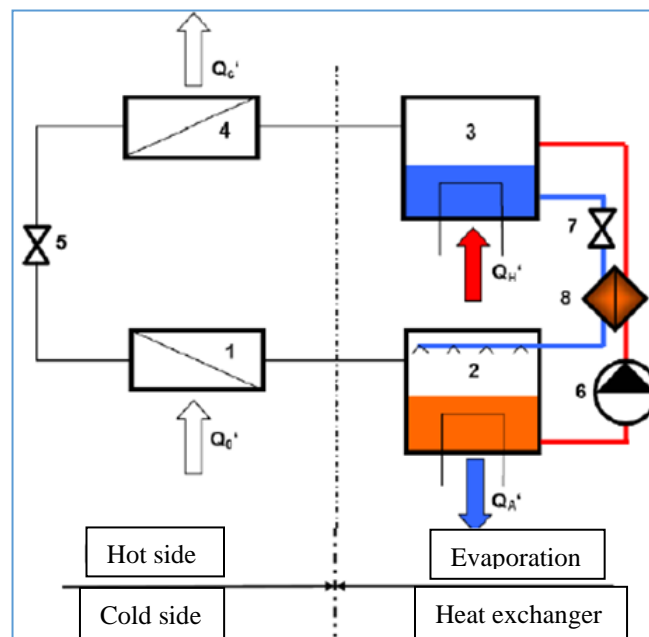


Figure 13. Schematic structure of the absorption refrigerator [8]

Signs in fig. 13:

1. evaporator
2. absorber
3. expulsive
4. condenser
5. expansion valve
6. pump
7. throttle
8. heat exchanger

From the generator the external heat causes the absorber steam to enter the condenser, where it becomes liquid under the influence of external cold energy, then evaporates through the choke when it draws heat from the hot material coming in the cooling circuit and liquefying. Upon entering the absorber, the poor solution returned from the generator is enriched and pumped back into the generator by the absorber pump. The intermediate heat exchanger improves efficiency by preheating the colder enriched medium, so less energy is required for re-expulsion.

Energy balance of the system:

$$Q'_o + Q'_H + P_P = Q'_C + Q'_A + Q'_V \quad (1)$$

Where:

- Q'_o = cold energy capacity (cooling capacity)
- P_P = pump drive performance
- Q'_A = warm energy (absorber power)
- Q'_H = heat dissipation (heating)
- Q'_C = condensation power (heat absorption)
- Q'_V = losses

Cold energy performance:

$$Q'_o = \epsilon_h (Q'_H + P_P) \quad (2)$$

Where COP: $\epsilon_h = 0,85-1,2$.

In this case, the available heat output is 350 kW, the cold power output of the absorption machine is ~ 340-355kW (this has not been validated yet).

3.3. The implemented system consists of two parts (Figure 14)

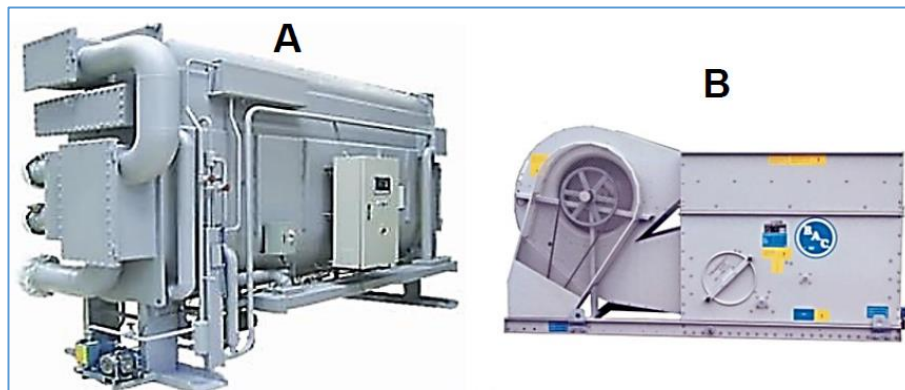


Figure 14. Chiller (A) and connected outdoor air cooler for absorber cooling (B)

The cooling unit:

The type of cooling unit is: 16JLH007. Manufacturer: Carrier CLK Corporation. Cold power output: 131 kW. Feed hot water: 90°C, mass flow: 7.5m³/h. The returning water temperature is 70°C. Refrigerant LiBr: 55% aqueous dilution. Total power of internal pumps: 2.1 kW. The cold side: inlet 12°C, outlet 6°C, mass flow 21.1 m³/h.

The external air cooler:

- Manufacturer: Baltimore Aircoil. Type VTL-E082-K.
- Drive motor: 7.5 kW, air delivery 10.6 m³/s.

3.4. Cost calculation for refrigerated storage

(The cost of kWh is made of the cost of investment and fuel [18]. Due to simplification, it was performed only for the normally required cooling period of 8 months)

- a) The 120kW system generates 660 000 kWh of electricity in 8 months (5 500 operating hours) to meet its own energy needs in other areas of the plant. Thus, at the current price of 10 € cent/kWh, it saves 119 459 €.
- b) If 124 kg/h of quality wood waste (0.054 €/kg) is used during the operating period, 35 135 € will be issued.
- c) The operating heat demand of the installed 131 kW absorption chiller 720 500 kWh over an 8-month period, which is waste heat, so it means no expense. If you buy electricity and the chiller works with 1.2 SPF, you will save 156 756 € (10 € cent/kWh electricity). With a good approximation, the energy requirement for storing one ton of fruit is ~ 100kWh (over 8 months). With this system, 7 200 tons can be stored at ~ 6°C.
- d) Due to the operation of the system, an additional ~ 70 kW of waste heat is available, which, when used or sold, means a profit of 124 324 € (at a price of 8.6 €/GJ).
- e) The investment cost of the system is 432 432 €.
- f) With these values, calculated with a simple return: the investment pays off in 3.3 years, i.e. it is already profitable in the fourth year.

(It would be less favourable, if the cooling facilities were solved with an electric heat pump, which would require ~ 360MWh of main electricity (including 2.0-2.5 SPF) (excluding the unit's own electricity consumption), which is ~ 65 135 € expenditure (excluding depreciation of the system).

2. Summary

In our study, we presented an environmental-friendly, energy-efficient system for the use of primary- and waste biomass. Biomasses with significant energy and cellulose content are well suited for the system, but require some preparation. The fragmentation and water content of the materials must be adequate for the beneficial operation of the system.

In the case of the developed pyrolysis (so-called thermal decomposition [19]) equipment, 0.9-1.15 kg of wood (containing 15 - 20% moisture) is needed to produce 1.0 kWh of electricity. During its operation, it generates 1.1-1.3 times more thermal energy than electricity, which can be used in its entirety (can be recuperated). This heat energy comes from the cooling of the gas generated during pyrolysis and the waste heat generated by the operation of the gas engine. It can be used entirely for community purposes, e.g., for heating, or domestic hot water, etc.

In this research, they are used to produce cold energy, namely to drive an absorption chiller, which e.g. provides the cold energy demands of storing fruits.

The economic calculation shows that given current electricity and firewood prices, the application of the system is particularly economical and even suitable for profit generation. It is even more advantageous to have biomass as waste in the operating environment, or even to pay for its destruction. The system is environmental-friendly, part of the so-called “circular farming”, but its environmental benefits are also significant. The resulting high mineral content ash and residual biochar are returned to the soil, increasing its productivity and water storage capacity. Compared to the natural fermentation of biomass, methane emissions are reduced and this contributes to the reduction of methane produced in agriculture as a strong greenhouse gas, and ultimately to the reduction of environmental pollution.

Acknowledgement

Thanks to GINOP-2.1.2-8-1-4-16 “Development of a complex energy system for the implementation of about 95% efficient, circulating decentralized energy production” entitled research and development, the processing of which provided substantive assistance.

References

- [1] **Downie A, Crosky A, Munroe P.:** (2009) Physical properties of biochar. In ‘Biochar for environmental management’, Science and technology, Sterling, VA, USA. pp. 13-32.
- [2] https://railsafe.hu/wp-content/uploads/2022/04/RAILSAFE_GINOP-2.1.2-8-1-4-16-2017-00075.pdf
- [3] <https://csolmontage.hu/szolgalatasaink/kfi-mernoki-tevekenyseg-es-muszaki-tanacsadas/>
- [4] **Tóth L.:** (2012) Alternatív energiaellátási rendszerek az agrárgazdaságban, Szaktudás Kiadó, Budapest, ISBN 978-615-5224-22-5. pp. 320.

- [5] **Madár V., Tóth L.:** (2012) Fagázgenerátor üzemű bio-kiserőmű és öntözőberendezés, *Mezőgazdasági Technika*, ISSN 0026 1890. 52. évf. Nr.09, pp. 3-8.
- [6] **Madár V., Tóth L., Madár Gy., Schrempf N.:** (2014) Kísérleti fagázgenerátor, *Mezőgazdasági Technika*, ISSN 0026 1890. 55. évf. Nr.4. pp. 2-5.
- [7] **Madár V., Tóth L., Schrempf N., Madár Gy., Gubó J., Szegvári P.:** (2016) Kísérleti pirolízis kiserőmű tüzeléstechnikai vizsgálata, *Mezőgazdasági Technika*, ISSN 0026 1890. 58. évf. Nr.02, pp. 2-6.
- [8] **Madár V., Tóth L., Schrempf N., Madár Gy., Gubó J.:** (2016) GG100 típusú fagázgenerátoros kiserőmű, *Mezőgazdasági Technika*, 58. évf. Nr.11, pp. 2-5.
- [9] **Tóth L.:** (2021) Az állattartás és a klímaváltozás összefüggései, *Mezőgazdasági Technika*, 2021. június. pp. 2-6.
- [10] **Országos Hulladékgazdálkodási Terv 2014-2020**, pp. 76-86.
- [11] **Tóth L., Madár V., Bácskai I.:** (2019) Pirolízis berendezés fejlesztését megelőző vizsgálatok, *Energiagazdálkodás*, 60. évf. 1-2. pp. 27-33.
- [12] **Dhaundiyal, A., Bercesi, G., Atsu, D., and Toth, L.:** (2021) Development of a small-scale reactor for upgraded biofuel pellet, *Renewable Energy*, 170, pp.1197–1214. DOI: 10.1016/j.renene.2021.02.057 (IF:7.387)
- [13] **F. Guo, Y. Dong, L. Dong, C. Guo.:** (2014) Effect of design and operating parameters on the gasification process of biomass in a downdraft fixed bed: an experimental study, *Int J Hydrogen Energy*, 39, pp. 5625-5633.
- [14] **Di Blasi:** (2004) Modelling wood gasification in a countercurrent fixed-bed reactor, *AIChE J*, 50, pp. 2306-2319.
- [15] **Kocsis T.:** (2018) Bioszén és bioeffektor kombinációk hatása homoktalajok biológiai tulajdonságaira, *Doktori értekezés*, Szent István Egyetem. pp. 110.
- [16] **Martínez J. D., Lora E. E. S., Andrade R., V., Jaén R. L.:** (2011) Experimental study on biomass gasification in a double air stage downdraft reactor, *Biomass and Bioenergy*, Vol. 35, I.8, pp. 3465-3480.
- [17] **N. S. Barman, S. Ghosh:** (2012) Gasification of biomass in a fixed bed downdraft gasifier – A realistic model including tar, Elsevier, *Bioresource Technology* 107. sz., pp. 505-511.
- [18] **Fülek A.:** (2003) Földi Gázturbinák, *Repüléstudományi közlemények* 15. évf. 35. sz., pp. 153-162.
- [19] **Bácskai I.:** (2020) Pirolízisgenerátor hatékonyságának növelése *Doktori (PhD) értekezés*, Gödöllő, Műszaki Tudományi Doktori Iskola, pp. 9-10.

STRATEGY ANALYSIS OF INTERNATIONAL FORAGE LABORATORY NETWORKS

Author(s):

G. Kövesdi¹, Sz. Orosz¹, Cs. Fogarassy²

Affiliation:

¹ Livestock Performance Testing Ltd., 2100 Gödöllő, Dózsa György u. 58., Hungary;

² Institute of Agriculture and Food Economics - Hungarian University of Agriculture and Life Sciences, 2100 Gödöllő, Páter Károly u. 1., Hungary;

Email address:

gretakovesdi@gmail.com; orosz.szilvia@atkf.hu; fogarassy.csaba@uni-mate.hu

Abstract: Nowadays, there are some successful forage laboratory global networks owned privately. Their strategies have been extremely successful in the past decades, and have shown a similar pattern worth examining for its effectiveness. In recent study, the business and corporate strategy of international forage laboratory networks (Eurofins Agro, CVAS, Rock River, DairyLand, DairyOne) have been analysed. Porter's five-factor model and the SWOT analysis have been applied to find out the key factors of the forage laboratory network building strategy.

Keywords: NIR-analysis, laboratory service, forage analysis, development strategy

1. Introduction

In 1987, Henry Mintzberg defined five different interpretive concepts for strategy: plan, trick, vision, position and pattern [1] [2]. It is important to differentiate between content and process. In terms of content, it encompasses the different types of decisions that decision-makers will make in the future. This can be a type of prioritizing of environmental adaptation, growth or decline [4][7][8]. In business, the strategy and strategy-making management functions of firms are regularly examined. One of the most defining figures in defining strategy was Porter. In terms of business strategy, the goal is for the business unit to gain a competitive advantage, while corporate strategy decides in which industries and how the company's units participate [10]. In the 1990s, however, Porter approaches the concept with a triple definition. The first is positioning, which means building a valuable position, the second is creating a trade-off, choosing between incompatible activities, and finally integrating activities to create a competitive advantage [11][12]. Views on competitiveness can be divided into four different groups: 1. denial of the concept of competitiveness, 2. macroeconomic, 3. microeconomic, and 4. unified positions [8] Porter's view can be classified as a microeconomic approach, as in his view competitiveness can only be interpreted for companies and industries, not for national economies [10].

One of Porter's best-known models is the five-factor model, which divides corporate performance into two different parts: industry-standard activities and activities that the company is able to perform above average. [11][11]. He believes a company is successful if it can achieve the best possible competitive position in its industry. It uses a five-factor model to measure competitive advantage.

In recent study, the business and corporate strategy of international forage laboratory networks (Eurofins Agro, CVAS, Rock River, Dairyland, DairyOne) have been analysed. Porter's five-factor model and the SWOT analysis have been applied to find out the key factors of the forage laboratory network building strategy.

2. Materials and Methods

In our research, we analyzed international laboratory networks using two models. Porter's five-factor model was used to measure competitive advantage.

The other method we used to analyse the current state of networks is SWOT analysis, a popular and widely used method of analysis that helps discovering the capabilities of a company, product, or service. Of the four options, strengths and weaknesses appear in the internal environment of the business, while opportunities and threats are external factors [12][14].

The analysis of the laboratory networks was performed on the following companies.

Eurofins is an international group of companies that provides unique analytics services (forage, water, manure, plant tissues et. cet.) to its clients across multiple industries. Eurofins Agro has set up a laboratory network around the world, which currently has more than 900 so-called ‘satellite’ laboratories. The company uses the NIR testing method. NIR is an innovative spectroscopy-based procedure that uses the absorption or reflection of near-infrared light (physical measurement, no chemicals required). This is an indirect matching method based on a NIR database and a reference database (classical chemical or *in vitro* value database). NIR spectroscopy is used partially to check parameters indicative of the phenological phase (e.g., water content, protein, and fiber content) during the harvest season. In part, it has an important role in quality control of the forage bank and is also the basis for TMR formulation [15].

CVAS (Cumberland Valley Analytical Services) is a US-based company that also deals in forage analysis and was founded in 1992 as a small-capacity chemical laboratory. They have tools suitable not only for testing forage samples, but also for testing water, manure, and plant tissue. This US based company also uses the NIR system to test incoming forage samples. CVAS, like Eurofins, has set up an international network of companies. Although headquartered in the United States, they operate forage analysis laboratories around the world [16].

The Rock River Laboratory is also located in the US. In addition to forage analysis, they also deal with animal health issues and water quality analyses. Their main customers are in the United States, but they have also set up satellite laboratories in South America, Spain and Germany [17].

Dairyland Laboratories, Inc. is an independent, full-service agricultural testing laboratory that provides analysis of forage, soil, plant tissue, manure, water, mould, and mycotoxins. It measures with laboratory wet chemistry and NIR methods. Dairyland Laboratories has customers in 42 states and 20 foreign countries [18].

Dairy One Cooperative is a non-profit cooperative focusing on plant, manure, water, milk and forage testing. In addition to wet chemical testing, this laboratory also uses NIR technology as its main testing method. They have built up a global around the world (more than 30 satellite laboratories) [19].

3. Results

In the following, we present the strategy of the examined international, privately owned forage laboratory networks through Porter’s five-factor model (Fig. 1) and SWOT analysis (Fig. 2). We observe that analytical laboratories have gained a huge and unattainable market advantage over chemical analytical laboratories using NIR technology. The other trend is that several NIR laboratories have developed a worldwide network to take advantage of foreign opportunities. Therefore, the analysis of the strategic elements of successful networking can fill the gaps from an economic point of view.

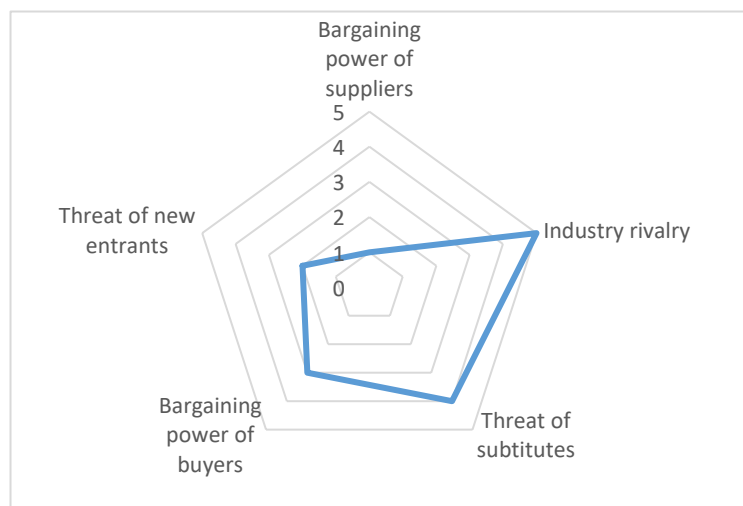


Figure 1. Application of Porter’s five-factor model for five international laboratory networks, highlighting commonalities

<p style="text-align: center;">Strengths</p> <ul style="list-style-type: none"> • Quick results • 'Multiparameter' measurements • Special parameters (parameters that cannot be determined by chemical analysis) • Value-for-money 'multi-parameter' packages • Diet formulation software input service • R&D takes place in a central laboratory • Standard protocols in satellite laboratories • 'Easy to install and manage' satellite laboratories 	<p style="text-align: center;">Weaknesses</p> <ul style="list-style-type: none"> • Acceptance of the NIR results • NIR database size - accuracy of results • 'Dry' NIR: the sample must be sent to the laboratory • Satellite laboratory: dependence on "mother laboratory", lack of its own calibration database
<p style="text-align: center;">Opportunities</p> <ul style="list-style-type: none"> • "Mother laboratory": R&D • Mobil in time 'wet' NIR development: the sample does not need to be sent to the lab 	<p style="text-align: center;">Threats</p> <ul style="list-style-type: none"> • Competitors • Macro-microeconomic environment • Mobile wet NIR displaces the laboratory and the 'dry' NIR

Figure 2. Application of SWOT analysis to five international laboratory networks, highlighting commonalities

4. Discussion

As a result of our research, the main, key elements of the strategic development of international forage laboratories are presented below. Furthermore, we found that the following parameters were very similar for the five networks examined:

- Independent laboratories (there is no feed company in the background, thus they can build a wide range of partners),
- Ability to test a wide range of different sample types (feed, water, manure, soil, etc.),
- The service is usually based on NIR measurement, because it is fast and accurate enough for practice (it took 20-30 years and a significant investment to create a database that allows internationally acceptable results, number of parameters and a wide range of sample types),
- Ability to measure many (20-30) parameters from a single forage sample (serving the demands of the crop manager, herd managers and nutritionist, respectively),
- They are also able to measure parameters with the NIR method, that cannot be routinely tested by classic chemical analytical methods (eg. *in vitro* digestibility)
- The parameters are offered in a package to their partners (convenient approach for the partner, makes ordering easier and secure)
- The operation also includes sampling services and advisory,
- In a so-called franchise system, a network of satellite laboratories has been set up. Satellite laboratories are required to measure and participate in internal audits according to uniform standard methods defined by the main company. The database is located in the centre, thus the satellite laboratories are in a dependent position as they get the results based on spectrum and pay for the results. So there is no need to send the sample physically, it just has to be transmitted online (this is one of the basics of the fast reports).
- As a result of nearly 30 years of developmental work, private research laboratories have a knowledge reproduced over decades, at a significant investment cost. Thus, creating an own calibration database (in a quality that is already existing at the level of global laboratory networks) is not a realistic strategic goal at either the private or at the state level. Because of this, the make-or-buy decision situation can not arise, if results to the partner is wanted to be quick). Therefore, for integration lab partners participating in a global network, a dependent relationship means immediate service opportunity and income, while stand-alone development would require years of investment without any revenue. Creating and maintaining this situation is one of the strategic cornerstones of building a laboratory network.
- The satellite laboratory in the country is supported by the "mother laboratory", as it works with it, shares knowledge and, in some cases, receives the necessary tools from them (NIR equipment, grinder). The

“mother laboratory” conducts research and development to maintain their competitiveness, which requires significant investment and huge infrastructural laboratory capacity.

- Formulation software servicing is also part of the strategy, as laboratories providing in-put data for multiple diet formulation software can gain market advantage. Also all this in the form of an xml input file (no need to manually enter the data for today’s software user). Therefore laboratory networks generally consult with developers of major software owners on parameters and IT issues.

After performing a five-factor analysis of Porter, we found that the bargaining position of suppliers is less dominant in the strategy of international forage laboratory networks. The threat of new entrants is not a significant factor due to its capital and time-consuming nature. However, the threat of substitutes is significant, as there may be more than one satellite laboratory in a country or region. These competitors can easily replace other laboratories due to the better price / value ratio. The bargaining power of the buyers is high, as the use of an optional service is of paramount importance to the laboratory, so meeting the needs set up by the customers is priority. The industry rivalry has the greatest impact on strategy. Due to continuous research and development, the needs of the market and the market itself are changing rapidly.

Based on the SWOT analysis, the following was established.

- **Strengths:** The strength of international forage laboratory networks is their ability to provide results fast (24-48 hours) and ‘multi-parameter’ data with special information (e.g. digestibility). All this is provided in affordable and convenient packages. In addition, they have a broad knowledge base across countries. Through developments, satellite laboratories are also be able to provide input data for major local and global software, providing a huge market advantage in collaboration with a feed company. The unified methodology operated within the network provides security that the applied methods are up-to-date and validated, which supports the authenticity through accuracy. Through the central research and development laboratory, it is possible that satellite laboratories do not require large infrastructural investment and a highly skilled workforce.
- **Weaknesses:** a weak point of the system is the acceptance of NIR over chemical analysis. Accuracy is determined by the size of the database, which can vary between networks. Samples for ‘dry’ NIR must be sent to the laboratory (drying, grinding, homogenisation), which is a disadvantage compared to the mobile NIR equipment. This will have a major impact in the distant future, when mobile NIR technology will be accurate enough for large-scale measurements. The dependent position of satellite laboratories may weaken the market position in a given area because they do not have their own calibration database. However, the developments also cover locally occurring special feeds, so this disadvantage can be mitigated by the central developmental laboratory. However, running a central research laboratory is expensive if it wants to stay competitive. Appropriate and innovative technological tools, their maintenance and use mean high and regular costs for the company.
- **Opportunities:** there is an increasing emphasis on central research and development in this area. If such a program is successfully completed in a centralized, high-capacity and well-equipped central laboratory, it will be a great opportunity for all satellite laboratories to stabilize their market position and improve their position. The latest development was particularly investment-intensive and significantly strengthened the position of satellite laboratories (calibration database of CNCPS model input data). The situation of central development and database significantly increases the economic efficiency of research and development (specifically cheaper than operating several local development laboratories) and data security (thus data theft is not possible). Mobile NIR can be both an opportunity and a threat to laboratories. On the one hand, the laboratory becomes unnecessary if the measurements can be performed on site. On the other hand, the laboratory can participate in the calibration of the mobile NIR and later provide it to its partners as a service.
- **Threats:** increasing competition in the sector poses a significant threat to the agricultural business [20]. Satellite laboratories (competitors) appearing on the market in more and more places are also a primary threat to networks. In some countries, there are already laboratories with a similar strategy and technology, thus taking revenue from each other. The market position of each satellite laboratory affects the performance of the entire network, as these are factors that interact with each other. Through developing their services, laboratories can prepare to reduce the risks.

5. Conclusions

As a result of the research, we explored the strategic foundations of how international laboratory networks executed their global network development. The key strategic elements were as follows, which can be found

for all 5 laboratory networks: centralized system (central database and database development), central well-equipped R&D chemical and *in vitro* laboratory (reference analyses), easy to install 'satellite' laboratories, standard protocols globally, NIR-technology, all-in-one hand (multifunctional NIR-services: forage, manure, soil, water), quick service, multiparameter-packages (20-30 parameters/sample), collaboration with formulation software owners. The study confirmed that this development strategy was detailed and extremely effective. That is the reason why many similarities have been found in the different laboratory networks studied.

References

- [1] **Porter, M.**, (1985) Competitive advantage, creating and sustaining superior performance. The Free Press, New York
- [2] **Mintzberg, H.**, (1987) The Strategy Concept II: Another Look at Why Organizations Need Strategies. California Management Review, vol.30.1, 25-53 doi:10.2307/41165264
- [3] **Porter, M.**, (1998) Clusters and the new economics of competitiveness. Boston: Harvard Business Review
- [4] **Seth, A., Zinkhan G.**, (1991) Strategy and the research process: A comment. Strategic Management Journal, vol. 12.1 75-82 doi:10.1002/smj.4250120107
- [5] **Ward, P.T., Leong, G.K., Synder, D.L.** (1990) Manufacturing Strategy: An Overview of Current Process and Content Models. Manufacturing Strategy 189-199 doi:10.1007/978-94-009-2189-4_19
- [6] **Porter, M.**, (1979) How competitive forces shape strategy? Boston: Harvard Business Review
- [7] **Porter, M.**, (1996) What is strategy? Boston: Harvard Business Review
- [8] **De Wit, B.**, (1997) Porter on business strategy. Perspectives on Strategy 7-18 doi:10.1007/978-1-4615-6179-8_2
- [9] **Lengyel, I.**, (1999) Régiók versenyképessége (A térségek gazdaságfejlesztésének főbb gazdasági fogalmai, alap gondolatai, tényezői az EU-ban). Kézirat, JATE Gazdaságtudományi Kar, Szeged
- [10] **Porter, M.**, (1990) The competitive advantage of nations. The Free Press, New York
- [11] **Porter, M.**, (1987) From competitive advantages to corporate strategy. Boston: Harvard Business Review
- [12] **Dobbs, E. M.**, (2014) Guidelines for applying Porter's five forces framework: a set of industry analysis templates. Competitiveness Review vol.24.1 32-45 doi:10.1108/CR-06-2013-0058
- [13] **Gürel, E.**, (2017) SWOT Analysis: A theoretical review. The Journal of International Social Research, 10, 994-1006. doi:10.17719/jisr.2017.1832
- [14] **Helms, M. M., Nixon, J.**, (2010) Exploring SWOT analysis – where are we now? A review of academic research from the last decade. Journal of Strategy and Management, vol3.3, 215-251 doi:10.1108/17554251011064837
- [15] **Eurofins** (2022) Our Strategy and objectives. Available at: <<https://www.eurofins.com/about-us/our-business/eurofins-strategy-and-objectives/>> (Accessed 2 March 2022)
- [16] **Cumberland Valley Analytical Services** (2022) Our mission. Available at: <<https://www.foragelab.com/>> (Accessed 2 March 2022)
- [17] **Rock River Lab** (2022) About us <<https://www.rockriverlab.com/pages/About.php>> / (Accessed 2 March 2022)
- [18] **Dairyland Laboratories, Inc.** (2022) History. <<https://www.dairylandlabs.com/about-us/history/>> / (Accessed 2 March 2022)
- [19] **Dairy One** (2022) Core Values <<https://www.dairyone.com/about/core-values/>> / (Accessed 2 March 2022)
- [20] **Namugenyi, C., Nimmagadda, S. L., Reiners, T.**, (2019) Design of a SWOT Analysis Model and its Evaluation in Diverse Digital Business Ecosystem Contexts. Procedia Computer Science 159, 1145-1154. Doi: 10.1016/j.procs.2019.09.283



SMALL SCALE EXPERIMENTS OF PM₁₀ DISPERSION AROUND OBSTACLES

Author(s):

A. Qor-el-aine¹, J. Benécs², A. Béres³, G. Géczí³

Affiliation:

¹ Doctoral School of Mechanical Engineering – Hungarian University of Agriculture and Life Sciences, 2100 Gödöllő, Páter Károly u. 1., Hungary;

² Institute of Process Engineering - Hungarian University of Agriculture and Life Sciences, 2100 Gödöllő, Páter Károly u. 1., Hungary;

³ Institute of Environmental Science - Hungarian University of Agriculture and Life Sciences, 2100 Gödöllő, Páter Károly u. 1., Hungary;

Email address:

Qor-El-Aine.Achraf@phd.uni-mate.hu; Geczi.Gabor@uni-mate.hu; Beres.Andras@uni-mate.hu;

Benecs.Jozsef.Istvan@uni-mate.hu

Abstract: Particulate matter (PM) is the main determinant of air pollution caused by a variety of natural and human-caused sources. Because it can be suspended in the atmosphere for long periods of time and travel long distances, it can cause a major health crisis for humans and damage the environment as well. Studies are still required to understand how the PM moves around obstacles, especially in urban areas. In this study, small scale experiments were carried out to look into the effects of simple obstacles, heights and distance from the source on the PM₁₀ concentration. Results show that when obstacle heights and distance from the source increase, the PM₁₀ average concentration decrease. Also, turbulence created by the obstacles affects the PM₁₀ concentration in both sensors before and after the obstacle, mainly in cases of high wind speed. In addition, the use of incense sticks as a source of PM pollution illustrated that moderate burning of incense sticks in indoor places could skyrocket the PM₁₀ concentration to an unhealthy level.

Keywords: PM₁₀ concentration; PM₁₀ dispersion; Incense sticks; Obstacles; Wind speed

1. Introduction

Particulate matter (PM) is a broad term that encompasses a wide range of particle sizes. It includes particles with a diameter ranging from a few nanometers to 100 micrometers. Carbonaceous particles with adsorbed organic chemicals and reactive metals make up the PM component of air pollution. Nitrates, sulfates, polycyclic aromatic hydrocarbons, endotoxin, and metals such as iron, copper, nickel, zinc, and vanadium are all common components of PM [1]. These are usually divided into two basic particle metrics, PM₁₀ (coarse particle with diameter <10 μ m) and PM_{2.5} (fine particles with diameter <2.5 μ m), in order to ensure adequate monitoring and regulation [2]. Coarse particles come from a variety of natural as well as anthropogenic sources, but they rarely make it past the upper bronchus of the lung. Fine particles are produced when fossil fuels are burned, and they pose a greater health risk than coarse particles because they penetrate into the small airways and alveoli (very small balloon air sacs, with the function of moving oxygen and carbon dioxide molecules into and out of the bloodstreams) [3]–[5]. Furthermore, High levels of PM have been linked to serious diseases such as silicosis, lung cancer, cardiovascular disease, and chronic obstructive pulmonary disease, so exposure to PM can have a serious impact on human health [6]–[8]. Besides that, PM exposure was associated with an increased risk of death [9]. According to the World Health Organization (WHO), exposure to high concentrations of PM₁₀ and PM_{2.5} were linked to a high mortality rate [10].

The dispersion and the transport of PM plume in urban areas are still an open field due to its complexity. Many studies were conducted to understand more how the PM plumes are moving around different types of obstacles and how different parameters can influence it [12]–[14]. Building height variability and wind have

effects on PM plume dispersion [15]–[17]. Simplified wind tunnel experiments and Computational Fluid Dynamics (CFD) simulations investigated the PM and air pollutants dispersion in simplified urban models [18]–[21].

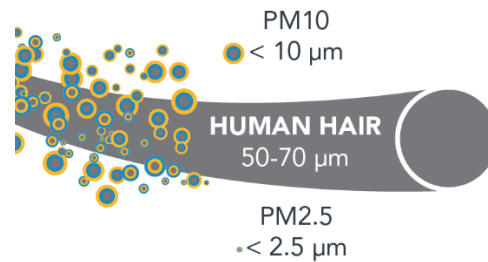


Figure 1. Particulate matter size comparison [11]

In this paper, small scale experiments were conducted in order to investigate the effects of obstacles, heights and distance from the source on the PM10 concentration. The goal was to understand the changing of the PM10 concentration around obstacles in a simple environment.

2. Materials and Methods

The experiments were done in an isolated laboratory room on the built table. The table had 3 PM10 sensors with a 50 cm distance between each sensor. The room temperature was stable during the experiments ($25 \pm 1^\circ\text{C}$); the same was for the Relative Humidity (RH) ($50\% \pm 3$).

2.1 Experiment set up

The experiments were done with two different wind speeds (2.9 and 1 m/s) provided by two different small ventilators. The use of the ventilators is to make sure that the PM plume will follow the wind direction toward the sensors and to avoid the spreading of the plume around the room. As mentioned, three sensors were used, sensors A, B and C, as shown in Figure 2, sensor C is placed near the source, sensor B is in the middle and sensor A is 1 meter away from the source. The obstacle was placed at three different distances between sensors A and B, with changing of the obstacle height (120, 240 and 360 millimetres).

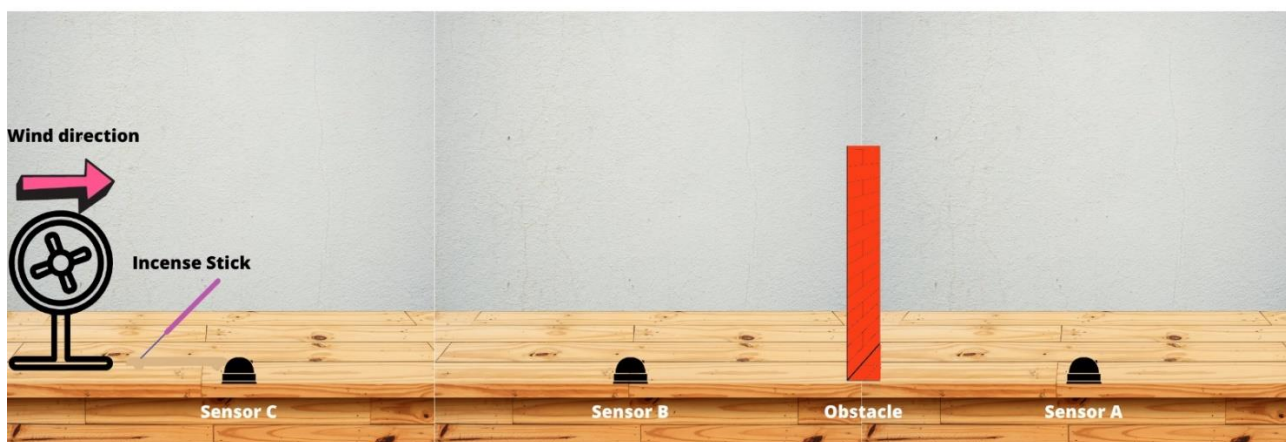


Figure 2. Experimental set-up

The incense sticks were used as a source of PM10 plumes due to the number of particles emitted from incense smoke in a short time. There were many research studies that investigated the effect of the use of incense sticks on PM10 concentrations. Numerous studies point out that during the burning of the incense sticks, the particle concentration increase dramatically, and so is the concentration of PM2.5 and PM10 to extreme levels; not only the PM concentration that increases during the incense stick burning but also the level of Carbone Oxide (CO), Nitrogen Oxides (NOx) and Sulfur dioxide (SO₂) concentrations go up [22]–[27].

Each experiment took 15-20 minutes by burning one incense stick with fixed wind speed, obstacle distance from the source and obstacle height. The total number of variations (experiments) was 18.

2.2 Data analysis

Measurements were registered continuously in a programmed excel sheet during each experiment for every 30 seconds. The results present the average PM10 concentration in each test and are presented in graphs depending on the obstacle height and distance from the source for the three sensors.

3. Results

The results of the experiments showed some interesting aspects for the understanding of the PM10 dispersion around the simple obstacle (Walls).

3.1. Sensor A

Sensor A is the sensor behind the obstacle. Figure 3 shows the average concentration of PM10 during each experiment in the function of Obstacle heights and distance from the source. The average PM10 concentration increase with increasing the obstacle distance from the source at higher wind speed, while at low wind speed, it is almost stable. At a wind speed of 2.9m/s, the average PM10 concentration was the same for obstacle heights of 240 and 360mm, while it was at its peak when obstacle height was 120mm. While for the wind speed of 1m/s, the peak average PM10 concentration was at the obstacle height of 360mm and almost the same at the other two heights.

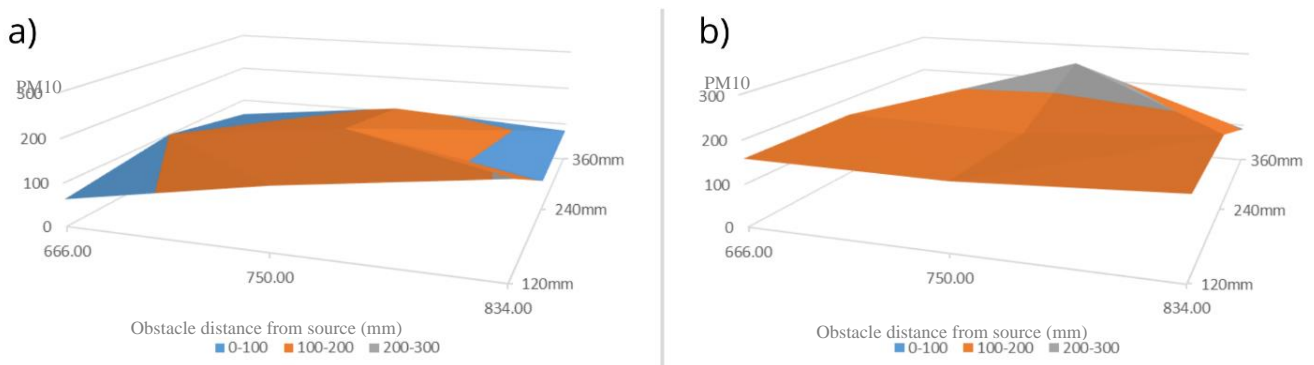


Figure 3. graphs of Average PM10 concentration registered by Sensor A in the function of Obstacle heights and distance from the source in case of a) wind speed 2.9 m/s and b) wind speed 1 m/s

3.2. Sensor B

For sensor B, which is the sensor placed before the wall, the PM10 average concentration was higher in the case of wall height of 240 and 360mm, and wall distance of 750mm at a wind speed of 1m/s (Figure 4).

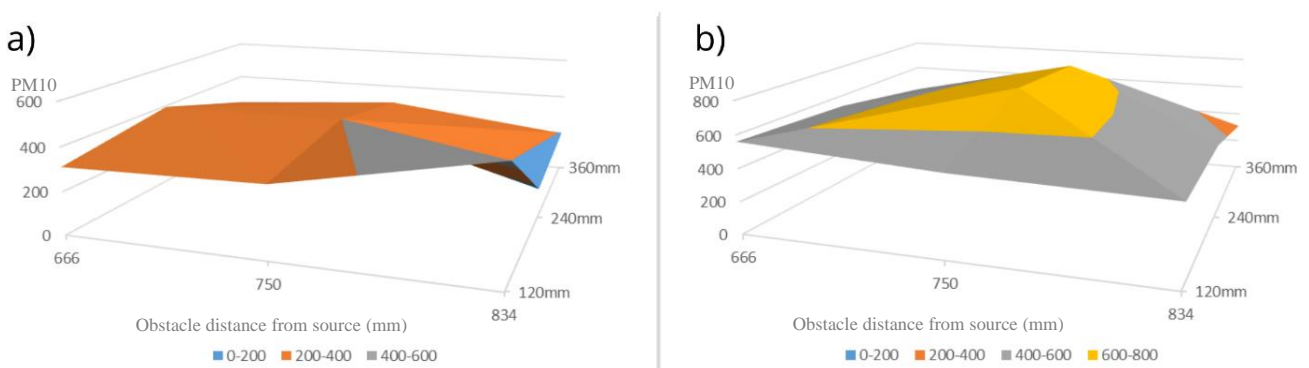


Figure 4. Graphs of Average PM10 concentration registered by Sensor B in the function of Obstacle heights and distance from the source in case of a) wind speed 2.9 m/s and b) wind speed 1 m/s

While it reaches the maximum when the obstacle distance from the source is 834mm, obstacle height is 120mm and wind speed of 2.9m/s.

3.3. Sensor C

The sensor C placed near the source registered almost the same average concentration of PM10 at a wind speed of 1m/s with a decrease in concentration in case of obstacle height of 360mm and distance from the source of 834mm (Figure 5). On the other hand, it was changing at a wind speed of 2.9m/s. The peak average PM10 concentration was the same as sensor B when the obstacle distance from the source was 834mm, and the obstacle height was 120mm.

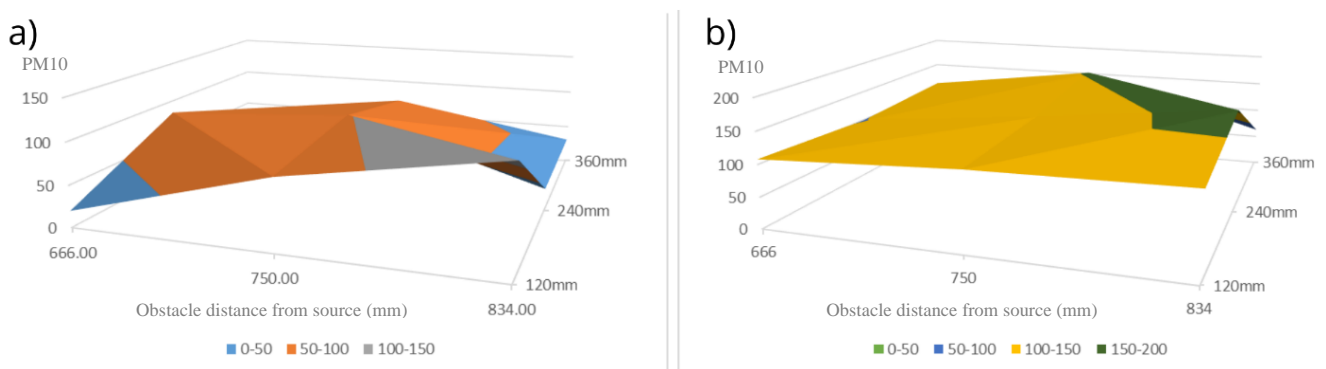


Figure 5. Graphs of Average PM10 concentration registered by Sensor C in the function of Obstacle heights and distance from the source in case of a) wind speed 2.9 m/s and b) wind speed 1 m/s

4. Discussion

The results of this research concluded that there is a significant positive effect on Obstacle heights, the distance of the obstacle from the source, and the wind speed. The PM10 average concentration decrease significantly in sensor A (behind the wall) when the obstacle height increases and also when the obstacle distances from the source increase also in case of the two-wind speed (1m/s and 2.9m/s) with higher concentrations registered in case of wind speed is 1m/s. While, changes in the PM10 average concentration were also seen in the case of Sensor B (in the middle) and sensor C (near the source), especially in the case of high wind speed (2.9m/s) and, that is due to the turbulence created before and after the walls when the wind hits it, in addition to the reflection of PM plumes by the obstacle.

Generally, the PM10 average concentration tends to decrease when obstacle heights increase but are also combined with the position of the obstacle far from the source.

Moreover, using Incense sticks as a source of PM pollution showed that while the stick is burning, it continues to spike the PM10 concentration, as before the experiments, the background concentration of PM10 was $7 \pm 3 \mu\text{g}/\text{m}^3$, and during the experiments, it can reach $700 \mu\text{g}/\text{m}^3$, which manifest the short-term effect of burning the incense stick and its risk of affecting the indoor air quality if used in excess.

5. Conclusions

This paper investigated the PM10 dispersion around the wall of different heights and distances from the source in a simple environment. Two wind speeds were used in the experiments (1m/s and 2.9m/s) and variations of three wall heights (120, 240 and 360mm) constructed by simple breaks and three different distances from the source (666, 750 and 834mm).

The results showed higher average PM10 concentrations were registered in case of low wind speed (1m/s); increasing the wind speed results in decreasing the PM10 concentration. As the Obstacle height goes up, the PM10 concentration goes down, especially in position after the obstacle. Moreover, the PM10 concentration decrease by going far from the source and decreases, even more when an obstacle is placed between source and sensor. The turbulence created by the effects of the walls also the before and after wall sensors measurements.

Even so, more research is needed, and more parameters should be considered for a deep understanding of the PM plume dispersions around different types of obstacles.

Additionally, burning of the incense stick increases the PM10 concentration dramatically in the experiment room, and excessive use of it deteriorates the indoor air quality.

References

- [1] **R. B. Hamanaka and G. M. Mutlu**, “Particulate Matter Air Pollution: Effects on the Cardiovascular System,” *Frontiers in Endocrinology*, vol. 9, 2018, Accessed: Apr. 05, 2022. [Online]. Available: <https://www.frontiersin.org/article/10.3389/fendo.2018.00680>
- [2] **A. Thorpe and R. M. Harrison**, “Sources and properties of non-exhaust particulate matter from road traffic: A review,” *Science of The Total Environment*, vol. 400, no. 1, pp. 270–282, Aug. 2008, doi: 10.1016/j.scitotenv.2008.06.007.
- [3] **M. R. Miller, C. A. Shaw, and J. P. Langrish**, “From particles to patients: oxidative stress and the cardiovascular effects of air pollution,” *Future Cardiology*, vol. 8, no. 4, pp. 577–602, Jul. 2012, doi: 10.2217/fca.12.43.
- [4] **C. A. Pope**, “Epidemiology of fine particulate air pollution and human health: biologic mechanisms and who’s at risk?,” *Environmental Health Perspectives*, vol. 108, no. suppl 4, pp. 713–723, Aug. 2000, doi: 10.1289/ehp.108-1637679.
- [5] **M. T. Chin**, “Basic mechanisms for adverse cardiovascular events associated with air pollution,” *Heart*, vol. 101, no. 4, pp. 253–256, Feb. 2015, doi: 10.1136/heartjnl-2014-306379.
- [6] **K. Khamraev, D. Cheriyan, and J. Choi**, “A review on health risk assessment of PM in the construction industry – Current situation and future directions,” *Science of The Total Environment*, vol. 758, p. 143716, Mar. 2021, doi: 10.1016/j.scitotenv.2020.143716.
- [7] **N.-H. Hsieh and C.-M. Liao**, “Assessing exposure risk for dust storm events-associated lung function decrement in asthmatics and implications for control,” *Atmospheric Environment*, vol. 68, pp. 256–264, Apr. 2013, doi: 10.1016/j.atmosenv.2012.11.064.
- [8] **H. Kim, H. Kim, and J.-T. Lee**, “Effects of ambient air particles on mortality in Seoul: Have the effects changed over time?,” *Environmental Research*, vol. 140, pp. 684–690, Jul. 2015, doi: 10.1016/j.envres.2015.05.029.
- [9] **F. Lu et al.**, “Systematic review and meta-analysis of the adverse health effects of ambient PM2.5 and PM10 pollution in the Chinese population,” *Environmental Research*, vol. 136, pp. 196–204, Jan. 2015, doi: 10.1016/j.envres.2014.06.029.
- [10] **World Health Organization**, *WHO global air quality guidelines: particulate matter (PM2.5 and PM10), ozone, nitrogen dioxide, sulfur dioxide and carbon monoxide*. Geneva: World Health Organization, 2021. Accessed: Apr. 07, 2022. [Online]. Available: <https://apps.who.int/iris/handle/10665/345329>
- [11] **California Air Resources Board**, “Inhalable Particulate Matter and Health (PM2.5 and PM10) | California Air Resources Board.” <https://ww2.arb.ca.gov/resources/inhalable-particulate-matter-and-health>
- [12] **H. Merbitz, F. Detalle, G. Ketzler, C. Schneider, and F. Lenartz**, “Small scale particulate matter measurements and dispersion modelling in the inner city of Liège, Belgium,” *International Journal of Environment and Pollution*, vol. 50, no. 1–4, pp. 234–249, Jan. 2012, doi: 10.1504/IJEP.2012.051196.
- [13] **L. Liang and P. Gong**, “Urban and air pollution: a multi-city study of long-term effects of urban landscape patterns on air quality trends,” *Sci Rep*, vol. 10, no. 1, Art. no. 1, Oct. 2020, doi: 10.1038/s41598-020-74524-9.
- [14] **M. J. Davidson, W. H. Snyder, R. E. Lawson, and J. C. R. Hunt**, “Wind tunnel simulations of plume dispersion through groups of obstacles,” *Atmospheric Environment*, vol. 30, no. 22, pp. 3715–3731, Nov. 1996, doi: 10.1016/1352-2310(96)00103-3.
- [15] **J. Hang, Y. Li, M. Sandberg, R. Buccolieri, and S. Di Sabatino**, “The influence of building height variability on pollutant dispersion and pedestrian ventilation in idealized high-rise urban areas,” *Building and Environment*, vol. 56, pp. 346–360, Oct. 2012, doi: 10.1016/j.buildenv.2012.03.023.
- [16] **Z.-L. Gu, Y.-W. Zhang, Y. Cheng, and S.-C. Lee**, “Effect of uneven building layout on air flow and pollutant dispersion in non-uniform street canyons,” *Building and Environment*, vol. 46, no. 12, pp. 2657–2665, Dec. 2011, doi: 10.1016/j.buildenv.2011.06.028.

- [17] **S. Di Sabatino, R. Buccolieri, B. Pulvirenti, and R. Britter**, “Simulations of pollutant dispersion within idealised urban-type geometries with CFD and integral models,” *Atmospheric Environment*, vol. 41, no. 37, pp. 8316–8329, Dec. 2007, doi: 10.1016/j.atmosenv.2007.06.052.
- [18] **J. Dehai, W. Jiang, H. Liu, and J. Sun**, “Systematic influence of different building spacing, height and layout on mean wind and turbulent characteristics within and over urban building arrays,” *Wind and Structures*, vol. 11, pp. 275–289, Aug. 2008, doi: 10.12989/was.2008.11.4.275.
- [19] **J. Hang, M. Sandberg, Y. Li, and L. Claesson**, “Pollutant dispersion in idealized city models with different urban morphologies,” *Atmospheric Environment*, vol. 43, no. 38, pp. 6011–6025, Dec. 2009, doi: 10.1016/j.atmosenv.2009.08.029.
- [20] **S. Brusca, F. Famoso, R. Lanzafame, S. Mauro, M. Messina, and S. Strano**, “PM10 Dispersion Modeling by Means of CFD 3D and Eulerian–Lagrangian Models: Analysis and Comparison with Experiments,” *Energy Procedia*, vol. 101, pp. 329–336, Nov. 2016, doi: 10.1016/j.egypro.2016.11.042.
- [21] **S. Brusca, F. Famoso, R. Lanzafame, A. M. C. Garrano, and P. Monforte**, “Experimental Analysis of a Plume Dispersion Around Obstacles,” *Energy Procedia*, vol. 82, pp. 695–701, Dec. 2015, doi: 10.1016/j.egypro.2015.11.794.
- [22] **X. Ji et al.**, “Characterization of particles emitted by incense burning in an experimental house,” *Indoor Air*, vol. 20, no. 2, pp. 147–158, Apr. 2010, doi: 10.1111/j.1600-0668.2009.00634.x.
- [23] **S.-C. Lee and B. Wang**, “Characteristics of emissions of air pollutants from burning of incense in a large environmental chamber,” *Atmospheric Environment*, vol. 38, no. 7, pp. 941–951, Mar. 2004, doi: 10.1016/j.atmosenv.2003.11.002.
- [24] **L. K. Tran et al.**, “The impact of incense burning on indoor PM2.5 concentrations in residential houses in Hanoi, Vietnam,” *Building and Environment*, vol. 205, p. 108228, Nov. 2021, doi: 10.1016/j.buildenv.2021.108228.
- [25] **S. Wei See, R. Balasubramanian, and U. M. Joshi**, “Physical characteristics of nanoparticles emitted from incense smoke,” *Science and Technology of Advanced Materials*, vol. 8, no. 1–2, pp. 25–32, Jan. 2007, doi: 10.1016/j.stam.2006.11.016.
- [26] **A. Goel, R. Wathore, T. Chakraborty, and M. Agrawal**, “Characteristics of Exposure to Particles due to Incense Burning inside Temples in Kanpur, India,” *Aerosol Air Qual. Res.*, vol. 17, no. 2, pp. 608–615, 2017, doi: 10.4209/aaqr.2016.04.0146.
- [27] **J. J. Jetter, Z. Guo, J. A. McBrien, and M. R. Flynn**, “Characterization of emissions from burning incense,” *Sci Total Environ*, vol. 295, no. 1–3, pp. 51–67, Aug. 2002, doi: 10.1016/s0048-9697(02)00043-8.

MICROCLIMATIC AND ENERGETIC FEASIBILITY OF AGRIVOLTAIC SYSTEMS: STATE OF THE ART

Author(s):

I. Khele^{1,2*}, M. Szabó²

Affiliation:

¹ Doctoral School of Mechanical Engineering, Hungarian University of Agriculture and Life Sciences, Páter K. u. 1, Gödöllő, H-2100, Hungary.

² Department of Building Engineering and Energetics, Hungarian University of Agriculture and Life Sciences, Páter K. u. 1, Gödöllő, H-2100, Hungary.

* Corresponding author

Email address:

Issam.Khele@phd.uni-mate.hu ; Szabo.Marta@uni-mate.hu

Abstract: Agrivoltaic systems have been proposed as the most prominent synergetic application of agricultural and energetic sectors. Integrating solar power generating with agricultural activities is relatively new; however, it has started with implementing the PV panels into the greenhouses. Comparatively, open-field agrivoltaics systems are still growing and under-development in many locations around the world. The urge to explore innovative solutions for the increasing demand for electricity and food has been the main motivation for the research centers, researchers, and governments to escalate agrivoltaics development globally. In this paper, the current and most recent projects and studies of open-field agrivoltaic systems are presented, compared, and analyzed in order to anticipate the potential and path of development for agrivoltaics in the near future. Several pieces of research from different countries globally were included to illustrate the main features and performance indicators of agrivoltaic systems. The paper concludes that the agrivoltaics system has the potential to grow to big-scale projects in different climatic regions because it provides benefits either by increasing the Land Equivalent Ratio (LER), protecting the plants from severe ambient weather, and diversifying the income for farmers. New technologies and methods have been integrated with the agrivoltaics systems in different projects to optimize the model; however, many aspects of development could be introduced in the near future.

Keywords: Agrivoltaics, Agrophotovoltaics, dual-use land, crop production

1. Introduction

The increasing need for energy worldwide has been accompanied with increasing demand for food due to the constant population explosions. That elaborated a (food vs. energy) dilemma, especially in countries with scarce arable lands [1]. Moreover, since renewable energy sources onshore (mainly solar and wind energy) require huge areas of land for the infrastructure in order to generate a sufficient amount of electricity, the dilemma of exploiting the arable lands for energy-generating purposes has been debatable, especially in the last decade. Therefore, sustainable solutions have to be proposed to allow the dual use of land, especially in countries with no arid or semi-arid lands (like most European countries), which can be exploited mainly for solar energy harnessing.

Agrivoltaic systems (APV) have emerged to provide a synergetic solution for both energetic and agricultural sectors, allowing for the dual-use of the land leading to maximizing the benefit and diversifying the income. Agrivoltaics could simultaneously meet the growing demands on energy and food and reduce fossil fuel emissions. [2][3][4] Therefore, the installed capacity has increased exponentially from 5 megawatts (MW_p) peak in 2012 to at least 2.8 gigawatts peak (GW_p) in 2020. [5]

On the other hand, the key feature of agrivoltaic systems, which is the synergy that can be created between agricultural and energetic sectors, is what causes the complexity of optimizing the system. (APV) evaluation

is not just impacted by the performance of the photovoltaic modules, the tilt angle, or the losses factor. Many aspects shall be considered since the agricultural performance is as essential as the energetic performance, and in some cases, it may be prioritized.

In this paper, the current state of the art of the agrivoltaic systems is presented and discussed to assess the current barriers and challenges, explore the new technologies and methods, and the potential technologies to be used in the field.

The article is organized as follows. Section 2 presents the research method and the keywords used for the literature review. In section 3, a brief definition and background were provided to illustrate the context of agrivoltaics development. Section 4 is dedicated to expressing and discussing the current state of the art of agrivoltaic systems. Finally, the main conclusions are discussed in section 5.

2. Materials and Methods

To collect relevant research publications, a review process was conducted, and the following keywords were used in (Google Scholar), (Web of Science), and (Scopus): (Agrivoltaics, Agrophotovoltaics, dual-use land, Solar sharing).

It should be noted that the chosen papers and scientific papers of research focused on the open-field agrivoltaic systems. The papers that only focus on the greenhouses integrated with photovoltaics were excluded from the review.

3. Background of Agrivoltaics

No universal definition can be found in the standards for agrivoltaic systems; however, Fraunhofer ISE Institute defined the agrivoltaic systems as "Agrivoltaics allows the simultaneous use of land for both agriculture and photovoltaic power generation. Food crops and electricity can be harvested on the same plot of land." [5]

Table 1. Different terms used worldwide for agrivoltaics

Term	Region	Reference
Agrivoltaics - Agrophotovoltaics	Germany- France- US	[7][8][9]
Colocated systems		[10] [11]
Horticulture PV		[12]
Agrovoltaico	Italy	[13]
Solar sharing	Japan	[14] [15]

Figures (1,2) are respectively illustrating the two most spreaded types of open-field agrivoltaic. The first (Figure 1) is for Fraunhofer ISE research plant at Lake Constance, which is horizontal-tilted and stilted PV panels above the crops, and one of the main advantages of this structure is the ability to use machinery under the panels for higher accessibility. The second (Figure 2) is the vertical PV panels agrivoltaic implemented in Donaueschingen-Germany and mainly use bifacial modules [6]. The vertical-mounting structure is cost-effective since it does not need to be 3-4 meters in height. Moreover, it would benefit from mitigating the wind effect on the crops; however, this structure has fewer light-management options than the stilt-mounted agrivoltaics.[5]

The term used for referring to agrivoltaic systems is different based on the country or region. In the following table, we included the most used terms for this method of integration between agriculture and solar power.

Agrivoltaic systems can be classified based on multiple aspects regarding function, mobility, structure, or farming type. Figure (3) shows the classification proposed by Fraunhofer ISE for the agrivoltaic systems.

Generally, two main structures of agrivoltaic systems can be found in the studies currently, interspace PV (either vertical or horizontal PV panels), which is more focused on providing sufficient space between the PV rows to be used. The other is overhead PV, in which the PV panels are mounted on 2-4 m of height. Also, tracking systems are essential in the case of agrivoltaics. The function and the number of tracking axis systems could characterize the system. Moreover, the microclimate underneath is a crucial variable since it directly affects the crop yield.



Figure 1. The Fraunhofer ISE agrivoltaic research plant at Lake Constance. @Fraunhofer ISE



Figure 2. Bifacial modules installed vertically, Donaueschingen-Germany. @Next2Sun GmbH

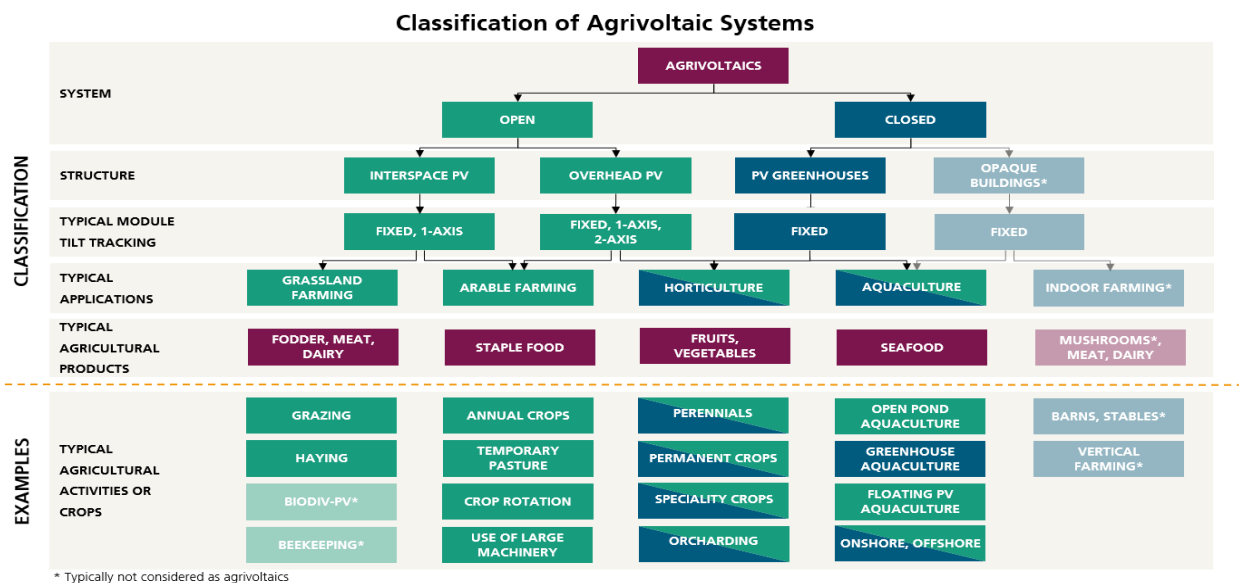


Figure 3. Classification of agrivoltaic systems. proposed by Fraunhofer ISE. @Fraunhofer ISE

Figure (4) shows a more simplified classification proposed by [16]. The objective-based classification has been added to this classification since it is important, especially in the planning phase, to determine the objective of the planned agrivoltaic system if it is energy or agriculture centric or integrated centric. [17]

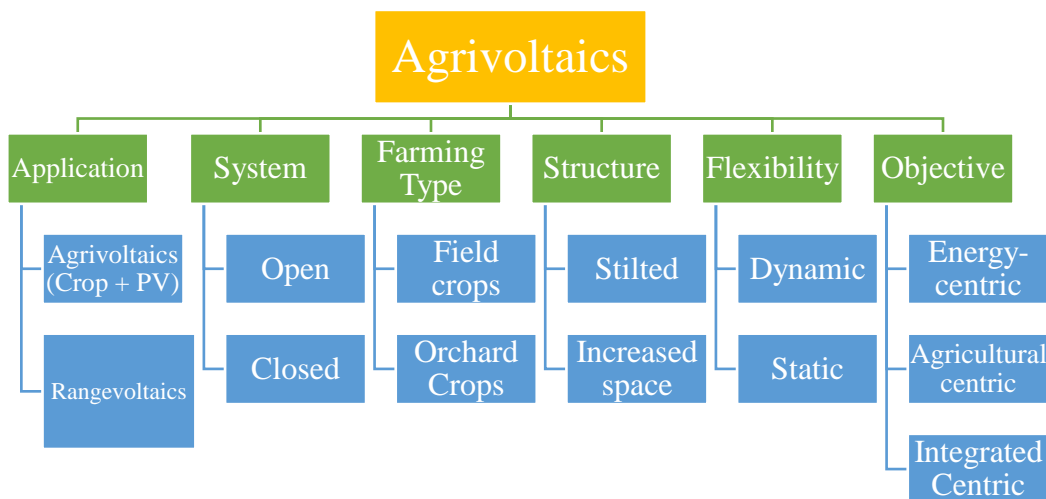


Figure 4. Classification of agrivoltaic systems proposed by [16]

4. State of the art of the agrivoltaic systems

4.1. Agrivoltaics evolution and workflow

Under the new definition of agrivoltaics, the first agrivoltaics farm was installed in Montpellier, France, and several studies were carried out there by [4] [18] [8]. Durum wheat was initially chosen as a test crop in the (STICS) crop model to investigate the performance of the crops under the shade of solar panels [4]. The results showed an increase of 60-70% in overall land productivity using the agrivoltaic system.

In the same facility, another study was carried out to assess the effect of shade caused by the panels of two densities on the crop yield [8]. The two PV panels densities, Full Density (FD) and Half Density (HD), resulted in shade levels of 50 and 70% of solar irradiation. Four varieties of lettuce were used as cultivated crops under stilt mounted PV panels of 4m height and tilted angle 25. In that research, the lettuce approved its ability to adapt to the new shading amount caused by the solar panels, which were connected to morphological leaf development changes.

Fraunhofer-ISE institute launched the project (APV-RESOLA) in Germany, to be Germany's largest agrivoltaic research facility. [7] used the facility to build a simulation model in order to analyze the electrical performance and the behavior and productivity of four crops (Potato, Celeriac, clover grass, and winter wheat). This research facility has a unique design with solar panels' height of 5 m, and the distance between the rows is up to 19 m to allow the use of large machines as shown in Figure 5.

The simulation results conducted in this research presented the system's viability in the aspects of orientation, row distance (density of panels), and electricity yield. It was found that by combining the electrical and crop yield, (LER) mean for 2017 and 2018 between 1.71 and 1.76 was achieved. However, the research stated that the row distance is vital in the aspect of balancing the electrical and crop yield and that agrivoltaics bears the chance to enhance the resilience of farming systems against future drought.

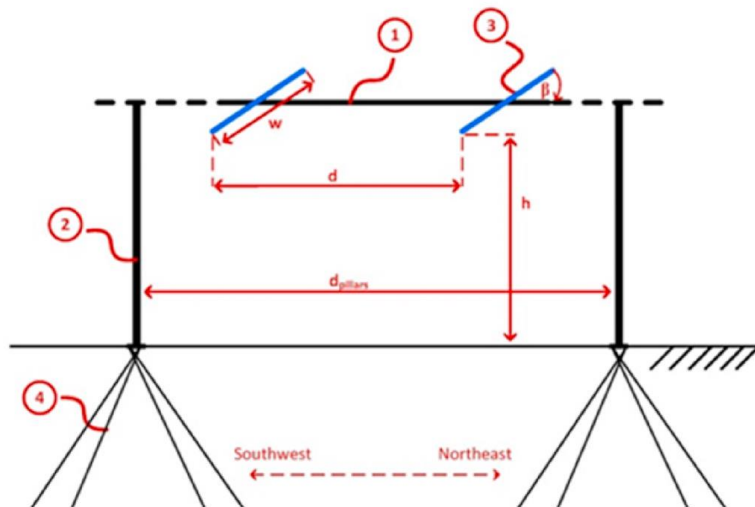


Figure 5. Sketch of lateral view of an APV system in Fraunhofer ISE in Heggelbach. 1 = longitudinal beam, 2 = pillar, 3 = PV module, 4 = Spinnanker foundation; w = module width, β = tilt angle, d = row distance, d_{pillar} = width clearance, h = vertical clearance. The source[7]

Agrivoltaics systems were also attractive in the USA, where [9] proposed agrivoltaics in Phoenix Metropolitan Statistical Area (MSA) intending to reduce the energy production from conventional sources, preserve the agricultural land, and help the local community to accept and adopt agrivoltaics as a sustainable solution. A large-scale simulation assessment was carried out to investigate the potential of the agrivoltaic system on the agricultural land in Phoenix. The analysis has been conducted using (Sketchup Pro), (Skelion), and (SunHorus) plugins and the panels were placed at 4m height. Half and quarter-density PV panel distribution patterns over the agricultural land were analyzed in this study. The farmers growing Alfalfa, Cotton, and Barley can generate 5, 4.7, and 1.5 times the current residential energy requirement. The future energy needs of the MSA can also be met using agricultural land. With half-density panel distribution, the agricultural land would receive about 60% of the direct sunlight compared to land without panels. The agricultural land would receive about 80% of the direct sunlight with quarter-density panels. Analysis shows

that the energy used in crop production is less than 1% of the total energy generated using agrivoltaic systems. It is observed that 50% of the agricultural land would make up for the sale price of the land within two years with agrivoltaic systems.

Also, in the USA, [19] performed their research on the applicability of agrivoltaic systems in California at SunPower research center (Figure 6). A variety of crops used in this study included: Kale, Swiss chard, broccoli, bell peppers, tomato, and smooth leaf spinach.

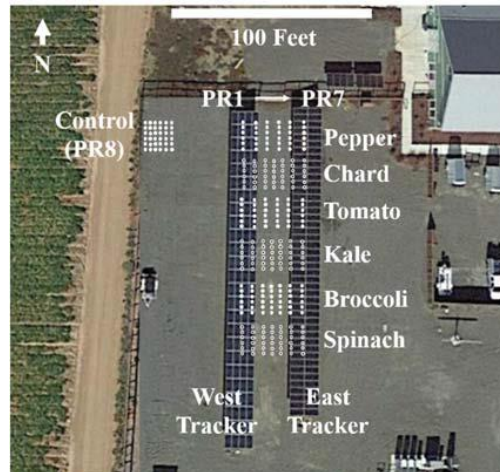


Figure 6. Layout of the shade treatments among the PV at the SunPower Research center in Davis, California. Circles show individual, container-grown plants of the indicated crops. Image source[19]

It was found that Kale produced the same amount within all PAR levels between (55-85%) of FS (Full Sun). Chard yield was the same in PAR levels of 85% and greater. Also, Tomatoes produced the same yield in all PAR levels greater than 55% of FS.

The research suggested that crops like Kale, chard, and tomatoes can be planted throughout the solar array with only a limited yield penalty as long as light levels are at least 55% of full-sun irradiance. Other crops like spinach are not advisable among solar panel arrays due to their strong dependence on high irradiance for best crop yields.

4.2. Design parameters, performance indicators, and their impact

Usually, the tilted PV panels can optimize the tilt angle based on the annual local solar irradiation [12] [20]. Also, the possibility of deriving the tilt angle of the optimal situation in the critical growth stage for the crop was mentioned by (Elborg 2017) in the manually controlled tracking system cases. Moreover, in addition to the operation temperature, which is determined by the ambient temperature, wind speed, and solar irradiation, the dust caused by the agricultural activities can impact the power generated. The amount of dust collected on the PV panels has an inverse relationship with the tilt angle. [21] [3].

Crop-Sim, a Decision Support System (DSS), is an interesting method used to anticipate and optimize crop status and energy yield under a dynamic agrivoltaic system to achieve the highest possible energy yield without impacting the crop (Chopard et al., 2021). This (DSS) defines a plant's well-recognized three abiotic indicators associated with crop development under panels. 1-the predawn water potential (leaf water potential measured just before dawn) 2-the canopy temperature, and 3-the amount of carbon produced through photosynthesis. And these indicators would allow anticipating the plant's performance throughout the year. The function of Crop-Sim is to simulate the soil, the plant, the atmosphere, and the interactions between them.

In order to conduct the first study on agrivoltaics under organic field management conditions. [22] [23] in Germany investigated how celeriac would be affected by cultivating under agrivoltaics system and the impact of solar panels on the microclimate underneath. Cultivating celeriac was part of a four-year crop rotation consisting of Celeriac, Potato, winter wheat, and grass-clover as in Figure 7.

The research stated that PAR was reduced by 29.5% on average under agrivoltaics, while irradiance reduction was between 12-60% depending on the agrivoltaics setup. Despite the differences in some variables, the crop yields were not significantly reduced, and the research stated that celeriac could be considered a suitable crop under agrivoltaics.

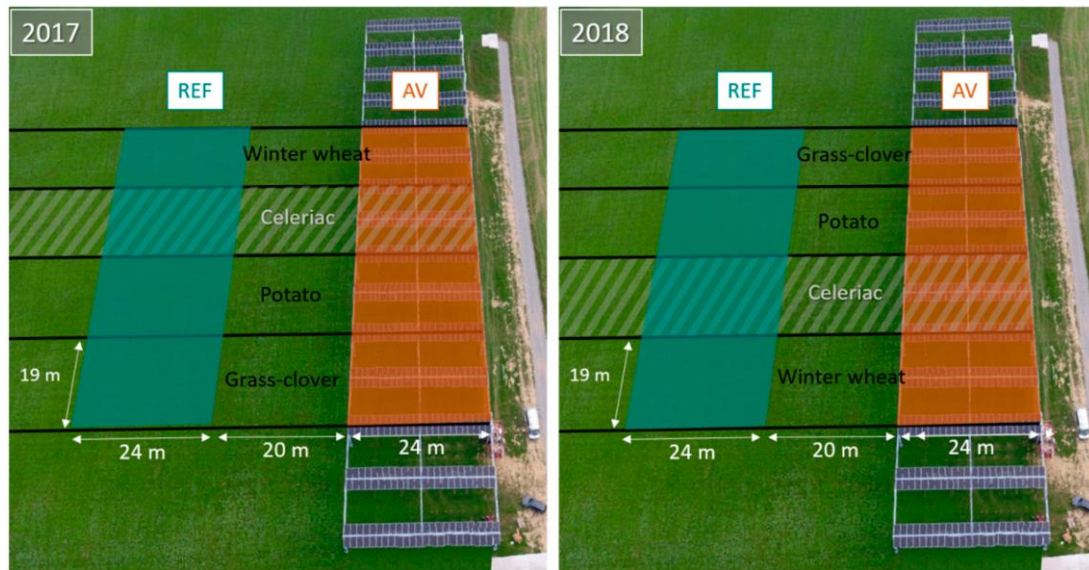


Figure 7. Setup of the field experiment in 2017 and 2018 with the location of celeriac within the crop rotation. The source [22]

Considering the viability of a crop such as rice, especially in Asia, the yield should not fall below 80% of crops grown under normal conditions in the surrounding area [14] [24]. To assess the applicability of agrivoltaics systems over rice crops, [25] carried out a comprehensive study in four different farms in Japan with different ratios of projected shade under solar panels to the total surface area and to optimize agrivoltaics in the case of rice yield. Also, [24], in an MSc thesis, conducted simulation and experimental assessment to estimate rice yield integrated with energy yield under an agrivoltaic system. The research reported experimental data to refer to a reduction in the grain yield by 22.6% under partial shading compared to full sun condition; even delaying the harvest didn't change the reduction percentage. The model has been performed accurately, and the experimental results validated it.

4.3. Innovative solutions and applications

Not only stationary PV panels were investigated in the agrivoltaics systems, but also mobile PV panels were proposed by [26]. The study conducted a comparative assessment of the performance of stationary and mobile agrivoltaics systems over lettuce in the aspect of energy production and yield biomass using (LER). The sun-tracking solar panels were installed beside the typical stationary panels in the field with the flexibility to control the microclimate under the agrivoltaic system. Physiological traits should be measured in a crop as the projected area, leaf number, specific leaf area, leaf shape. Two types of lettuce were cultivated under the panels (Kiribati, Madelona). The experiment was well prepared by dividing the field into three main areas: 1-Mobile Panels with solar tracking (ST) 2- Mobile Panels with controlled tracking (CT) 3- Stationary panels area which contains Half Density (HD) and Full Density (FD) areas. Also, full sun condition (FS) was placed in the south of the agrivoltaic system as a control for the crop yield. Three experiments in spring, summer, and autumn were carried out.

Interestingly, all of the cases studied in that experiment achieved an (LER) bigger than 1, which indicates that in all the cases, the agrivoltaic system reduced the required area to produce the same amount of electricity and yield biomass. Notably, both types of mobile agrivoltaics achieved higher (LER) than the stationary system due to the significantly increased power generated and slightly increased biomass. Even though ST mobile systems achieved better electricity generation than CT systems, the latter provided a crop yield at levels close to the control FS systems yield, introducing it as a solution for different crops that may be more shading intolerant.

A patented agrivoltaic solar tracking system named (Agrovoltaico) (Figure 8) was investigated using simulation with a maize crop by [27] in northern Italy. One of the unique traits of this system is the tensile structure of the stilts which minimize the use of land.



Figure 8. The tensile structures of the Agrovoltaico systems. The source[13]a

The study used Generic Crop Growth Simulator (GECROS) with coupled radiation and shading models. A simulation model was used in this study in (Scilab) software platform, and the crop model was prepared using (GECROS). The simulation provides results for the years (1976-2014).

After a comprehensive analysis, the grain yield was higher and more stable under Agrovoltaico than full sun conditions under the drought stress, while it is slightly lower when water is not limited. Using (LER) method, always Agrovoltaico achieved more than 1.

Arid and semi-arid lands are a suitable location for conventional PV farms because of the high potential yield and because it is usually far from the centers of human activity. In the arid and semi-arid lands in Northeastern India, [10] investigated an agrivoltaic system as a compromise between the conventional installation of solar panels and cultivation (Aloe vera) as shown in Figure 9, which is xerophytic and doesn't require special requirements of solar infrastructure. (Aloe vera) has a short growth stature and low maintenance.



Figure 9. (a) Colocation of solar PV and vegetation in Colorado, USA. (b) Aloe vera cultivation in Rajasthan, India. Source[10]

The research investigated the aspects of energy inputs/outputs, water use, greenhouse gas emissions, and the solar installation system's economics compared to aloe vera cultivation, another widely promoted and economically important land use in these systems. The life cycle analysis showed that agrivoltaics are economically beneficial in rural areas and could create better rural economic growth opportunities. The water inputs for cleaning solar panels are similar to the amounts required for annual aloe vera productivity. The authors recommended integrating the two systems to maximize land and water use efficiency. A life cycle analysis of a hypothetical colocation indicated higher returns per m^3 of water used than either system alone.

Choosing the appropriate module and technology for the solar panels is still under study, and the emergence of bifacial modules opened the door for comparison between them and monofacial modules. The comprehensive analysis of agrivoltaics in Paras, Maharashtra, India [12] recommended using bifacial solar panels after the practical measurements. The bifacial modules produced 6.4% of electric yield, more than the monofacial modules.

[28] in their research investigated the performance of vertical East-West oriented bifacial modules computationally compared to the conventional tilted North-South oriented monofacial modules (Figure 10).

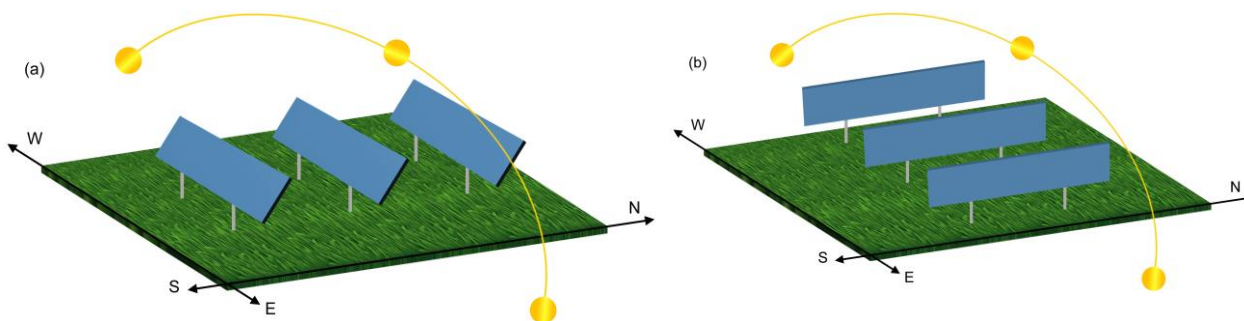


Figure 10. (a) Tilted monofacial south-facing (mono-N/S), and (b) vertical bifacial east-west facing (bi-E/W) solar modules. The source [28]

In some areas, power loss due to soiling can reach 10% per day for lightly soiled panels and 40% for heavily soiled panels. This effect could be mitigated by shifting the tilt from horizontal to vertical [29]. The potential of vertical bifacial solar is high because it can mitigate soiling losses, making it important to assess its performance, especially in arid areas.

[28] in their research, stated that the performance of the bifacial panels is affected by the density of solar rows. When the farm is half-density, the vertical panels produce the same energy as the tilted conventional one. Also, the combined PAR/Energy yields for the vertical bifacial farm is not always superior, and the study suggested that it could still be an attractive choice for agrivoltaics due to its distinct traits such as minimizing the land coverage, more flexibility to the farm machinery, ability to mitigate soiling losses, in addition to the cost advantages due to potentially reduced elevation, in the cases when the elevation is not a requirement for the system.

Interesting experimental research was conducted to use tinted semi-transparent solar panels in agrivoltaics systems [30], as presented in Figure 11, where spinach and basil were the crops under the solar panels. Physiological/metabolic variations of the crops were analyzed, and the relative content of lipid, carbohydrates and protein from plants under agrivoltaics compared to control plants. The main trait of tinted semi-transparent panels was the selectivity of the electromagnetic spectrum so the photovoltaic system and the plant can harness different parts of the spectrum. The sum of experimental data showed that agrivoltaics could provide an overall financial gain of +2.5% for Basil and +35% for spinach. Also, the amount of protein extracted from both plants increased despite the loss of marketable biomass for basil and spinach plants.

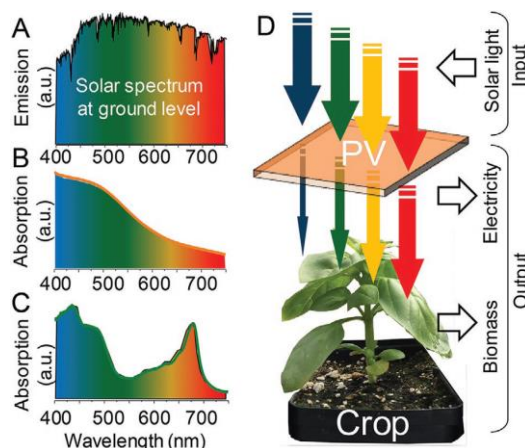


Figure 11. Agrivoltaics for food and energy double-generation implemented with tinted semi-transparent solar panel. A) Solar radiation spectrum in the visible range at the ground level. B) Absorption spectrum for the tinted semi-transparent solar PV panel (a-Si single-junction) used in this study. C) Absorption spectrum for a basil plant leaf. D) Schematic representation of the input (solar energy) and the two contextual outputs of agrivoltaics (i.e., electricity and biomass). The source [30]

The possibility of cultivating grape as a shade-intolerant crop under agrivoltaics in Nashik, Maharashtra, India, was assessed using simulation [31]. The ground coverage ratio was about 0.26, to decrease the effect of shade as much as possible. The research estimated an increase in the revenue of 15 times when using agrivoltaics system on the grape lands than in the case of conventional grape farming. However, actual experiments are needed to verify and validate the model to check the effect of shade on crop yield performance.

Agrivoltaic systems are developing rapidly, researchers all over the world are reporting advancements on agrivoltaics performance. A new configuration of agrivoltaic system was proposed lately by [32] named the Even-Lighting Agrivoltaic System (EAS) against what so-called Conventional Agrivoltaic System (CAS) in both Fuyang city and Hefei City, Anhui province, China (Figure 12). The essential concept in this system is to reduce 1/3 of the solar panel and replace it with a grooved glass plate, and this plate is designed to distribute the light evenly over the shadowed cultivated area by scattering the incident light into three parts by refraction.

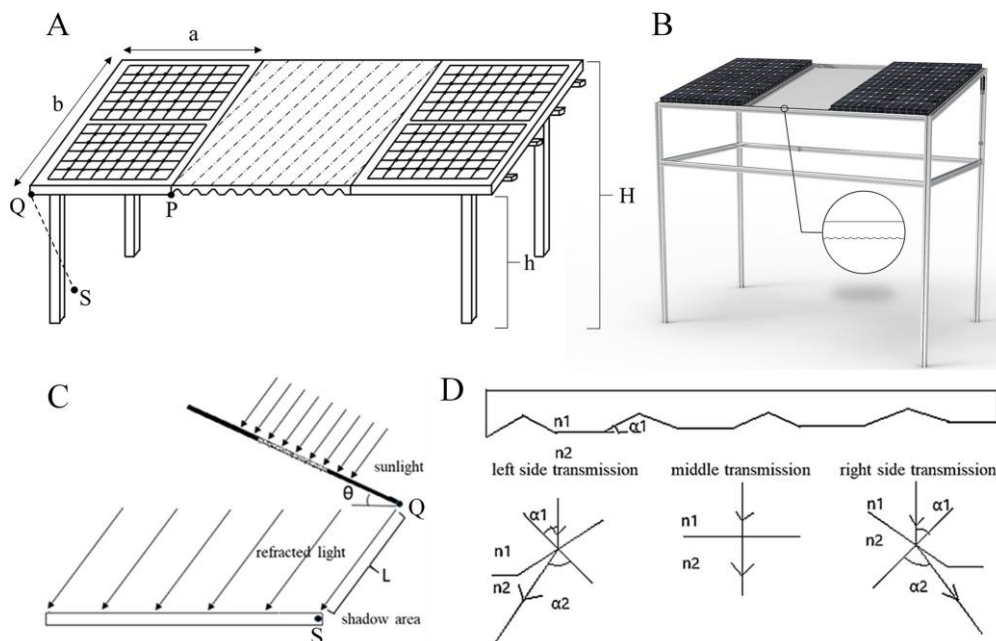


Figure 12. The structure of the EAS (A). The rendered output diagram of EAS structure (B). The side view of the EAS (C). The structure of the grooved glass plate. The source [32]

The crop cultivated under solar panels is lettuce for the small-scale facility, and broccoli, shallot, garlic sprouts, garlic, rape, broad bean, and Jerusalem artichoke in the large-scale facility. The research stated that using EAS is most similar to the control land in the aspect of crop yield. The yield of crops fell by 5% except for broccoli and rape, while Jerusalem artichoke yield was 23% higher. EAS improved the irradiation for the crops by 47.38% compared to CAS, Land Equivalent Ratio (LER) for the crops range between (1.55-1.9) under EAS. An interesting enhancement was combining supplementary LED lamps with the EAS, which increased the soluble sugar content of lettuce by 72.14% and decreased nitrate content by 21.51%.

4.4. Environmental and economic centric studies

To provide a holistic approach over (Agrovoltaico) system, the environmental and economic performance of the system was modeled by [13] to provide a Life Cycle Assessment for the system and investigate the implementing costs' details compared to other PV applications or sources of electricity can be found in the Italian market.

It was found that in the aspects of climate change, ecosystem quality, air quality, and resources depletion, the agrivoltaico systems have a similar performance to the ground or roof-mounted PV due to the tensile construction, although the first release of (Agrivoltaico) systems with the huge concrete basements and large poles made the environmental performance of these proposed systems worse than the conventional ground or roof-mounted PV applications and even than coal electricity.

The environmental impact of agrivoltaic systems is another important aspect to consider. [33] assessed the environmental impacts and viability of energy production efficiency of agrivoltaic systems compared to other forms of energy production, by comparing three different solar array designs as shown in Figure 13; the first emphasizes maximizing the crop yield per area unit by providing the optimal conditions for it, the second emphasizes maximizing the energy production per area unit, and the third was developed to be balanced between crop and solar production. The panels were ground mounted with 0.61 m height above the ground. The Tool for the Reduction and Assessment of Chemical and other Environmental Impacts (TRACI) was used to analyze the environmental performance of the agrivoltaic system by considering ten different impact categories. The research stated that even though agrivoltaic systems have a higher Global Warming Potential (GWP) than traditional PV, this difference is insignificant compared to the amount of space that agrivoltaics saved by co-existing solar panels and agriculture. Also, agrivoltaics was recommended for maximizing land-use efficiency.

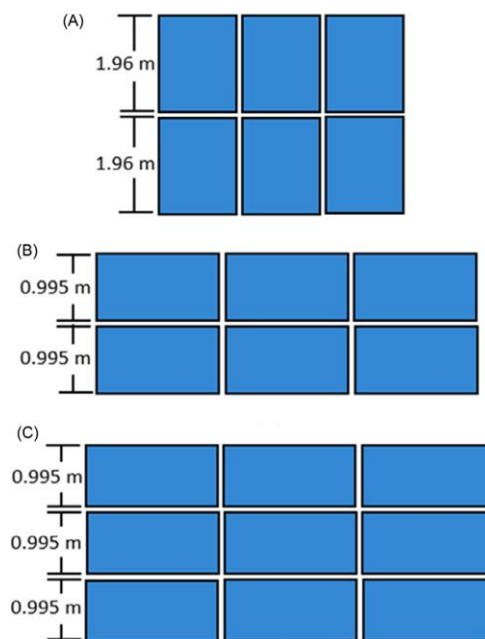


Figure 13. Front views of PV array system design 1 (A), 2 (B), and 3 (C). The source [33]

4.5. Microclimate under the panels

To emphasize the importance of assessing the patterns of shade and availability of PPFD and DLI within the agrivoltaic system, [34] quantified the spatial and temporal availability variability of PPFD and DLI under the Agrivoltaic system in Jodhpur, India. Three blocks of PV modules were installed on an area of 32*32m and 35 KW_p for each (Figure 14).

The measurements were carried out around the winter solstice because in this period, the day length is the minimum, and the magnitude of shade is greatest in the northern hemisphere. A major obstacle reported in this study was the absence of (DLI) and (PPFD) standards for the field crops, while in the literature, the greenhouse crops standards can be found. Also, in the case of high stilted panels (5 m, for example), the issue of cleaning the panels from the dust in such a dry region in India was encountered. The research results proved that in the region of Jodhpur, the availability of PPFD was not a constraint in order to meet the photosynthesis requirements. The shaded area in the interspace during the winter solstice varied from 18 to 58% of the total interspace area. The proportion of shaded area was greater in the single row PV array design than in the double row PV array and triple row PV array designs of the AVS. It was suggested that standardizing the required amount of (DLI) and (PPFD) and mapping spatial and temporal distribution of these parameters to optimize the crop yield and choose the optimal crop.

Generally, under agrivoltaic systems, there is shade and light fluctuation during the day [35] because of the sun's position. Due to that, the stomatal conductance process that indicates plant water status will be affected. [36] focused in their research on modeling the water budget and crop growth of irrigated lettuce under an agrivoltaic system, concerning stomatal conductance as a variable that considers the short-term alternation of sunlight and shade in the intersections between panels. Four devices were considered in the

study compared to the control plot, Full Density (FD), Half Density (HD), Solar Tracking (ST), and Control Tracking (CT). By averaging all the tested cases in this study, it was found that the (LER) of the proposed agrivoltaic system value is 1.21. The mean overall effects of the tested artificial shading conditions were a reduction of plant water demands by -20%, a delay in maturity of about 5–7 days in the agrivoltaic installation concerning the control plot, or a decrease of agricultural yield by -15% to -25%.

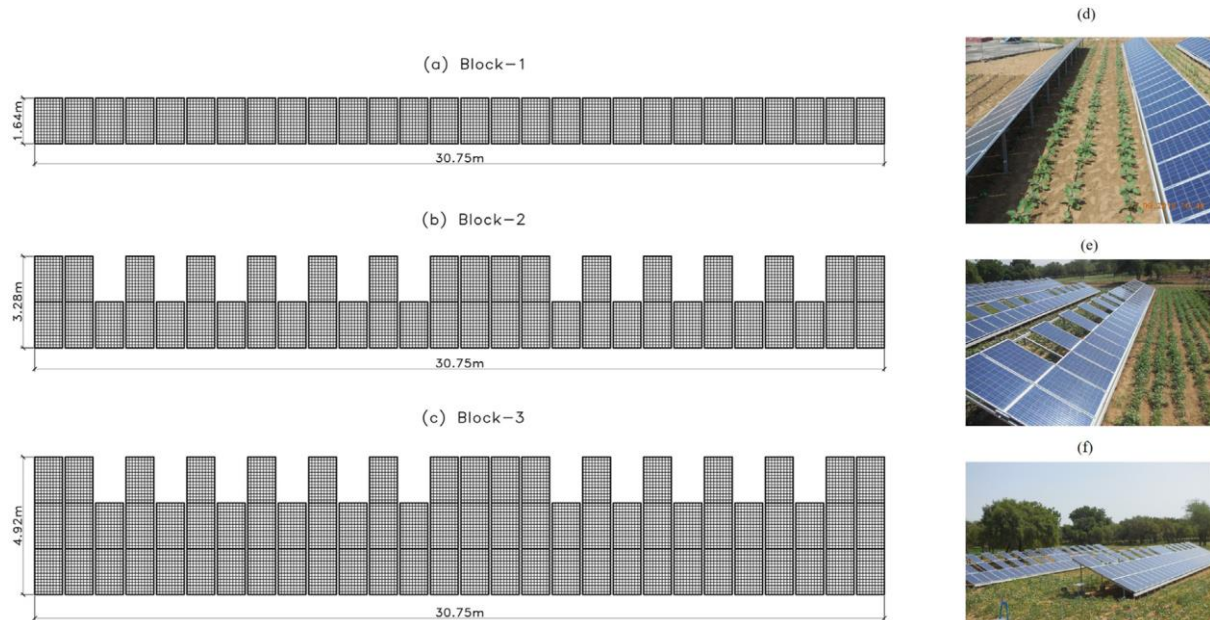


Figure 14. Agrivoltaic system (AVS) at ICAR-CAZRI, Jodhpur; (a-c) design of PV array in three field blocks of the AVS and (d-f) field photographs of the installed AVS in block 1, block 2, and block 3, respectively.
Source[34]

As mentioned previously, using agrivoltaics as a shelter from severe environmental conditions is popular. In Ongjin-Gun, the Republic of Korea [15] installed an agrivoltaic system over the grape crop to protect the crops from heavy rain. Acryl panels were added to the structure mounted on its top for that purpose. And the shading rate was controlled to be 30% of the total roof area. The experiment consisted of three sections with three different module technologies, 1-conventional opaque monofacial solar panels, 2- bifacial solar panels, and 3- transparent solar panels with three relevant control sites to compare the results of each type. Experimental data of the microclimate under agrivoltaics were collected (Carbon dioxide, Illuminance, and soil temperature), in addition to the germination process monitoring and the sugar content of the grape fruit. These variables were monitored to investigate each technology performance of agrivoltaics system compared to control conventional cultivation. The research stated that the coloring and growth of the test-site grapes were delayed compared to the control site due to the solar irradiance reduction and temperature change under the panels. However, by delaying the second harvest time by ten days after the first, the researchers reported a grape yield quality in the agrivoltaic site as equal to the quality under the control site at the first harvest time.

Coupling agrivoltaics with shade-intolerant crops was addressed by [37] to assess the performance of corn as a shade-intolerant crop under stilted mounted PV panels as presented in Figure 15. The experiment was carried out on a farm in Ichihara city, Chiba prefecture, Japan. The farm contains three sub-configurations: low module density, high module density, control area (no modules).

The study stated that high-density agrivoltaic land revenue could be 8.3 times larger than the control one, while the low density was 4.7 times larger. Speaking in detail, the biomass of corn stover under a high-density system was 96.9% of the control biomass, while the biomass under a low-density system was interestingly larger than under control by 4.9%. The authors proposed that light saturation point is the key to understanding these results, so when the plant is photosynthetically saturated, no more light is required to boost photosynthesis. In addition, to the shelter provided by solar panels from too much light, and increasing the water efficiency.

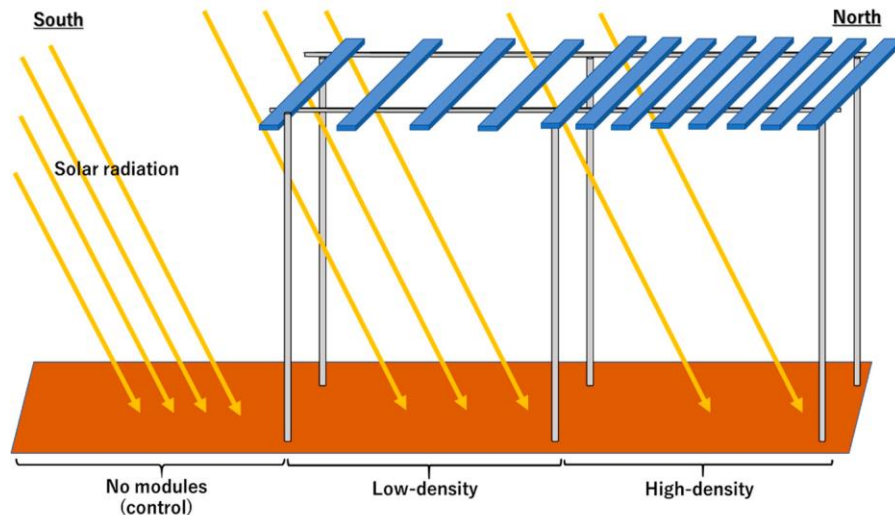


Figure 15. PV module configurations at the agrivoltaic experimental farm in [37]

5. Conclusion

Agri-voltaics systems are one of the most promising synergetic technologies that allow the dual-use of land, which is more significant for countries with a scarcity of land. Moreover, many studies reported the efficiency of using agrivoltaic systems in the arid and semi-arid areas where different crops would benefit from the effect of solar panels' existence on the microclimate underneath, as it mitigates the ambient impact, which could harm the yield.[37][34][38] Along with the attractive trait of diversifying the farmers' income and providing more rural services. [39]

The aspects of developing agrivoltaics systems are diverged into the technology by using Semi-Transparent PV [30] and tracking systems [26][36]. Innovative structure optimizing methods like using acrylic-panels to protect the crops from heavy rain [15], or dynamic system which can be moved along the land [40].

The publicity of agrivoltaics systems is expected to increase and be promoted more by the governments. More researchers, institutions, and research centers are working on the optimization process of the system, which can not be an easy task due to the high number of variables and the complexity of modeling the crops to anticipate the output of the project during the planning stage.

References

- [1] **D. Ketzer, P. Schlyter, N. Weinberger, and C. Rösch** (2020) "Driving and restraining forces for the implementation of the Agrophotovoltaics system technology – A system dynamics analysis," *J. Environ. Manage.*, vol. 270, no. May, 2020, doi: 10.1016/j.jenvman.2020.110864.
- [2] **A. S. Pascaris, C. Schelly, and J. M. Pearce** (2020) "A first investigation of agriculture sector perspectives on the opportunities and barriers for agrivoltaics," *Agronomy*, vol. 10, no. 12, 2020, doi: 10.3390/agronomy10121885.
- [3] **H. Dinesh and J. M. Pearce** (2016) "The potential of agrivoltaic systems," *Renew. Sustain. Energy Rev.*, vol. 54, pp. 299–308, 2016, doi: 10.1016/j.rser.2015.10.024.
- [4] **C. Dupraz, H. Marrou, G. Talbot, L. Dufour, A. Nogier, and Y. Ferard** (2011) "Combining solar photovoltaic panels and food crops for optimising land use: Towards new agrivoltaic schemes," *Renew. Energy*, vol. 36, no. 10, pp. 2725–2732, 2011, doi: 10.1016/j.renene.2011.03.005.
- [5] **Fraunhofer ISE** (2020) *Agri-voltaics: Opportunities for agriculture and the energy transition - A guideline for Germany*, no. October. 2020.
- [6] "Homepage - next2sun." <https://www.next2sun.de/en/homepage/> (accessed Mar. 05, 2022).
- [7] **M. Trommsdorff et al.** (2021) "Combining food and energy production: Design of an agrivoltaic system applied in arable and vegetable farming in Germany," *Renew. Sustain. Energy Rev.*, vol. 140, no. January, 2021, doi: 10.1016/j.rser.2020.110694.
- [8] **H. Marrou, J. Wery, L. Dufour, and C. Dupraz** (2013) "Productivity and radiation use efficiency of lettuces grown in the partial shade of photovoltaic panels," *Eur. J. Agron.*, vol. 44, pp. 54–66, 2013, doi: 10.1016/j.eja.2012.08.003.

- [9] **D. Majumdar and M. J. Pasqualetti** (2017) "Dual use of agricultural land: Introducing' agrivoltaics' in Phoenix Metropolitan Statistical Area, USA," *Landsc. Urban Plan.*, vol. 170, no. May 2017, pp. 150–168, 2018, doi: 10.1016/j.landurbplan.2017.10.011.
- [10] **S. Ravi et al.** (2016) "Colocation opportunities for large solar infrastructures and agriculture in drylands," *Appl. Energy*, vol. 165, pp. 383–392, 2016, doi: 10.1016/j.apenergy.2015.12.078.
- [11] **J. Macknick, B. Beatty, and G. Hill** (2014) "Overview of opportunities for colocation of solar energy technologies and vegetation," *Sol. Energy Sites Considerations Areas Veg. or Contam. Disturb. Lands*, no. December, pp. 1–21, 2014.
- [12] **M. Trommsdorff et al.** (2019) "Feasibility and Economic Viability of Horticulture Photovoltaics," no. July 2021. 2019, [Online]. Available: https://www.eupvsec-planner.com/presentations/c49900/a_standardized_classification_and_performance_indicators_of_agri_voltaic_systems.htm.
- [13] **A. Agostini, M. Colauzzi, and S. Amaducci** (2020) "Innovative agrivoltaic systems to produce sustainable energy: An economic and environmental assessment," *Appl. Energy*, vol. 281, no. June 2020, p. 116102, 2021, doi: 10.1016/j.apenergy.2020.116102.
- [14] **M. Elborg** (2017) "Reducing Land Competition for Agriculture and Photovoltaic Energy Generation - A Comparison of Two Agro-Photovoltaic Plants in Japan," *Int. J. Sci. Res.*, vol. 6, no. 9, pp. 1–5, 2017, doi: 10.21275/1081704.
- [15] **J. Cho, S. M. Park, A. Reum Park, O. C. Lee, G. Nam, and I. H. Ra** (2020) "Application of photovoltaic systems for agriculture: A study on the relationship between power generation and farming for the improvement of photovoltaic applications in agriculture," *Energies*, vol. 13, no. 18, pp. 1–18, 2020, doi: 10.3390/en13184815.
- [16] **B. Willockx, B. Uytterhaegen, B. Ronsijn, B. Herteleer, and J. Cappelle** (2020) "A Standardized Classification and Performance Indicators of Agrivoltaic Systems," *Eu Pvsec 2020*, pp. 1–4, 2020, [Online]. Available: https://www.eupvsec-planner.com/presentations/c49900/a_standardized_classification_and_performance_indicators_of_agri_voltaic_systems.htm.
- [17] **A. Scognamiglio and C. Toledo** (2021) "Agrivoltaic systems design and assessment: A critical review, and a descriptive model towards a sustainable landscape vision (three-dimensional agrivoltaic patterns)," *Sustain.*, vol. 13, no. 12, 2021, doi: 10.3390/su13126871.
- [18] **H. Marrou, L. Guillioni, L. Dufour, C. Dupraz, and J. Wery** (2013) "Microclimate under agrivoltaic systems: Is crop growth rate affected in the partial shade of solar panels?," *Agric. For. Meteorol.*, vol. 177, pp. 117–132, 2013, doi: 10.1016/j.agrformet.2013.04.012.
- [19] **T. Hudelson and J. H. Lieth** (2021) "Crop production in partial shade of solar photovoltaic panels on trackers," *AIP Conf. Proc.*, vol. 2361, no. June, 2021, doi: 10.1063/5.0055174.
- [20] **E. D. Mehleri, P. L. Zervas, H. Sarimveis, J. A. Palyvos, and N. C. Markatos** (2010) "Determination of the optimal tilt angle and orientation for solar photovoltaic arrays," *Renew. Energy*, vol. 35, no. 11, pp. 2468–2475, 2010, doi: 10.1016/j.renene.2010.03.006.
- [21] **G. Talbot, S. Roux, A. Graves, C. Dupraz, H. Marrou, and J. Wery** (2014) "Relative yield decomposition: A method for understanding the behaviour of complex crop models," *Environ. Model. Softw.*, vol. 51, pp. 136–148, 2014, doi: 10.1016/j.envsoft.2013.09.017.
- [22] **A. Weselek, A. Bauerle, S. Zikeli, I. Lewandowski, and P. Högy** (2021) "Effects on crop development, yields and chemical composition of celeriac (*Apium graveolens* L. var. *rapaceum*) cultivated underneath an agrivoltaic system," *Agronomy*, vol. 11, no. 4, 2021, doi: 10.3390/agronomy11040733.
- [23] **A. Weselek, A. Bauerle, J. Hartung, S. Zikeli, I. Lewandowski, and P. Högy** (2021) "Agrivoltaic system impacts on microclimate and yield of different crops within an organic crop rotation in a temperate climate," *Agron. Sustain. Dev.*, vol. 41, no. 5, 2021, doi: 10.1007/s13593-021-00714-y.
- [24] **T. C. Hau** (2019) "Simulation Approach to Estimate Rice Yield and Energy Generation under Agrivoltaic System," The University of Tokyo, 2019.
- [25] **R. A. Gonocruz et al.** (2021) "Analysis of the rice yield under an agrivoltaic system: A case study in Japan," *Environ. - MDPI*, vol. 8, no. 7, pp. 1–18, 2021, doi: 10.3390/environments8070065.
- [26] **B. Valle et al.** (2016) "Increasing the total productivity of a land by combining mobile photovoltaic panels and food crops," *Appl. Energy*, vol. 206, no. July, pp. 1495–1507, 2017, doi: 10.1016/j.apenergy.2017.09.113.
- [27] **S. Amaducci, X. Yin, and M. Colauzzi** (2018) "Agrivoltaic systems to optimise land use for electric

- energy production," *Appl. Energy*, vol. 220, no. February, pp. 545–561, 2018, doi: 10.1016/j.apenergy.2018.03.081.
- [28] **M. H. Riaz, R. Younas, H. Imran, M. A. Alam, and N. Z. Butt** (2019) "Module Technology for Agrivoltaics: Vertical Bifacial vs. Tilted Monofacial Farms," pp. 1–8, 2019, [Online]. Available: <http://arxiv.org/abs/1910.01076>.
- [29] **A. Ullah, H. Imran, Z. Maqsood, and N. Z. Butt** (2019) "Investigation of optimal tilt angles and effects of soiling on PV energy production in Pakistan," *Renew. Energy*, vol. 139, pp. 830–843, 2019, doi: 10.1016/j.renene.2019.02.114.
- [30] **E. P. Thompson et al.** (2020) "Tinted Semi-Transparent Solar Panels Allow Concurrent Production of Crops and Electricity on the Same Cropland," *Adv. Energy Mater.*, vol. 10, no. 35, pp. 1–9, 2020, doi: 10.1002/aenm.202001189.
- [31] **J. M. Pearce, P. R. Malu, and U. S. Sharma** (2017) "Agrivoltaic potential on grape farms in India," *Sustain. Energy Technol. Assessments*, vol. 23, no. April, pp. 104–110, 2017, doi: 10.1016/j.seta.2017.08.004.
- [32] **J. Zheng et al.** (2021) "Increasing the comprehensive economic benefits of farmland with even-lighting agrivoltaic systems," *PLoS One*, vol. 16, no. 7 July, 2021, doi: 10.1371/journal.pone.0254482.
- [33] **E. M. Ott, C. A. Kabus, B. D. Baxter, B. Hannon, and I. Celik** (2020) *Environmental Analysis of Agrivoltaic Systems*, 2nd ed., no. 1982. Elsevier Inc., 2020.
- [34] **P. Santra, H. M. Meena, and O. P. Yadav** (2021) "Spatial and temporal variation of photosynthetic photon flux density within agrivoltaic system in hot arid region of India," *Biosyst. Eng.*, vol. 209, pp. 74–93, 2021, doi: 10.1016/j.biosystemseng.2021.06.017.
- [35] **G. Roccaforte** (2021) "Eclipse: A new photovoltaic panel designed for greenhouses and croplands," *AIP Conf. Proc.*, vol. 2361, no. June, 2021, doi: 10.1063/5.0054544.
- [36] **Y. Elamri, B. Chevion, J. M. Lopez, C. Dejean, and G. Belaud** (2017) "Water budget and crop modelling for agrivoltaic systems: Application to irrigated lettuces," *Agric. Water Manag.*, vol. 208, no. October 2017, pp. 440–453, 2018, doi: 10.1016/j.agwat.2018.07.001.
- [37] **T. Sekiyama and A. Nagashima** (2019) "Solar sharing for both food and clean energy production: Performance of agrivoltaic systems for corn, a typical shade-intolerant crop," *Environ. - MDPI*, vol. 6, no. 6, 2019, doi: 10.3390/environments6060065.
- [38] **S. Ates, A. C. Andrew, C. W. Higgins, M. Bionaz, and M. A. Smallman** (2021) "Pasture production and lamb growth in agrivoltaic system," *AIP Conf. Proc.*, vol. 2361, no. June, 2021, doi: 10.1063/5.0055889.
- [39] **R. Mahto, D. Sharma, R. John, and C. Putcha** (2021) "Agrivoltaics: A Climate-Smart Agriculture Approach for Indian Farmers," *Land*, vol. 10, no. 11, 2021, doi: 10.3390/LAND10111277.
- [40] **N. Loots** (2018) "Technologic, Biological and Economic analysis of a dynamic agrivoltaic system in the Dutch agriculture sector," 2018.

CONTENT OF No 40/2021

CONSTRUCTION OF A PACKED-BED PYROLYSIS REACTOR FOR CHARCOAL PRODUCTION

A. Dhaundiyal, G. Bercesi, L. Toth

Institute of Process Engineering, Hungarian University of Agriculture and Life Sciences (MATE), 2100 Gödöllő, Páter Károly u. 1., Hungary5

SOIL STRENGTH AND LOAD BEARING CAPACITY MEASUREMENT TECHNIQUES

A. E. Eltayeb Ahmed¹, A. El Hariri¹, P. Kiss²

¹ Mechanical Engineering Doctoral School – Hungarian University of Agriculture and Life Sciences, 2100 Gödöllő, Páter Károly u. 1., Hungary;

² Institute of Technology - Hungarian University of Agriculture and Life Sciences, 2100 Gödöllő, Páter Károly u. 1., Hungary16

THE MAIN INFLUENCING FACTORS OF MOBILE BANKING ADOPTION IN THE OPEN INNOVATION BUSINESS ENVIRONMENT (CASE STUDY)

T. Atobishi¹, M. Bahna¹, Cs. Fogarassy²

¹ Doctoral School of Management and Business Administration – Hungarian University of Agriculture and Life Sciences, 2100 Gödöllő, Páter Károly u. 1., Hungary;

² Institute of Agriculture and Food Economics - Hungarian University of Agriculture and Life Sciences, 2100 Gödöllő, Páter Károly u. 1., Hungary28

THE EFFECT OF PARTICLE SHAPE ON THE ANGLE OF REPOSE TEST BASED CALIBRATION OF DISCRETE ELEMENT MODELS

A. Bablena, N. Schrempf, I. Keppler

Institute of Technology - Hungarian University of Agriculture and Life Sciences, 2100 Gödöllő, Páter Károly u. 1., Hungary39

INTRODUCTION TO 3D PRINTING: TECHNIQUES, MATERIALS AND AGRICULTURAL APPLICATIONS

R. F. Faidallah¹, Z. Szakal², I. Oldal²

¹ Doctoral School of Mechanical Engineering – Hungarian University of Agriculture and Life Sciences, 2100 Gödöllő, Páter Károly u. 1., Hungary;

² Institute of Mechanical Engineering - Hungarian University of Agriculture and Life Sciences, 2100 Gödöllő, Páter Károly u. 1., Hungary47

TESTING AXIAL FLOW SOLAR CHIMNEY TURBINE USING WIND TUNNEL

W. M. A.-Elmagid^{1,2}

¹ Institute of Technology - Hungarian University of Agriculture and Life Sciences, 2100 Gödöllő, Páter Károly u. 1., Hungary;

² Dept. of Mech. Power Engineering, Faculty of Energy Engineering, Aswan University, Sahary, P.O. Box 81525, Aswan, Egypt59

ASSESEMENT AND MODELLING OF INDUSTRIAL-SCALE SOLAR THERMAL SYSTEM APPLICATION IN HUNGARY

R. Ghabour¹, P. Korzenszky²

¹ Doctoral School of Mechanical Engineering – Hungarian University of Agriculture and Life Sciences, 2100 Gödöllő, Páter Károly u. 1., Hungary;

² Institute of Technology - Hungarian University of Agriculture and Life Sciences, 2100 Gödöllő, Páter Károly u. 1., Hungary70

GENERATING COLD ENERGY USING WASTE HEAT FROM A PYROLYSIS GENERATOR (CHP)

V. Madar¹, N. Schrempf², A. Betovics², L. Toth²

¹ Pyrowatt Kft., 6120 Kiskunmajsa, Vágóhíd utca 91. Hungary;

CONTENT OF No 40/2021

² Institute of Technology - Hungarian University of Agriculture and Life Sciences, 2100 Gödöllő, Páter Károly u. 1., Hungary78

STRATEGY ANALYSIS OF INTERNATIONAL FORAGE LABORATORY NETWORKS

G. Kövesdi¹, Sz. Orosz¹, Cs. Fogarassy²

¹ Livestock Performance Testing Ltd., 2100 Gödöllő, Dózsa György u. 58., Hungary;

² Institute of Agriculture and Food Economics - Hungarian University of Agriculture and Life Sciences, 2100 Gödöllő, Páter Károly u. 1., Hungary91

SMALL SCALE EXPERIMENTS OF PM10 DISPERSION AROUND OBSTACLES

A. Qor-el-aïne¹, J. Benécs², A. Béres³, G. Géczi³

¹ Doctoral School of Mechanical Engineering – Hungarian University of Agriculture and Life Sciences, 2100 Gödöllő, Páter Károly u. 1., Hungary;

² Institute of Process Engineering - Hungarian University of Agriculture and Life Sciences, 2100 Gödöllő, Páter Károly u. 1., Hungary;

³ Institute of Environmental Science - Hungarian University of Agriculture and Life Sciences, 2100 Gödöllő, Páter Károly u. 1., Hungary96

MICROCLIMATIC AND ENERGETIC FEASIBILITY OF AGRIVOLTAIC SYSTEMS: STATE OF THE ART

I. Khele^{1,2}, M. Szabó²

¹ Doctoral School of Mechanical Engineering, Hungarian University of Agriculture and Life Sciences, Páter K. u. 1, Gödöllő, H-2100, Hungary;

² Department of Building Engineering and Energetics, Hungarian University of Agriculture and Life Sciences, Páter K. u. 1, Gödöllő, H-2100, Hungary102

